Some studies of Non-Minimal Universal Extra Dimension at the Large Hadron Collider

By

Saurabh Niyogi

Enrolment Number : PHYS08200804003

Harish-Chandra Research Institute, Allahabad

A thesis submitted to the

Board of Studies in Physical Sciences

In partial fulfillment of requirements

for the Degree of

DOCTOR OF PHILOSOPHY

of

HOMI BHABHA NATIONAL INSTITUTE

September, 2014

STATEMENT BY AUTHOR

This dissertation has been submitted in partial fulfillment of requirements for an advanced degree at Homi Bhabha National Institute (HBNI) and is deposited in the Library to be made available to borrowers under the rules of the HBNI.

Brief quotations from this dissertation are allowable without special permission, provided that accurate acknowledgement of source is made. Requests for permission for extended quotation from or reproduction of this manuscript in whole or in part may be granted by the Competent Authority of HBNI when in his or her judgement the proposed use of the material is in the interests of scholarship. In all other instances, however, permission must the obtained from the author.

Saurabh Niyogi
(Ph.D. Candidate)

Declaration

I, hereby, declare that the investigation presented in the thesis has been carried out by me. The work is original and has not been submitted earlier as a whole or in part for a degree or diploma at this or any other Institution/University.

Date: September 29, 2014

Saurabh Niyogi
(Ph.D. Candidate)

List of publications arising from the thesis

Journals

1. "Non-minimal universal extra dimensions: the strongly interacting sector at the Large Hadron Collider",
   AseshKrishna Datta, Kenji Nishiwaki and **Saurabh Niyogi**,
   JHEP 11 **(2012)** 154 [arXiv:1206.3987].

2. "Non-minimal Universal Extra Dimensions with Brane Local Terms: the top quark sector",
   AseshKrishna Datta, Kenji Nishiwaki and **Saurabh Niyogi**,
   JHEP 01 **(2014)** 104 [arXiv:1310.6994].

Others

1. "Broad resonances at the LHC and the nmUED",
   AseshKrishna Datta, Kenji Nishiwaki and **Saurabh Niyogi**,
   In preparation.

Dedicated to

Didi

and

my friends

Acknowledgments

This thesis is a result of contributions and help from many people in various ways. I take this opportunity to thank them all. Please forgive me whom I forget to mention.

First of all, I thank my supervisor, Prof. AseshKrishna Datta, for his guidance and help throughout my Ph.D years. I am really grateful to my collaborator Dr. Kenji Nishiwaki without whom this thesis would not be completed. His excellence in academic discussions helps me understand the subject better. His diligence and sincerity in his work is simply astounding.

I must thank to all the past and present members of the high energy phenomenology group at HRI. Specially, I am thankful to Prof. Biswarup Mukhopadhyaya for his help on various occasions. Thanks to Prof. Raj Ghandhi, Prof. V. Ravindaran, Prof. Sandhya Choubey, Dr. Santosh Rai, Dr. A. Nyffeler for many enlightening discussions. I would also like to thank Dr. Ujjwal Sen for agreeing to be a member of my thesis committee.

A very special thanks to my friends at HRI !! It is great fun to be with them. They make the struggles and miseries of the Ph.D life forgettable. Bhuru (Sourav Mitra), Tarat (Sabyasachi), Jonthu (Arunabha), Manoj, Ho-chi (Ujjal), Rambha (Saurabh Pradhan) – thanks to all of you for all the happy moments we share together ! I will always cherish the memories of our wonderful trips.

The seniors are always very helpful. They take me through the difficult situations. Mama (Arjunda), Shubhoda, Priyotoshda, Shamikda, Kaka (Kirtimanda), Joydeepda, Sanjoyda are more than just friends. The endless gibberish over the tea parties are never to forget. I must mention the influence of Sanjoyda in my life. He is more like elder brother to me. Thank you Sanjoyda, for being there !

Dhiraj, whom I knew from my undergraduate days, is a constant source of inspiration for me. I thank Satya for many useful discussions and many more not-so-sensible chatter! Arijit and Atri – I remember you as two computer geeks ! Thanks for fixing my computer whenever it gives trouble.

Friends are lifeline in a place like HRI. As seniors start leaving, juniors flock in. Narayan is always a very close companion. Swapnamoy, Masud, Avijit, Animesh, Shankha, Taushif, Aritra, Dibya, Nabarun, Arindam, Titas, Soumyarup are all very cordial and lively. Thanks for the tremendous atmosphere you people provide!! Hi-five to my football partners Samrat, Pallab, Bibek, Subhroneel to name a few. Thanks to Am-

bresh for the jokes we shared. Discussions with you are always very fruitful.

Paromita, Anushree and Ushoshi have become very good friends over the time. I have a nice time with them sharing many details of life. Utsa – I wonder how our friendship grows talking over phone. Those countless gossips on the most unimaginable topics I can only share with you. Our friendship is very special to me!

I feel lucky to be a part of this institution. HRI provides excellent academic environment and all the necessary facilities for research. I express my gratitude to all the non-academic members of this institute for their help and support. I am indebted to the workers and stuffs of HRI (specially to the mess workers) who are always ready at their service.

I am very grateful to have some excellent teachers throughout my academic career. My love for the subject grew over the years with their excellent teaching. It would be a blunder if I forget to mention the name of Swami Kripamayanandaji. His encouragement and support help me a lot to pursue this career. His influence is immense in shaping my future from my school days.

Finally, I thank my parent and grandparents for their support without which I may not arrive at this point of my life. Didi – simply thanking you will be less for what you mean to me. Over these years our bonding grows stronger even when we are far away. Your love and affection keep me going. You are the best person I have in my life.

Thank you all !!

SYNOPSIS

Although signals of physics beyond the standard model (SM) give the first phase run of the Large Hadron Collider (LHC) a miss, the hope to discover the same is still very much alive. Supersymmetry (SUSY) and compactified extra dimensions are the two most popular frameworks for going beyond the SM. However, even within these two broad scenarios, many possibilities are still open for closer studies. Therefore, at a time when the LHC is widening its search strategies to look for new physics signals, physicists are trying to exhaust various phenomenological possibilities which have not yet been studied in detail.

In the present thesis, we consider the TeV-scale extra dimensions. A particular variant of this scenario is the so-called Universal Extra Dimensions (UED) in which one extra, flat spatial dimension is introduced beyond the usual $1+3$ dimensions. This extra spatial dimension is compactified on a circle (S^1) of radius R. The use of S^1/Z_2 orbifolding makes the circle an interval. All the SM particles have universal (equal) access to the extra dimensional bulk. One of the important features of the compactified extra dimensional models is the presence of infinite towers of Kaluza-Klein (KK) states. In a given tower, states are labelled by the KK number (n). In UED, KK number is conserved in any given interaction at tree-level which is a consequence of momentum conservation along the extra dimension. However, the presence of boundary usually breaks KK number conservation. A discrete symmetry, called the KK parity $\left((-1)^n\right)$, still remains a conserved quantity. The minimal version of a UED scenario (the mUED) is a simple extension of the SM built on the same gauge group. The particle content is also the same except for the presence of additional KK states. Since mUED is a gauge theory in more than 4 dimensions, it is non-renormalizable. Therefore, it is expected to remain valid up to a certain scale Λ. The mUED scenario has three input parameters – the inverse radius of compactification (R^{-1}), the cut-off scale (Λ) and the Higgs mass (m_H).

The non-minimal Universal Extra Dimension (nmUED), as the name suggests, contains some new free parameters. Along with the bulk terms like in mUED, we include terms localized at the boundaries of the compactified extra dimension and call these as boundary (or, brane) localized terms (BLTs). These operators are of mass dimension 4

(*i.e.*, renormalizable) and are consistent with all the symmetries of the SM. Thus, one expects that such terms must be present in any consistent version of the theory. In mUED, these terms are implicitly assumed to be small (or zero) at the cut-off scale. However, this need not be the case. In fact, it can be shown by explicit calculations that these terms will eventually be generated when one considers higher order corrections. One has to add appropriate counter terms at the boundaries in order to cancel the divergences that appear in mUED 1-loop calculation in $5D$. Thus, a more general set-up demands the inclusion of boundary-localized terms at the low scale. Therefore, it seems legitimate to include these terms from the beginning. In this thesis, we are interested in such an extension of the mUED scenario at the tree-level.

We discuss the theoretical structure (namely the action) of this particular model in detail. The bulk fields can be decomposed in terms of Fourier basis (KK mode functions) as a functions of the extra dimensional coordinate. Integration of the KK mode functions over the extra dimension gives $4D$ effective theory. We call each of this integral an "overlap integral". In our first work, we consider the boundary-localized kinetic terms (BLKT) and the Yukawa terms (BLYT) for the strongly interacting sector. Later, when we talk about the phenomenology of the top quark sector, the Higgs BLKTs will automatically come into the picture. The BLTs are free parameters of this scenario. We consider equal boundary terms at both the boundaries to preserve KK parity. Our first observation is that the boundary terms change the mass spectrum in a non-trivial fashion. Unlike in mUED, the mass of a KK excitation is obtained by numerically solving a transcendental equation. In our first work, we provide a quantitative description of the masses of the level-1 KK quarks and the KK gluons with respect to appropriate brane-local parameters. Further, the presence of BLYT for quarks invokes mixing among the various chiral states at a particular KK level. The mixing is proportional to the mass of the corresponding SM quark. Hence, this kind of chiral mixing is rather interesting for the top quark due to its large mass. Apart from the chiral mixing between the $SU(2)$ doublet and singlet states, there can be characteristic mixing of the top quarks from different KK levels of similar parity. Such *level mixings* are primarily triggered by non-vanishing overlap integrals arising from the Yukawa sector. In a different work, we investigate the effect of such mixing among the level-0 (SM) and level-2 (KK) top quarks. This kind of mixing can potentially alter the masses to a great extent. This opens up the possibility to bring down the KK top quark masses significantly thus making them accessible at the LHC. We provide quantitative estimates of the masses of the level-1 and level-2 KK top quarks and discuss their phenomenological implications.

One of the most striking features of nmUED is that both the mass spectrum and couplings vary simultaneously with the input parameters. Effective couplings can depart from the corresponding SM values and, in particular, may become quite large due to the overlap integrals. This fact makes the scenario rather interesting for the LHC where the production and decay rates of various KK excitations would get directly affected by such modifications. The most relevant one is the interaction vertex involving a SM quark, a level-1 KK quark ($Q^{(1)}$) and a level-1 KK gluon ($G^{(1)}$). This vertex plays a major role in the production processes like $Q^{(1)}\bar{Q}^{(1)}$, $G^{(1)}G^{(1)}$ and $Q^{(1)}G^{(1)}$. We work out the analytical form of this coupling deviation factor. Further, we also probe the correlations of KK masses and deviations in this coupling as a function of brane-local parameters. This coupling is equally important for the top quark sector. However, tree-level couplings of level-2 KK top quark with a pair of SM states have greater implications for the LHC. This interaction violates KK number and is not present in mUED at tree-level. Now, a level-2 KK top quark ($t^{(2)}$) can directly decay to much lighter SM particles. These would then be heavily boosted and may serve as a "smoking gun" signal at the LHC. We also discuss the deviation in couplings with the Higgs boson which may become dominant in case of top quark.

Next, we discuss the phenomenology of level-1 KK gluon and level-1 KK quarks from the first two generations at the 8 TeV and the 14 TeV runs of the LHC. Variations of cross sections of different production processes have been discussed in detail with varying parameters. We try to understand the role of simultaneous variations of the couplings and masses on various production rates. One important aspect of this work is our attempt to understand how nmUED can fake a popular scenario like, SUSY (MSSM) or mUED in a suitable set-up. We compare the cross sections for all the three scenarios. Since in nmUED, we can tune both the masses and the couplings at the same time, we have greater freedom at our disposal. We come to the conclusion that the difference in production cross sections of various final states of mUED and nmUED are not large enough to clearly distinguish one of the models. Even, in many different regions of the parameter space, nmUED cross sections could yield the corresponding SUSY numbers. We also take up an ATLAS analysis for the $jets + E_T^{\rm miss}$ final state at $\sqrt{s} = 7$ TeV and translate the ATLAS bound into an approximate constraint on the nmUED scenario. It is found that $R^{-1} = 1$ TeV can be ruled out under some reasonable assumptions. We select three benchmark points which satisfy the relevant experimental constraints. We study some important production processes (*i.e.,* pair production, single production, associated production) involving KK top quarks for the selected benchmark points. Particularly, the production modes of $t^{(2)}\bar{t}$, $t^{(2)}\bar{b}$, $t^{(2)}\bar{t}H$

(and their charge-conjugate modes) are found to be of special importance.

The possibility of enhanced couplings and the presence of KK-number violating interactions at the tree-level could result in large decay widths $\Big(\ (\Gamma/M) \gg 10\%\ \Big)$ for some KK excitations in the nmUED scenario. In this context, the level-2 KK gauge boson resonances are of immediate interest. The narrow-width approximation (NWA) usually adopted in collider studies becomes inadequate for such "fat" resonances. On top of that, even the Breit-Wigner form of the resonant propagator is bound to get distorted under the circumstances. These compels us to consider the related effects in the Drell-Yan type process and study their implications for current and future runs of the LHC. This is the subject matter of the third work which is in preparation.

The thesis is primarily intended to present an alternative scenario in the form of nmUED which could have rich phenomenology at the colliders. Working out the theoretical framework of the model lays down a platform for such analyses. The scenario has been implemented in MadGraph-5, an event generator, with the help of FeynRules which is a Mathematica-based package for implementing various particle physics models.

Contents

List of Figures

List of Tables

Chapter 1

Standard Model and beyond

1.1 General features

The Standard Model (SM) of particle physics [1] is a field theory which describes the interaction among elementary particles. In quantum field theory, elementary particles are described by fields, local in space-time, with definite transformation properties under some particular symmetries of nature. Symmetries have long been powerful guiding principles of particle physics. SM is also based on some symmetries and resulting conservation laws borne out of experiments over several decades. These are :

1) **Poincaré symmetry** is a symmetry of space-time which states that laws of nature are independent of rotation, translation or boost. Fields transform in a particular way under the Poincaré transformation. The Lagrangian of the theory must be Poincaré invariant.

2) **Gauge symmetry** is one that requires invariance under certain "continuous local transformations" i.e. transformation parameters depend on space-time points.

Apart from these, there are three discrete symmetries : charge conjugation (C), parity transformation (P), and time reversal (T) which shape the structure of the SM. Parity transformation flips left-handed fields to right-handed ones and vice-versa. Similarly, charge conjugation replaces particles with its own anti-particles. Experiments have shown that the electromagnetic and the strong interaction respect C and P (hence their product operation CP). But this is not necessarily true for the weak force which violates C, P as well as CP. The fact that parity is violated is an important one since it determines

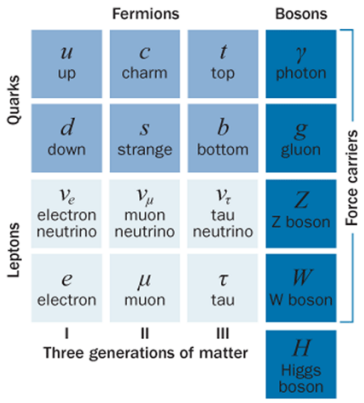

Figure 1.1: Particle content of the Standard Model.

the form of the weak interaction. Moreover, unitarity (conservation of probability) and stability of the vacuum (the lowest energy state) are also assumed in the formulation of the SM.

The requirement of renormalizability, although not a fundamental one, is another condition imposed on SM. In a renormalizable theory, the ultra-violet (short distance) divergences are absorbed through careful redefinition of bare fields and parameters of the Lagrangian. By treating SM as a renormalizable theory, one assumes that no unknown physics is required to explain discovered experimental evidences.

1.2 Particle content of the SM and their properties

The observable universe is primarily made of matter which is described by fermions of spin-$\frac{1}{2}$. It consists of quantum fields of six flavours of quarks, three flavours of charged leptons and the associated neutrinos. Interactions between matter fields are mediated by spin-1 bosons.

In a more compact notation, the continuous, local (gauge) symmetry can be conveniently described in the language of group theory. We focus on the continuous symmetry group called Lie group which is specified by some Hermitian operators known as the generators of the group. Any symmetry is labeled as a good symmetry if the Hamiltonian of the theory commutes with the symmetry transformation. An element g of the group can be written as $g = \exp(i\epsilon_a T^a)$ with T^a as the generators. Associated with each of the generator, there is a vector field (also called gauge boson). They are a consequence of local gauge symmetry. SM is invariant under the unitary product group

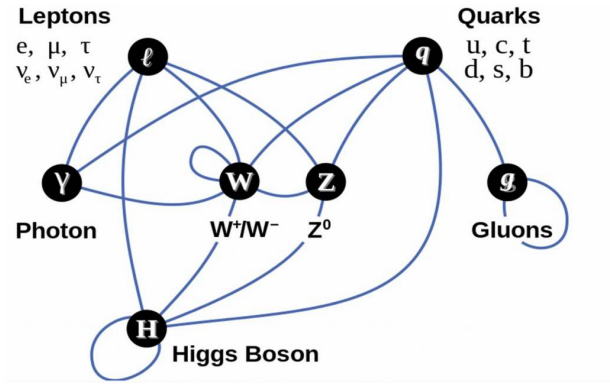

Figure 1.2: Standard Model interactions.

$SU(3)_C \otimes SU(2)_L \otimes U(1)_Y$. These three different gauge groups describe the three fundamental forces of nature. $SU(3)_C$ gauge group describes strong interaction where 'C' stands for the colour charge. According to Noether's theorem, a symmetry transformation results in a conserved quantity called Noether charge. All the fields which transform under the symmetry group carry this charge. The conserved charge of the $SU(3)_C$ transformation is called the colour charge. Quarks are the only matter fields which take part in strong interaction. Eight massless gluon fields corresponding to eight generators of $SU(3)_C$ group mediate strong interaction among quarks. Similarly, $SU(2)_L$ group governs weak forces where 'L' signifies that only left-handed fermions transform under this group operation. $U(1)_Y$ group is related to electromagnetic interaction and 'Y' denotes hypercharge. All quarks and leptons respond to the weak force whereas the electromagnetic force is felt only by electrically charged fields. Three massive gauge bosons ($W^{\pm}$ and Z) are the carriers of weak interaction. Finally a massless photon is responsible for carrying the electromagnetic force among the quarks and charged leptons.

The SM fields must be assigned a representation of the respective gauge groups under which they transform so that invariance under gauge transformation becomes manifest. The quark fields transform as fundamental (or, triplet) under $SU(3)_C$ group,

$$\mathbf{u} = \begin{pmatrix} \mathbf{u}^{\mathbf{red}} \\ \mathbf{u}^{\mathbf{green}} \\ \mathbf{u}^{\mathbf{blue}} \end{pmatrix}$$

where red, green and blue are the three colour quantum numbers associated with the group. SM is a chiral theory. Hence, its left-handed fields transform differently from the right-handed one under $SU(2)_L$ gauge transformation. The left-handed fermions are in the fundamental (or, doublet) representation of $SU(2)_L$ while the right-handed particles

are $SU(2)_L$ singlet. The representation of the quark and lepton fields under $SU(2)_L$ and $U(1)_Y$ groups are given as follows :

$$\textbf{Quark Doublets :} \quad \begin{pmatrix} \mathbf{u} \\ \mathbf{d}' \end{pmatrix}_{\mathbf{L}}, \begin{pmatrix} \mathbf{c} \\ \mathbf{s}' \end{pmatrix}_{\mathbf{L}}, \begin{pmatrix} \mathbf{t} \\ \mathbf{b}' \end{pmatrix}_{\mathbf{L}} \qquad (\mathbf{3}, \mathbf{2}, \frac{\mathbf{1}}{\mathbf{6}})$$

$$\textbf{Lepton Doublets :} \quad \begin{pmatrix} \boldsymbol{\nu}_{\mathbf{e}} \\ \mathbf{e}' \end{pmatrix}_{\mathbf{L}}, \begin{pmatrix} \boldsymbol{\nu}_{\boldsymbol{\mu}} \\ \boldsymbol{\mu}' \end{pmatrix}_{\mathbf{L}}, \begin{pmatrix} \boldsymbol{\nu}_{\boldsymbol{\tau}} \\ \boldsymbol{\tau}' \end{pmatrix}_{\mathbf{L}} \qquad (\mathbf{1}, \mathbf{2}, -\frac{\mathbf{1}}{\mathbf{2}})$$

$$\textbf{Quark Singlets :} \quad \begin{matrix} \mathbf{u_R}, & \mathbf{c_R}, & \mathbf{t_R}, \\ \mathbf{d}'_{\mathbf{R}}, & \mathbf{s}'_{\mathbf{R}}, & \mathbf{b}'_{\mathbf{R}} \end{matrix} \qquad \begin{matrix} (\mathbf{3}, \mathbf{1}, \frac{\mathbf{2}}{\mathbf{3}}) \\ (\mathbf{3}, \mathbf{1}, -\frac{\mathbf{1}}{\mathbf{3}}) \end{matrix}$$

$$\textbf{Lepton Singlets :} \quad \mathbf{e_R}, \ \boldsymbol{\mu}_{\mathbf{R}}, \ \boldsymbol{\tau}_{\mathbf{R}}, \qquad (\mathbf{1}, \mathbf{1}, -\mathbf{1})$$

Here, inside the brackets, the first number stands for the $SU(3)_C$ representation, the second number indicates the $SU(2)_L$ representation while the last number denotes the weak hypercharge quantum number. The electric charge Q of a field is defined in terms of hypercharge quantum number (Y) and third component of the $SU(2)_L$ charge (T_3) as $Q = T_3 + Y$. Note that the $U(1)_Y$ group does not represent the group for electromagnetic interaction directly and the corresponding quantum number is a derived quantity. We shall come to this point again in section 1.3.

The primed fields are actually in the mass-bases and are orthogonal combinations of the gauge (flavour) eigenstates *i.e.,*

$$d_i^{'} = \sum_j V_{ij} d_j$$

where d_i, $i = 1, 2, 3$, represent three down-type quarks d_L, s_L and b_L respectively. The matrix V is unitary (assuming universal weak coupling). It could have been formulated in the up-type quark sector as well. Such mixing arises for performing the field rotations for the up and down-type quarks in order to diagonalize the masses. Note that no such mixing occurs in the leptonic sector of the SM. This is because the neutrinos are massless in the SM and hence, no difference can be made between the flavour eigenstates and the mass eigenstates [1].

[1] However, after the discovery of neutrino mass, there happens to be similar mixing in the leptonic sector as well.

The massless fermion fields are described by the Dirac Lagrangian

$$\mathcal{L}_{\text{fermion}} = i\ \bar{\psi}\gamma^{\mu}\partial_{\mu}\psi, \tag{1.1}$$

where ψ denotes any general spin-$\frac{1}{2}$ fermion field which responds to all three gauge interactions and γ^{μ} are a set of four 4×4 matrices satisfying the following anticommutation relations

$$\{\gamma^{\mu},\gamma^{\nu}\} = \gamma^{\mu}\gamma^{\nu} + \gamma^{\nu}\gamma^{\mu} = 2g^{\mu\nu}\times 1_{4\times4}$$

However, this term is not invariant under the local gauge transformations of the field ψ :

$$\psi(x) \longrightarrow \psi^{'}(x) = e^{(ig_3\alpha_1^a(x)\lambda^a/2)}\ e^{(ig_2\alpha_2^a(x)\sigma^a/2)}\ e^{(ig_1\alpha_3(x)Y/2)}\psi(x)$$

where λ's are eight Gell-mann matrices (generators of $SU(3)_C$ group), σ's are three Pauli matrices (generators of $SU(2)_L$ group). g_i's ($i=1,2,3$) are the three coupling constants of the three gauge groups while α_i's ($i=1,2,3$) are the transformation parameters which are space-time dependent.

Note that we could not write a gauge invariant Lagrangian involving derivatives of ψ due to the presence of space-time dependent parameters. This leads to the idea of introducing gauge fields for each of the invariant gauge group generators for all the symmetry groups. Now, gauge invariance can be made manifest by promoting ordinary partial derivative to covariant derivative:

$$\partial_{\mu} \longrightarrow D_{\mu} = \partial_{\mu} - ig_3\frac{\lambda^a}{2}G_{\mu}^a - ig_2\frac{\sigma^a}{2}W_{\mu}^a - ig_1\frac{Y}{2}B_{\mu}$$

where G_{μ}^a's ($a=1,2,..8$) are the eight gluon fields of the $SU(3)_C$ gauge group. Similarly, W_{μ}^a ($a=1,2,3$) are the three weak gauge bosons corresponding to the $SU(2)_L$ group and B_{μ} is the one for the $U(1)_Y$ group. The fermion-gauge boson interaction vertex can be derived from $\mathcal{L}_{\text{fermion}}$.

Gauge fields transform like adjoint representation of the corresponding gauge groups. The kinetic terms of the gauge fields are given as follows,

$$\mathcal{L}_{\text{gauge}} = -\frac{1}{4}G_{\mu\nu}^a G^{a\mu\nu} - \frac{1}{4}W_{\mu\nu}^a W^{a\mu\nu} - \frac{1}{4}B_{\mu\nu}B^{\mu\nu} \tag{1.2}$$

where $G_{\mu\nu}^a$, $W_{\mu\nu}^a$ and $B_{\mu\nu}$ are the field strength tensors for $SU(3)_C$, $SU(2)_L$ and $U(1)_Y$ gauge fields respectively. They have the following forms

$$G_{\mu\nu}^a = \partial_{\mu}G_{\nu}^a - \partial_{\nu}G_{\mu}^a + g_3 f^{abc}G_{\mu}^b G_{\nu}^c \tag{1.3}$$

$$W_{\mu\nu}^a = \partial_{\mu}W_{\nu}^a - \partial_{\nu}W_{\mu}^a + g_2\epsilon^{abc}W_{\mu}^b W_{\nu}^c \tag{1.4}$$

$$B_{\mu\nu} = \partial_\mu B_\nu - \partial_\nu B_\mu \tag{1.5}$$

f^{abc} and ϵ^{abc} being the structure constants of $SU(3)_C$ and $SU(2)_L$ groups respectively. $B_{\mu\nu}$ being linear in the B_μ, there appears no term more than quadratic order in field. On the other hand, $W^a_{\mu\nu}$ and $G^a_{\mu\nu}$ are both quadratic in fields. This is an artifact of non-Abelian gauge theory. Hence, for W^a_μ and G^a_μ gauge fields, one finds triple and quartic gauge boson interaction vertices. This is an important difference between Abelian and non-Abelian theory.

The weak charged-current interaction for the quarks can be written as,

$$\mathcal{L}_{\text{cc}} = \frac{g_2}{2}(\bar{u}\ \ \bar{c}\ \ \bar{t})_i \gamma_\mu \left(V_u V_d^\dagger\right)_{ij} \begin{pmatrix} d \\ s \\ b \end{pmatrix}_j$$

The 3×3 unitary matrix $V = V_u V_d^\dagger$ is known as the Cabibbo-Kobayashi-Maskawa [2] (CKM) matrix [2]. It contains three real parameters and one complex phase factor. The presence of complex phase is important since it provides the only source of CP violation within the SM. There are many ways to parameterize the CKM matrix. Currently, the best-fit values of the various entries of the CKM matrix obtained from experiments are [3],

$$\begin{pmatrix} |V_{ud}| = 0.974 & |V_{us}| = 0.225 & |V_{ub}| = 0.0035 \\ |V_{cd}| = 0.225 & |V_{cs}| = 0.973 & |V_{cb}| = 0.041 \\ |V_{td}| = 0.00867 & |V_{ts}| = 0.0404 & |V_{tb}| = 0.999 \end{pmatrix}$$

The interesting observation is that the diagonal elements are close to unity. Since the CKM matrix describes the probability of a transition from one quark flavour 'i' to another quark 'j', the most probable transition takes place only within a given generation.

Gauge symmetry prohibits mass terms for the gauge fields. However, various experiments have confirmed that mediators of the weak force ($W^\pm$, Z) are massive. Moreover, mass terms for fermions have not been included in eqn 1.1. The mass term in a Lagrangian consists of both the left and right chiral fields ($m(\psi_L\psi_R + \text{h.c.})$). Hence, we cannot simply write a gauge invariant mass term for fermions as well.

Thus, generating masses for the weak bosons as well as the fermion fields were a long standing problem. One of the major triumph of modern day physics is the concept of

[2]The corresponding mixing matrix in the leptonic sector is known as the Pontecorvo-Maki-Nakagawa-Sakata (PMNS) matrix.

spontaneous symmetry breaking (SSB) which solves the problem of mass generation. In SSB, there could be a situation where the Lagrangian is still symmetric under the gauge group, but the choice of non-vanishing value at the minimum energy state (called vacuum) breaks the symmetry. This is achieved by introducing a weakly coupled spin-0 complex scalar field, called the Higgs field, which is a doublet under $SU(2)_L$ transformation. A single Higgs field is sufficient to generate masses for both the electroweak gauge bosons and the fermions in the SM. The formalism is known as the Brout-Englert-Higgs (BEH) mechanism which we discuss in the next section.

1.3 Brout-Englert-Higgs mechanism

It has been already mentioned that in quantum field theory one could be in a situation where the Lagrangian of a theory is invariant under a symmetry but the vacuum is not. The mechanism is known as the spontaneous symmetry breaking (SSB). The idea of SSB [4] was first proposed by Nambu in the context of superconductivity. Nambu and Jona-Lasinio then went on to suggest that masses of elementary particles might arise in a similar way [5]. Goldstone, on the other hand, provided a general theorem (known as Goldstone theorem) on existence of a massless particle in a spontaneously broken theory [6]. In the context of an explicitly relativistic theory, a general proof was provided by Goldstone, Salam and Weinberg [7].

It was the work of Higgs which exhibited in a very simple manner to generate mass in a relativistically invariant theory [8]. Higgs' treatment was purely classical. At the same time, Englert and Brout suggested the same idea in a quantum mechanical way [9]. They also pointed out that the same mechanism could work in non-Abelian models as well. Guralnik, Hagen and Kibble, on the other hand, showed how to evade Goldstone theorem using a different formalism [10].

The idea was brought into particle physics to provide masses to the gauge bosons for the first time by Weinberg and Salam. Finally, a very important step was the proof of renormalizability of such a spontaneously broken gauge theory was given by 't Hooft [11]. Thus, based on Glashow's idea [12] of extending the gauge group from $SU(2)_L$ to $SU(2)_L \times U(1)_Y$ (thus providing unified description of the electromagnetic and weak interactions), the work of Weinberg and Salam completed the Standard Model of particle physics [13] (also known as Glashow-Weinberg-Salam model) where masses of the gauge bosons and fermions are generated via the BEH mechanism.

SSB is achieved with a spin-0 complex scalar field which carries both $SU(2)_L$ and $U(1)_Y$

charge. The field Φ is in doublet representation under $SU(2)_L$ group.

$$\Phi = \begin{pmatrix} \phi^+ \\ \phi_0 \end{pmatrix} \qquad (\mathbf{1}, \mathbf{2}, \frac{\mathbf{1}}{\mathbf{2}})$$

Lagrangian of this field is given by,

$$\mathcal{L}_{\text{Higgs}} = \frac{1}{2}(D_\mu \Phi)^\dagger (D^\mu \Phi) \; - \; V(\Phi) \tag{1.6}$$

where the scalar potential has the form $V(\Phi) = \frac{1}{2}\mu^2 \Phi^\dagger \Phi \; - \; \frac{1}{4}\lambda(\Phi^\dagger \Phi)^2$. μ^2 can be positive or negative, however, the potential is dominated by the quartic interaction Φ^4 for large Φ. Consequently, it is bounded from below (for positive λ) irrespective of the magnitude or sign of the mass term. The minimum of the potential lies at $\frac{\partial V}{\partial \Phi} = 0$. There can be two situations :

(a) For $\mu^2 > 0$, the minimum of the scalar potential remains at zero.

$$\langle 0|\phi_0|0\rangle = 0 \tag{1.7}$$

This situation cannot give masses to the gauge bosons.

(b) However, if $\mu^2 < 0$, then

$$\langle 0|\phi_0|0\rangle = \pm\sqrt{\frac{-\mu^2}{2\lambda}} \equiv \pm\frac{v}{\sqrt{2}} \tag{1.8}$$

$v = \sqrt{\frac{-\mu^2}{\lambda}}$ is called the vacuum expectation value (vev). Thus, the vacuum state becomes degenerate and the choice of a particular solution breaks both $SU(2)_L$ and $U(1)_Y$ gauge symmetries. The corresponding gauge bosons now become massive. However, if the vacuum is still left invariant by some subgroup of the original gauge transformations, then the gauge bosons associated with this subgroup remain massless. In this case, the Lagrangian remains invariant under the unbroken subgroup $U(1)_{\text{EM}}$ with a single generator $Q = T_3 + Y$. This is called the electromagnetic charge. The corresponding gauge boson (photon) remains massless. Thus, it is said that, $SU(2)_L \otimes U(1)_Y$ symmetry is spontaneously broken down to $U(1)_{\text{EM}}$. In the unitary gauge,

$$\Phi = \frac{1}{\sqrt{2}} \begin{pmatrix} 0 \\ v + H(x) \end{pmatrix}$$

where $H(x)$ is the physical Higgs field which is basically a perturbation about the vacuum.

1.3.1 Masses of the gauge bosons

The kinetic term of the Higgs field is the following,

$$D_\mu \Phi = \left(\partial_\mu - i g_2 \frac{\sigma^a}{2} W_\mu^a - i g_1 \frac{Y}{2} B_\mu \right) \Phi$$

Expanding the equation 1.6 after putting the expression of Φ,

$$\left| \begin{pmatrix} g_2 W_\mu^3 + g_1 B_\mu & g_2(W_\mu^1 - i W_\mu^2) \\ g_2(W_\mu^1 + i W_\mu^2) & -g_2 W_\mu^3 + g_1 B_\mu \end{pmatrix} \begin{pmatrix} 0 \\ \frac{v}{\sqrt{2}} \end{pmatrix} \right|^2$$

This term provides all the gauge boson-Higgs interaction vertices. The physical gauge fields are defined as the following linear combinations

$$\begin{aligned} W_\mu^\pm &= \frac{1}{\sqrt{2}}(W_\mu^1 \mp i W_\mu^2) \\ Z_\mu &= \frac{g_2 W_\mu^3 - g_1 B_\mu}{\sqrt{g_1^2 + g_2^2}} \\ A_\mu &= \frac{g_2 W_\mu^3 + g_1 B_\mu}{\sqrt{g_1^2 + g_2^2}} \end{aligned}$$

Hence, we realize that W_μ^3 and B_μ fields are not the physical states, but their orthogonal combinations provide the physical fields. We define weak mixing angle θ_W which quantifies the mixing between them. Thus, the physical states can be written as,

$$\begin{pmatrix} Z_\mu \\ A_\mu \end{pmatrix} = \begin{pmatrix} \cos\theta_W & -\sin\theta_W \\ \sin\theta_W & \cos\theta_W \end{pmatrix} \begin{pmatrix} W_\mu^3 \\ B_\mu \end{pmatrix}$$

It is now easy to verify that the $SU(2)_L$ and $U(1)_Y$ coupling constants are also related to each other with the same mixing angle as

$$\cos\theta_W = \frac{g_2}{\sqrt{g_1^2 + g_2^2}}, \qquad \sin\theta_W = \frac{g_1}{\sqrt{g_1^2 + g_2^2}}.$$

On properly identifying the mass terms as $\left(M_W^2 W_\mu^+ W^{-\mu} + \frac{1}{2} M_Z^2 Z_\mu Z^\mu + \frac{1}{2} M_A^2 A_\mu A^\mu \right)$ one obtains,

$$\begin{aligned} M_W &= \frac{1}{2} g_2 v \\ M_Z &= \frac{1}{2} v \sqrt{g_1^2 + g_2^2} \end{aligned}$$

and the photon is massless. The potential term provides the mass term for the Higgs itself : $M_H = 2v^2\lambda$. It also predicts cubic and quartic self couplings of the Higgs boson.

1.3.2 Masses of the fermions

We introduce a new interaction known as the Yukawa interaction between the fermions and Higgs boson.

$$\mathcal{L}_{\text{Yukawa}} = -\lambda_e \bar{L}\Phi E_R - \lambda_d \bar{Q}_L \Phi D_R - \lambda_u \bar{Q}_L \tilde{\Phi} U_R + h.c. \tag{1.9}$$

where $\tilde{\Phi} = i\sigma_2\Phi^*$. λ_e, λ_d, λ_u are the Yukawa couplings of the down-type leptons, down-type quarks and up-type quarks respectively. Once Φ gets vev, one obtains mass terms for the fermions with $m_f = \lambda_f v/2$. The Yukawa couplings are free parameters in the SM as they are fixed by the masses of the fermions.

1.4 Experimental verification of the SM

Now that we have a renormalizable gauge theory, it is important to look for its experimental verifications. Investigation of electroweak theory began long back in the muon decay process where measurement of the Fermi constant (G_F) had been made. As higher energies become achievable for the collider experiments, direct evidence of weak gauge bosons becomes apparent. Charged current interaction was first observed at CERN SPS $p\bar{p}$ collider with center-of-mass energy of 540 GeV. Mass and width of $W^{\pm}$ bosons were measured. The SM predictions were very close to the experimental values. Next, at the large electron-positron collider (LEP) neutral Z boson was discovered. Various observables were measured precisely which were in close agreement with the SM predictions. Beyond the tree level, LEP precision measurements even provided a good verification of SM as a renormalizable field theory. Later on, top quark has been discovered at Tevatron. Recently, the last missing piece of the SM, the Higgs boson, has also been discovered at the Large Hadron collider (LHC). Thus, the SM is a tremendously successful as a theory of elementary particles and it has been able to explain almost all the phenomena observed at various experiments so far. Fig 1.3 shows production cross sections of various SM processes where the numbers closely agree, within the uncertainties, with values expected from the SM.

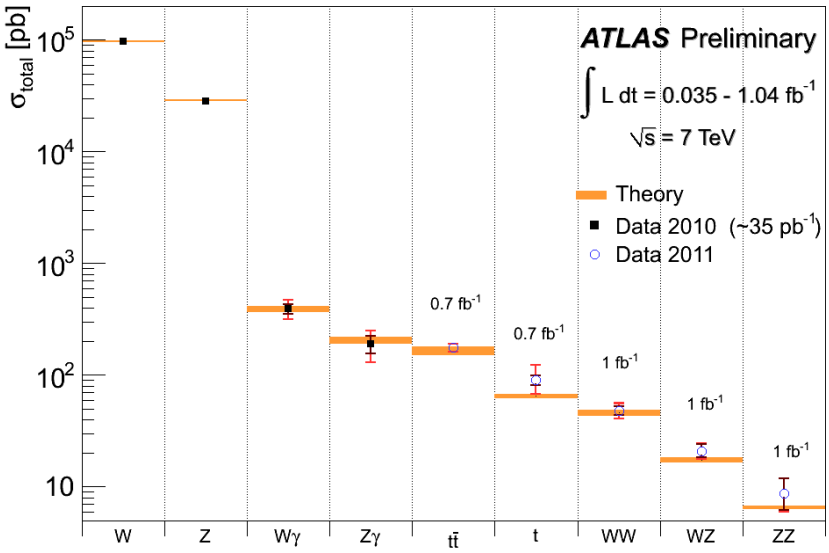

Figure 1.3: Summary of total production cross sections of several SM processes from the ATLAS collaboration compared to the corresponding theoretical expectations [14].

1.5 Need to go beyond the SM: Motivations

The discovery of the Higgs boson at the LHC completes the particle spectrum of the SM. It is very successful in explaining all, but one, experimental observations made till date. The existence of neutrino mass, as evident from neutrino oscillation experiments is a major issue confronting the SM. There is no right-handed neutrino in SM and hence, no conventional mass term can be written for the neutrinos. Also, the neutrino mixing pattern uncovered by various experiments is quite different from that of the mixing in the quark sector. All these facts demand proper explanation which lead us towards new physics beyond SM.

Astrophysical (and cosmological) observations provide indirect confirmation of existence of another kind of matter which cannot be explained in terms of the particle spectrum available in the SM. Nature and composition of such matter, called dark matter, are not yet known. The important fact is that this new type of (non-baryonic) matter constitute 23% of the universe. In 1933, F. Zwicky first observed from galaxy rotation curves that there should be more matter than just the visible matter in the universe [15]. Later on, gravitational lensing studies of the Bullet Cluster are claimed to provide the best evidence for the existence of dark matter [16,17]. From the SM, only the neutrinos can be the candidate for non-baryonic dark matter. However, study shows that neutrinos with ex-

tremely small mass could jeopardize large scale structure formation. Hence dark matter needs to be some new kind of particles and is believed to be one of the major hint of new physics. In addition, the universe contains more matter than anti-matter, a fact known as baryon asymmetry. SM has no appropriate mechanism to explain such observation.

Apart from these observational evidences, there are other compelling theoretical questions that confront SM as the ultimate theory. Stability of Higgs mass against large radiative correction is regarded as a very serious concern for a long time. The unitarity argument requires the Higgs boson mass below 1 TeV. But the correction to Higgs mass squared due to top Yukawa coupling (λ_t) is found to be quadratic in the cut-off scale Λ,

$$\delta m_H^2 = -\frac{\lambda_t^2}{8\pi^2}\,\Lambda^2 + ..$$

If SM remains valid upto a very high scale, then the mass corrections really becomes larger than the Higgs mass itself. The only way to retrieve physical Higgs mass $\sim \mathcal{O}(1\ )$TeV, is to have some 'unnatural' cancellation between the bare mass and its large correction. This is known as the Naturalness problem (often termed as 'fine tuning' problem because of the extreme accuracy required for such cancellations to take place).

Conversely, one can assume the cut-off Λ to a lower value. In that case, the theory ceases to exist above that scale. The only other scale known is the Grand Unified scale ($\sim 10^{16}$ GeV) or the Planck scale ($\sim 10^{19}$ GeV). Hence, there is a huge terrain in the energy scale which lies empty between the weak scale ($\mathcal{O}$(TeV)) and the GUT (or Planck) scale. This large hierarchy in energy scales is termed as "hierarchy problem". This is one of the most aesthetic reasons to believe in the existence of new physics above the TeV scale.

Further, the masses of all the fermions, although derived from the same SSB mechanism, are hugely different from each other. The ratio $\frac{m_{\text{electron}}}{m_{\text{top}}} \sim 10^{-6}$ points towards large mass hierarchy in fermion sector in the SM. There is no natural understanding of such differences (even, present within the quark and lepton sectors separately). Moreover, the SM provides no explanation of the existence of three families each for the quark as well as the lepton sector. Therefore, the SM, in many ways, is unlikely to be the ultimate theory. All these motivate one to go beyond the SM.

The thesis tries to capture one such scenario beyond the SM (BSM) which incorporates extra spatial dimensions. This thesis consists of the following chapters. In chapter 2, we discuss general theoretical aspects of the known extra dimensional scenarios. We introduce minimal universal extra dimension (mUED) model in a brief but self-contained manner. Later, we move on to non-minimal version of universal extra dimensional (nmUED)

scenario and discuss its theoretical setup. Chapter 3 contains the study of boundary localized kinetic terms (BLKTs) and the Yukawa terms (BLYTs) for the strongly interacting sector comprising of KK gluon and KK quarks and discuss their phenomenology at the LHC. In chapter 4, we discuss the basic phenomenology of the KK top quarks at the LHC by outlining their production and decay patterns for certain benchmark points. In chapter 5 we discuss broad resonance case at the LHC which is a characteristic of nmUED scenario. Finally, in chapter 6 we make a statement regarding the overall achievement of this thesis and conclude.

Chapter 2

Non-Minimal Universal Extra Dimension

2.1 Introduction

The idea of having an extra compactified spatial dimension was first proposed by Kaluza and Klein in order to unify Maxwell's theory of electro-magnetism and Einstein's theory of gravity [18–20]. Much later, in string theory we also find extra space dimensions to play crucial role in order to explain the quantum nature of gravity. The size of the extra dimensions is known to play crucial roles in scenarios with extra dimensions. Of course, if such extra dimensions exist at all, they must be smaller than the smallest distance probed by the experiments till date [1]. These suggest that the length of the extra dimensions can only be less than few hundreds of microns (10^{-6} m).

During early 90s, Antoniadis considered extra dimensional scenarios in relation to supersymmetry breaking [22]. Many theoretical ideas emerged in string theory in the context of extra dimension during this period. Hierarchy problem continues to be a serious concern in theoretical physics. This is related to the radiative corrections received by the squared Higgs mass in the SM (see section-1.5) which is quadratic in the cut-off scale. If the Planck scale ($M_{pl} \sim 10^{19}$ GeV) is the only energy scale next to the electroweak scale ($\sim 10^2$ GeV), then the corrections to the Higgs mass becomes enormously large compared to the bare Higgs mass itself. This is a consequence of huge separation of these two energy scales and is referred to as the hierarchy problem. The electromagnetic, weak and strong forces are all predominant at the electroweak scale. On the other hand, the existence of gravity can only be felt at/near the Planck scale. Note that the gravitational force has

[1] For reviews on extra dimensional theory, see refs. [21]

been measured only at large distance. One can pose the question the other way round: why the gravitational interaction is so weak compared to other forces of the SM at the electroweak scale. Extra dimensions as an answer to this question was first proposed by Arkani-Hamed, Dimopoulous and Dvali (ADD) [23,24]. They showed that if there exists at least two millimeter-sized (large) extra dimensions in which only gravity can propagate, then the weakness of gravitational force can be explained. The large volume of the extra dimensions dilutes the strength of the gravity as we see in ordinary $4D$. In this model, the extra dimension is assumed to be flat. This model requires the SM particles to remain confined to usual four dimensions. Some further important issues of this scenario, such as proton stability, gauge coupling unification and supersymmetry breaking have been discussed in ref. [25]. The carrier of gravitational force is a spin-2 field, called graviton. In four dimensions, the effect of a compactified extra dimension appears as infinite number of Fourier modes (called Kaluza-Klein (KK) tower) of the particles which propagate into the extra dimensional space. The KK gravitons can be directly produced at the collider experiments, like LHC. KK Gravitons interacts with SM fields gravitationally. Since gravity is very weak, they escape detection at the collider thus leading to missing transverse energy, E_T^{miss}. The virtual exchange of KK graviton can also be possible in certain processes. However, results from LHC put very stringent bound on this model. ATLAS analysis in $jets + E_T^{miss}$ channel has ruled out $(4 + n)$-dimensional Planck scale upto 4.3 TeV in ADD scenario with $n = 2$ [26].

Another variant of extra dimensional theory is proposed by Randall and Sundrum (RS) [27, 28]. The compact extra dimension, in this case, has two boundaries which are 4 dimensional slices of the $5D$ bulk. They are like surfaces enclosing the higher dimensional space-time and are called branes. In RS model, gravity resides in one of the branes, called the Planck brane, whereas our world (the SM) is stuck in another brane (the weak brane). To explain the weakness of gravity at the electroweak scale, Randall and Sundrum suggest the bulk to be extremely curved (warped). The curvature is introduced as a warp factor (parameterized by κ/M_{pl}) in the metric. As a result, the graviton wave function becomes extremely large at the Planck brane and it drops exponentially towards the weak brane. Thus the gravity is localized only at the Planck brane. In this case, the extra dimension need not be large to dilute gravity as in the case of the ADD model. Interesting signature of RS scenario includes a virtual graviton decaying into two photons which provides a clean signal at the LHC. A limit of around 2.6 TeV on graviton mass has been placed from the study of the dilepton final state (Drell-Yan production via graviton) by the ATLAS experiment for $\kappa/M_{pl} = 0.1$ [29].

These are some well-motivated extra dimensional scenarios for looking beyond the SM. In the above models, only gravity[2] can propagate into the extra dimensional bulk. There is yet another alternative framework, known as Universal Extra Dimensions (UED) [33], where the SM is embedded in any number of extra dimensions and in which all the SM fields have universal access to the extra dimensions. The minimal version of such a scenario is UED with only one extra spatial dimension compactified on S^1/Z_2 orbifold and with a minimal set of input parameters. This is called the minimal universal extra dimension (mUED). In this thesis, we consider an extended version of such a scenario, called the non-minimal Universal Extra Dimension (nmUED). As the name suggests, the model contains more numbers of free parameters. Before going into the theoretical details of the non-minimal model, we first give an overview of minimal version of universal extra dimension.

2.2 Minimal Universal Extra Dimension: A brief review

Universal extra dimension allows all the SM particles to propagate into the flat five [3] dimensional bulk which is compactified on S^1/Z_2 with an extra Z_2 symmetry called Kaluza-Klein (KK) parity. We will explain the meaning of the jargons in proper context. Although, UED does not have the virtue of solving the hierarchy problem, still the motivations for studying this particular scenario are many.

Unification of gauge couplings can take place in the presence of extra dimension accessible to the SM fields [40, 41]. Various models of neutrino mass generation can be fit into such scenarios [42]. Such a scenario could provide mechanism for supersymmetry breaking [22]. Extra dimensional models provide explanation for mass hierarchy in the fermion sector [40, 43, 44]. Moreover, scenarios with dynamical electroweak symmetry breaking have been studied for extra dimensional theories [45]. If the SM fields are allowed to propagate in TeV-scale extra dimensions, then a tightly bound composite state of top quarks can be found which has the same quantum numbers as the SM Higgs doublet [46]. This composite Higgs can then trigger electroweak symmetry breaking and no fundamental Yukawa interaction is needed. A very important aspect of the UED scenario is that it can provide a viable dark matter candidate [47–53]. The relic density calculated in such a framework agrees with its estimated value from various cosmological experi-

[2] Although this is not necessary in all the warped models [30–32].

[3] UED with two extra spatial dimensions ($6D$ UED) is also another interesting possibility and its phenomenology has been studied in refs. [34–39]

ments [54,55]. The UED excitations (higher KK modes) contribute to various electroweak observables which have been measured accurately at LEP and other experiments, only at loop level [56–59]. Its contributions to the electroweak precision variables are thus well suppressed and hence, the bounds on this model are only moderate. The scenario has a rich phenomenology at the collider. The UED excitations can be directly produced at the colliders. Recent collider experiments have already become sensitive to their production and hence its predictions can be tested at the ongoing collider experiments.

In UED, the gauge structure and the particle content of the SM have been kept intact. The extra dimension is compactified on a circle (S^1) of radius R. The $5D$ gauge couplings have negative mass dimensions. Such a theory is fundamentally non-remormalizable from a naive dimensional argument. Therefore, the theory is expected to remain valid only up to a certain scale Λ. In the minimal version of UED (mUED) scenario, there are only three input parameters: the compactification radius (R), the cut-off scale (Λ) and the Higgs mass (m_H) .

We label the coordinates as x^M = ($x^\mu, x^5 = y$) where $M = 0, 1, 2, 3, 5$ and μ runs over $0, 1, 2, 3$. $x^5 = y$ is the coordinate of the extra dimension. The flat metric in $5D$ is given by $g^{MN} = (+ - - - -)$. As the extra dimensional coordinate is compactified on a circle, any point y is identified with $(y + 2\pi R)$. Hence, the fields are periodic in y-direction. To illustrate, we consider a scalar field $\Phi(x, y)$. It satisfies periodic boundary condition: $\Phi(x, y) = \Phi(x, y + 2\pi R)$. This results in the expansion of $5D$ fields into an infinite series of Fourier modes:

$$\Phi(x, y) = \frac{1}{\sqrt{2\pi R}} \sum_n \phi^{(n)}(x) \ e^{iny/R}. \tag{2.1}$$

$\phi^{(n)}$s are called n^{th} Kaluza-Klein (KK) modes and the zero mode ($\phi^{(0)}$) is identified with the corresponding SM particle. Such tower of infinite KK states appear for each SM particles in $4D$. They carry exactly same quantum numbers as the corresponding SM fields. The mode (level) number n is also known as KK number. In mUED KK number is conserved in any given interaction at tree-level which is a consequence of momentum conservation along the extra dimension.

The $5D$ action of a massive scalar field is given by,

$$S_{5D} = \frac{1}{2} \int d^4x \int dy \Big[(\partial_M \Phi)(\partial^M \Phi) - m_0^2 \Phi^2 \Big] \tag{2.2}$$

where m_0 is the mass originating from the conventional electroweak symmetry breaking

mechanism. By plugging in the expansion of Φ in 2.1 into eqn. 2.2 and integrating over the extra dimensional coordinate y, we obtain the $4D$ effective action,

$$S_{4D} = \frac{1}{2}\int d^4x \sum_n \left[\left(\partial_\mu \phi^{(n)}(x)\right)\left(\partial^\mu \phi^{(n)}(x)\right) - \left(m_0^2 + \frac{n^2}{R^2}\right)\phi^{(n)}(x)\phi^{(n)}(x)\right] \tag{2.3}$$

Thus, the n^{th} KK mode $\phi^{(n)}$ has a tree-level mass $m_n^2 = m_0^2 + \frac{n^2}{R^2}$. For large R^{-1}, $m_0^2 \ll \frac{n^2}{R^2}$ and all the KK masses at a given level n are almost degenerate. However, masses of the KK states receive radiative corrections which can cause significant shift in the spectrum [60]. The total one loop correction includes both bulk and boundary contributions. But in mUED, boundary corrections are generally considered to be small or zero. One loop mass renormalization by the bulk interaction removes the mass degeneracy. The radiative corrections for KK gluon is the largest simply because of its large coupling strength and multiplicative colour factor. Corrections to KK quark masses are greater than KK leptons for similar reasons. Level-1 KK photon remains the lightest KK particle (LKP).

Generalized $\gamma^5 (= i\gamma^0\gamma^1\gamma^2\gamma^3)$ matrix in any odd dimensions does not anticommute with rest of the γ matrices as required by Clifford algebra. Hence, chiral projection operators cannot be defined in odd space-time dimensions. But the KK modes are 4 dimensional objects. Therefore, we can assign chirality to the KK states. KK modes of SM fermions are vector-like in nature. Vector-like fermions are those for which both chiral components have same transformation properties under the electroweak gauge group $SU(2) \times U(1)$. But this is not the case in SM where an $SU(2)_L$ doublet field is purely left handed and a $SU(2)_L$ singlet field (carries only hypercharge quantum number) is purely right handed. One has to retrieve the SM chiral fermions in $4D$, *i.e.*, extra components of

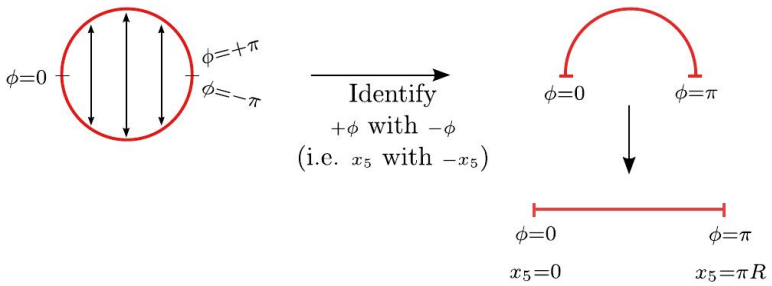

Figure 2.1: Orbifolding the circle to an interval (taken from the first reference in [21].)

the zero mode fields must be removed. This is achieved by a technique called "orbifolding" which is described as follows. Over the compactified extra dimension, we impose a

Z_2 symmetry in which two points on each half of the circle (as shown in the fig.2.1) are identified. This is essentially a discrete parity transformation $(y - \pi R) \to -(y - \pi R)$. We realize that the action 2.2 remains invariant if a generic scalar field Φ transforms in the following manner

$$\Phi(x, y - \pi R) \to \pm\Phi(x, -(y - \pi R)) \tag{2.4}$$

This is called S^1/Z_2 orbifolding. Information of one half of the circle is sufficient to know the details of the other half thus making one half redundant. This essentially makes the circle an interval of length πR. $y = 0$ and $y = \pi R$ are the two orbifold fixed points – the boundaries where the brane and the bulk meet. The fields transforming like $\Phi(x, -y^{'}) = +\Phi(x, y^{'})$ are called 'even' and $\Phi(x, -y^{'}) = -\Phi(x, y^{'})$ are termed 'odd' under Z_2 symmetry where $y^{'} = (y - \pi R)$. We denote even and odd fields by Φ_+ and Φ_- respectively. The fields obey different boundary conditions at the two orbifold fixed points. Φ_+ obeys Neumann boundary condition $\partial_y \Phi_+(x)\Big|_{y=0,\pi R} = 0$. Φ_- obeys Dirichlet boundary condition $\Phi_-(x)\Big|_{y=0,\pi R} = 0$. The KK expansions are also quite different for the two types of fields as shown below.

$$\Phi_+(x, y) = \frac{1}{\sqrt{\pi R}}\phi_-^{(0)}(x) + \frac{2}{\sqrt{\pi R}}\sum_n \phi_+^{(n)}(x)\cos\frac{ny}{R} \tag{2.5}$$

$$\Phi_-(x, y) = \frac{2}{\sqrt{\pi R}}\sum_n \phi_-^{(n)}(x)\sin\frac{ny}{R} \tag{2.6}$$

The KK decomposition of a vector field can be done in a similar manner. A vector field V^M in $5D$ has 5 components. We realize that V^μ are even while V^y is odd under Z_2 transformation mentioned above. Similar boundary conditions are also imposed for the even and odd type of vector fields: $\partial_y V^\mu(x)\Big|_{y=0,\pi R} = 0$ and $V^y(x)\Big|_{y=0,\pi R} = 0$. As a result, the KK expansion of a vector field can be written in a way so that there remains no zero mode of the 5th component:

$$V^\mu(x, y) = \frac{1}{\sqrt{\pi R}}V^{\mu(0)}(x) + \frac{2}{\sqrt{\pi R}}\sum_n V^{\mu(n)}(x)\cos\frac{ny}{R} \tag{2.7}$$

$$V^y(x, y) = \frac{2}{\sqrt{\pi R}}\sum_n V^{y(n)}(x)\sin\frac{ny}{R} \tag{2.8}$$

As for fermions, $SU(2)$ singlet field ($\psi(x, y)$) requires to satisfy the following boundary conditions: $\psi_L(x)\Big|_{y=0,\pi R} = 0$ and $\partial_5\psi_R(x)\Big|_{y=0,\pi R} = 0$. These boundary conditions set the

following mode expansion:

$$\psi_R(x,y) = \frac{1}{\sqrt{\pi R}}\psi_R^{(0)}(x) + \frac{2}{\sqrt{\pi R}}\sum_n \psi_R^{(n)}(x)\cos\frac{ny}{R} \tag{2.9}$$

$$\psi_L(x,y) = \frac{2}{\sqrt{\pi R}}\sum_n \psi_L^{(n)}(x)\sin\frac{ny}{R} \tag{2.10}$$

The boundary conditions are just opposite for a $SU(2)$ doublet field $\Psi(x,y)$. Since, in this case, we have to get rid of right handed zero mode, we set: $\Psi_R(x)\Big|_{y=0,\pi R} = 0$ and $\partial_5\Psi_L(x)\Big|_{y=0,\pi R} = 0$. The KK expansions are,

$$\Psi_L(x,y) = \frac{1}{\sqrt{\pi R}}\Psi_L^{(0)}(x) + \frac{2}{\sqrt{\pi R}}\sum_n \Psi_L^{(n)}(x)\cos\frac{ny}{R} \tag{2.11}$$

$$\Psi_R(x,y) = \frac{2}{\sqrt{\pi R}}\sum_n \Psi_R^{(n)}(x)\sin\frac{ny}{R} \tag{2.12}$$

The important point is that after demanding the fields to be even/odd under the discrete parity transformation, suitable boundary conditions remove the unwanted fields. However, the higher fermionic KK modes are necessarily vector-like. The Z_2 parity is known as KK parity which is defined as $(-1)^n$ where n stands for the KK level. In any mUED interaction, KK parity is assumed to be always conserved. Hence, any odd level KK partners must be produced in pair at the collider experiments. Conservation of KK parity also leaves the lightest KK particle (LKP) stable and provides a good dark matter candidate [47, 48, 52]. The LKP is the level-1 KK photon in the mUED scenario.

We now introduce the notations for various fields following reference [61]. For the $5D$ gauge fields we continue to use the similar notations as we did for the corresponding SM fields in chapter-1: B_M, W_M^a and G_M^a for the $5D$ gauge fields of $U(1)$, $SU(2)$ and $SU(3)_C$ groups respectively. The fermionic sector of the scenario is presented in table 2.1.

Now we are in a position to describe the action of the theory of minimal universal extra dimension (mUED). The various components of the action are as follows,

$$S_{\text{gauge}} = \int d^4x \int_0^{\pi R} dy \Big(-\frac{1}{4}B_{MN}B^{MN} - \frac{1}{4}W^a_{MN}W^{aMN} - \frac{1}{4}G^a_{MN}G^{aMN}\Big), \tag{2.13}$$

$$S_{\text{gf}} = \int d^4x \int_0^{\pi R} dy \Big(-\frac{1}{2\xi}(\partial^\mu B_\mu - \xi\partial_5 B_5)^2 - \frac{1}{2\xi}(\partial^\mu W^a_\mu - \xi\partial_5 W^a_5)^2$$

[4]Note that we have dropped the subscript 'L' for $SU(2)$ which we kept in chapter-1. 'L' stands for left handed, whereas a KK level SU(2) doublet field has both left and right handed components.

$SU(2)$ representations [4]	SM mode	KK modes
Quark doublet	$Q_L(x) = \begin{pmatrix} U_L(x) \\ D_L(x) \end{pmatrix}$	$Q_L^{(n)}(x) = \begin{pmatrix} U_L^{(n)}(x) \\ D_L^{(n)}(x) \end{pmatrix}, Q_R^{(n)}(x) = \begin{pmatrix} U_R^{(n)}(x) \\ D_R^{(n)}(x) \end{pmatrix}$
Lepton doublet	$L_L(x) = \begin{pmatrix} \nu_L(x) \\ E_L(x) \end{pmatrix}$	$L_L^{(n)}(x) = \begin{pmatrix} \nu_L^{(n)}(x) \\ E_L^{(n)}(x) \end{pmatrix}, L_R^{(n)}(x) = \begin{pmatrix} \nu_R^{(n)}(x) \\ E_R^{(n)}(x) \end{pmatrix}$
Quark Singlet	$u_R(x)$	$u_R^{(n)}(x), u_L^{(n)}(x)$
Quark Singlet	$d_R(x)$	$d_R^{(n)}(x), d_L^{(n)}(x)$
Lepton Singlet	$e_R(x)$	$e_R^{(n)}(x), e_L^{(n)}(x)$

Table 2.1: Fermion content of the minimal UED model. $SU(2)$-doublets ($SU(2)$-singlets) are denoted with capital (lowercase) letters. KK modes carry a KK index n. We omit the index "0" for the SM fields to match the notations in chapter-1.

$$- \frac{1}{2\xi}(\partial^\mu G_\mu^a - \xi \partial_5 G_5^a)^2\Big), \tag{2.14}$$

$$S_{\text{leptons}} = \int d^4x \int_0^{\pi R} dy \sum_j \Big(i\overline{L_j}\Gamma^M D_M L_j + i\overline{E_j}\Gamma^M D_M E_j \Big), \tag{2.15}$$

$$S_{\text{quarks}} = \int d^4x \int_0^{\pi R} dy \sum_j \Big(i\overline{Q_j}\Gamma^M D_M Q_j + i\overline{U_j}\Gamma^M D_M U_j + i\bar{D}_j\Gamma^M D_M D_j \Big), \tag{2.16}$$

$$S_{\text{Yukawa}} = \int d^4x \int_0^{\pi R} dy \sum_j \Big(Y_{ij}^u \overline{Q_i}\tilde{\Phi} U_j + Y_{ij}^d \overline{Q_i}\Phi D_j + Y_{ij}^l \bar{L}_i \Phi E_j \Big), \tag{2.17}$$

$$S_{\text{Higgs}} = \int d^4x \int_0^{\pi R} dy \Big((D_M\Phi)^\dagger (D^M\Phi) + \mu^2 \Phi^\dagger\Phi - \lambda(\Phi^\dagger\Phi)^2 \Big). \tag{2.18}$$

Here, we describe some more notations: $\Gamma^M = \gamma^\mu$ and $i\gamma^5$; Y_{ij}^u, Y_{ij}^d and Y_{ij}^l are $5D$ up, down and lepton Yukawa couplings respectively and $\tilde{\Phi} = i\sigma^2\Phi^*$ with the Pauli matrix σ^2. The gauge field strength tensors in $5D$ are given by,

$$\begin{aligned} B_{MN} &= \partial_M B_N - \partial_N B_M \\ W_{MN}^a &= \partial_M W_N^a - \partial_N W_M^a + g_2^{(5)} \epsilon^{abc} W_M^b W_N^c \\ G_{MN}^a &= \partial_M G_N^a - \partial_N G_M^a + g_3^{(5)} f^{abc} G_M^b G_N^c \end{aligned}$$

where $g_i^{(5)}$s are the 5 dimensional gauge coupling constants of $U(1)$, $SU(2)$ and $SU(3)_C$ groups respectively. The interactions between a gauge field and the fermions are set up by fermion kinetic term with partial derivative (∂_M) properly replaced by a covariant derivative (D_M) as shown in chapter-1. For example, the general form of the covariant

derivative for the quark fields which interact with all three gauge fields is given by,

$$D_M = \partial_M - ig_3^{(5)}\frac{\lambda^a}{2}G_M^a - ig_2^{(5)}\frac{\sigma^a}{2}W_M^a - ig_1^{(5)}\frac{Y}{2}B_M \tag{2.19}$$

λ^as ($a = 1-8$) are eight Gell-mann matrices, σ^a ($a = 1-3$) are the three Pauli matrices and Y is the hypercharge quantum number. Hypercharge numbers assigned to different fermions are exactly the same as in SM: $Y_Q = \frac{1}{6}$, $Y_u = \frac{2}{3}$, $Y_d = -\frac{1}{3}$, $Y_L = -\frac{1}{2}$ and $Y_e = -1$. The covariant derivatives corresponding to other fermion fields will be of similar form but only differ by the gauge interaction they respond to.

We now discuss briefly some guiding principles for deriving the interactions among various KK modes of different particles. $5D$ gauge coupling constants are dimensionful parameters. We must recover the exact SM coupling starting from the $5D$ Lagrangian. From the action given in eqns. 1.13-1.18, we first pick up an interaction term and write all the fields in terms of their respective KK expansions (with general mode numbers). For example, an interaction between a gauge boson(V_μ) a pair of fermions (Ψ) in $4D$ can be obtained from the fermion kinetic term in eqn. 1.17,

$$i\bar{\Psi}(x,y)\Gamma^M D_M \Psi(x,y) \longrightarrow i\bar{\Psi}(x,y)\gamma^\mu D_\mu \Psi(x,y)$$

We consider a simple covariant derivative with one gauge interaction with coupling constant $g^{(5)}$: $D_\mu = \partial_\mu - ig^{(5)}V_\mu$. The interaction term turns out to be $g^{(5)}\bar{\Psi}(x,y)\gamma^\mu V_\mu(x,y)\Psi(x,y)$. We now plug in the KK decomposition of the fields from equations 2.8, 2.12 in this expression to obtain

$$\begin{aligned} g^{(5)}\int d^4x \int dy \sum_{k,l,m}\Bigg(\frac{1}{\sqrt{\pi R}}\bar{\Psi}^{(0)}(x) + \frac{2}{\sqrt{\pi R}}\sum_n \bar{\Psi}^{(k)}(x)\cos\frac{ky}{R}\Bigg)\times \\ \Bigg(\frac{1}{\sqrt{\pi R}}V^{\mu(0)}(x) + \frac{2}{\sqrt{\pi R}}V^{\mu(l)}(x)\cos\frac{ly}{R}\Bigg)\times \\ \Bigg(\frac{1}{\sqrt{\pi R}}\Psi^{(0)}(x) + \frac{2}{\sqrt{\pi R}}\Psi^{(m)}(x)\cos\frac{my}{R}\Bigg) \end{aligned}$$

The SM interaction involving all the zero mode excitations can be reproduced as,

$$\begin{aligned} &\frac{g^{(5)}}{\left(\sqrt{\pi R}\right)^{\frac{3}{2}}}\int d^4x\ \bar{\Psi}^{(0)}(x)V^{\mu(0)}(x)\Psi^{(0)}(x)\int_0^{\pi R}dy \\ &\longrightarrow \quad \frac{g^{(5)}}{\sqrt{\pi R}}\int d^4x\ \bar{\Psi}^{(0)}(x)V^{\mu(0)}(x)\Psi^{(0)}(x), \end{aligned}$$

where $\frac{g^{(5)}}{\sqrt{\pi R}}$ must be equal to the SM coupling: $g^{(4)} = \frac{g^{(5)}}{\sqrt{\pi R}}$. Note that the proper normalization of the fields are essential to match the $5D$ gauge coupling with the exact SM coupling. As for the interaction involving KK level is concerned, we are allowed to pick only those mode numbers which satisfy a general selection rule fixed by the conservation of KK number. In the previous example, the next allowed interactions are $k = 1$, $l = 1$, $m = 0$ and all their permutations. One of the combination yields a level-0 gauge boson interacting with two level-1 fermions. This is a new vertex not present in SM and it is essential for the production of level-1 fermions at the LHC.

$$\frac{g^{(5)}}{\left(\sqrt{\pi R}\right)^{\frac{3}{2}}} \int d^4x\ \bar{\Psi}^{(1)}(x) V^{\mu(0)}(x) \Psi^{(1)}(x) \int_0^{\pi R} dy\ \cos^2 \frac{y}{R}$$

$$\longrightarrow \quad \frac{g^{(5)}}{\sqrt{\pi R}} \int d^4x\ \bar{\Psi}^{(1)}(x) V^{\mu(0)}(x) \Psi^{(1)}(x)$$

Using the integrals of various trigonometric functions (generally called orthonormal relations), one can easily derive the vertices. Note that the effective coupling again comes out to be the same as the SM coupling. In fact, all mUED vertices will appear exactly equal to the corresponding SM interaction vertices. Another important interaction could be a level-2 gauge boson interacting with two SM fermions. This vertex is particularly important for the resonance production of a level-2 gauge boson at the LHC. Note that such an interaction is prohibited at the tree level in mUED because of KK number conservation. There, it can only occur at one loop order and thus suppressed.

2.3 Phenomenology of mUED at the LHC

Phenomenology of the mUED scenario is primarily governed by the following factors

- mass spectrum
- conservation of KK number and KK parity

As we have already seen, mUED spectrum is highly compressed. The mass splittings essentially appear due to radiative corrections [60]. Besides, momentum conservation along the extra dimension gives rise to conservation of KK number at each interaction vertex. Hence, there is no tree level coupling with a level-2 gauge boson with SM fermions. Z_2 symmetry described as the KK parity $(-1)^n$ for a particle at level-n also remains conserved in any mUED interaction. As a result, level-1 KK particles are always produced

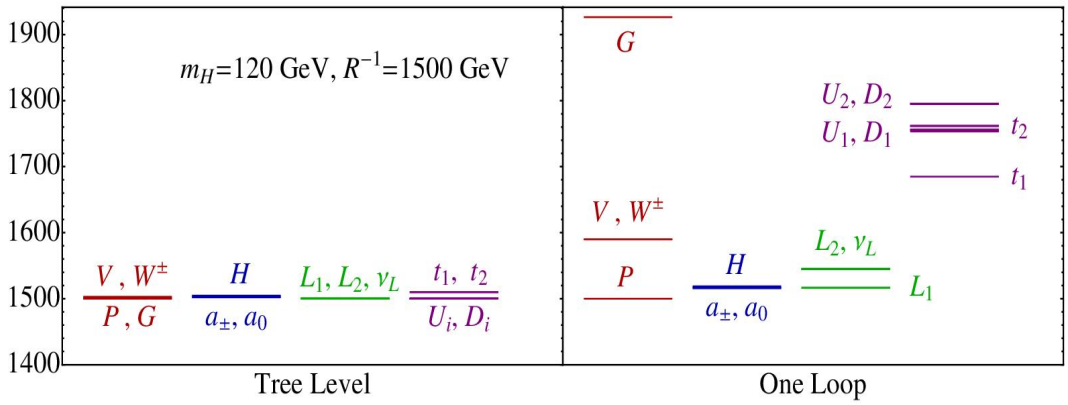

Figure 2.2: The level-1 KK mass spectrum of the mUED model at tree level (left) and at one loop (right) for R^{-1} = 1500 GeV, m_H = 120 GeV and ΛR = 20 [62].

in pair at the collider experiments. Conservation of KK parity ensures stability of the lightest KK particle (LKP). If, in addition, the LKP is a weakly interacting neutral particle, then it could serve a good candidate for cold dark matter (or a weakly interacting massive particle known as WIMP).

The level-1 coloured particles (KK quarks or KK gluons) can be copiously produced at the LHC. The KK quarks/gluons can, undergo then, cascade decays into a number of $jets$ or leptons (or both) and LKP which escapes the detector. A cascade results in a generic signal comprising n $jets$ + m leptons + E_T^{miss}. But as masses of the KK particles lie close, the $jets$ as well as the leptons are usually very soft and it is difficult to distinguish them from the SM background. Still, many search channels have been efficiently looked into by LHC experiments.

Supersymmetry (SUSY) is one of the most promising and extensively studied BSM scenario. However, there are many instances where mUED can fake possible SUSY signals [63–65]. R-parity conserving SUSY also provides a viable dark matter candidate. Although, it is true that SUSY (particularly, minimal supersymmetric standard model) provides a plethora of possibilities giving a variety of signatures at the colliders. However, there are two basic discriminators between mUED and SUSY scenarios. A typical feature of the UED scenario is the existence of towers of KK particles for each of the SM excitation. On the other hand, there is only one supersymmetric particle (known as sparticle) corresponding to each SM particle. Therefore, discovery of higher multiple massive states with similar quantum number may prove UED as a more viable BSM theory than SUSY. Another fundamental difference between such theories is the spin of the new excitations (sparticles or KK particles). SUSY predicts a spin-0 partner for every SM

fermion and a spin-$\frac{1}{2}$ fermion for every gauge boson. In contrast, KK particles are of same spin as their SM counterpart. Thus, spin correlation of the daughter particles in the decay chains can help distinguish the two competing scenarios. However, deciphering the spins of such new excitations is not an easy task. Thus, in the absence of any other hint, it is understood to be daunting task at the LHC to distinguish between a SUSY and an UED scenario once a signal is observed. We can also employ various angular asymmetry observables. Therefore, collider phenomenology becomes more complicated and needs careful consideration of many subtle points.

2.4 Experimental Constraints on mUED scenario

Several experimental observations put constraints on the mUED parameter space. The most severe constraints come from the electroweak precision variables which have been precisely measured at the LEP. Any new physics model may also contribute to these variables. But we expect their contribution to be small. S, T, U parameters are the corrections to the electroweak gauge boson propagators. They put stringent bounds on the mUED parameter space. One loop contributions from KK top quarks and KK Higgs states to these variables are significant. The bound has been set at $R^{-1} \gtrsim 680$ GeV [66].

Results from the Tevatron and LHC put limits on extra dimensional models. Bounds on UED scenarios are derived from the latest LHC analyses and other experiments searching for dark matter. These can be found in references [62, 67, 68]. The recent Higgs data also constrain UED models since the contributions from KK towers of various particles in loop affect both Higgs production and decay rates [69]. The constraints mainly come from $gg \to h \to \gamma\gamma, WW^*, ZZ^*$ channels. However, the most stringent bound comes from WW^* channel from both the ATLAS [70] and the CMS experiments [71]. The current ATLAS Higgs data combined for center-of-mass energies 7 TeV and 8 TeV at 25 fb^{-1} luminosity provides a constraint of $R^{-1} \gtrsim 460$ GeV. On the other hand, using CMS data, much stricter bound of $R^{-1} \gtrsim 1300$ GeV [72] can be put. The reason behind such difference is mainly the large difference in signal strengths (μ value) registered by the two experiments. However, one should be aware of the fact that bounds coming from such Higgs data are indirect in nature. The direct limit comes from trilepton signature at the LHC where the region $R^{-1} \lesssim 1200$ GeV has been excluded at the 95% C.L. for a large range of the cut-off scale Λ [62].

We have already mentioned that level-2 KK gauge bosons in mUED do not have tree level couplings with SM (level-0) fermions because these violate KK number. However,

an effective interaction among these particles occurs at 1-loop level that respect KK parity. This is of particular importance since it allows for the resonance production of level-2 gauge bosons at the LHC. Many new physics models with higher symmetry group predict additional gauge bosons ($Z^{'}$ or $W^{'}$). LHC usually searches for such spin-1 extra gauge bosons as massive resonance decaying into much cleaner leptonic final state. Results from such $Z^{'}$ or $W^{'}$-like signal can be reinterpreted in terms of specific scenarios. Level-2 electroweak gauge bosons in mUED ($\gamma^{(2)}$, $Z^{(2)}$ or $W^{(2)\pm}$) can be thought of such additional gauge boson candidates. Thus, absence of such signals, can lead to bounds on level-2 KK gauge bosons. CMS search for resonant $Z^{'}$ in the dilepton channel has resulted in a constraint of $R^{-1} \gtrsim 715$ GeV for mUED [73].

We have already mentioned that the LKP can be a prospective WIMP dark matter. The level-1 KK photon turns out to be the LKP and hence the dark matter candidate. The relic density is the amount of dark matter present in today's universe. The current value of relic abundance from recent Planck data is $\Omega_{DM}h^2 \sim 0.1189$ [54]. For an mUED scenario with a cut-off scale of $\Lambda = 20R^{-1}$, the value of R^{-1} which gives correct relic density is around 1300 GeV [74]. The relic density estimation for level-1 KK photon as the dark matter excludes large region of mUED parameter space. If the LKP is too massive, then it becomes too abundant and hence ruled out. The actual bound may vary depending on the nature of the dark matter and the mass splitting with other particles. But one can avoid the bounds in many possible ways. For example, constraints are less severe for a $Z^{(1)}$ WIMP or for a multi-component dark matter scenario. Of course, the constraints depend on various assumptions and in actual situation may be less restrictive. But one should keep the above information in mind while studying the mUED scenario.

With this overview on mUED, we now move on to extend this scenario. This would give us access to a variety of circumstances which may have rich phenomenology at the LHC. In the next section, we discuss the non-minimal universal extra dimension (nmUED) scenario .

2.5 From mUED to nmUED

The mUED model is minimal in the sense that it is based on a minimal set of parameters. In the non-minimal version, we add some more free parameters. In general, scenarios with less number of input parameters are more predictive and easy to rule out at experiments. But such models may not create much diverse possibilities which could be

equally valid new physics scenarios. For example, minimal supergravity (MSUGRA) is a well motivated scenario with only five input parameters. However, it is already heavily constrained by LHC results. On the other hand, nineteen parameter pMSSM gives rise to more varied possibilities.

Orbifold fixed point is the boundary of the brane and the bulk. Field theories on the orbifold have important consequences and are capable of altering the phenomenology at the low energy scale. Along with the bulk terms like in mUED, we include terms localized at the boundaries of the compactified extra dimension and call these as boundary (or, brane) localized terms (BLTs). In fact, it has been shown that these terms are unavoidable in certain circumstances. In an extra dimensional theory compactified over S^1/Z_2, translational symmetry is broken by the presence of orbifold fixed points. While calculating one loop radiative corrections to KK masses, additional divergences appear to be localized only at those fixed points. Hence, appropriate counterterms are to be placed at those boundaries in order to cancel the divergences [60]. In this sense such terms should necessarily be present. The coefficients of the boundary terms evolve with the renormalization group equations starting from the cut-off scale down to the weak scale. In case of mUED, all such boundary localized terms are assumed to be zero or negligibly small at the cut-off. But there is no reason to expect them to be small at the cut-off scale itself. Large boundary localized terms contribute significantly to the masses and mixings of the KK modes. Hence, it is logical to keep these terms from the beginning. BLTs are also consistent with the Lorentz symmetry and gauge symmetries of the theory. Therefore, inclusion of such terms definitely makes the theory more general. We must mention that such boundary term is not new in the literature and has been already mentioned in the refs. [75–81]. But detail phenomenological studies with BLTs keeping LHC in mind is still scarce. In this thesis, we want to explore such a scenario and investigate carefully the collider implications of such boundary localized terms. We introduce boundary localized kinetic terms (BLKT) for the fermions and the gauge bosons. We also include boundary localized Yukawa (BLYT) interactions. From now on, we interchangeably use the phrase 'brane-local' or 'boundary-local' for such terms. The coefficients of the boundary terms are the new parameters in this scenario. The scenario presented here is one version of a non-minimal universal extra dimension (nmUED). In the next section, we discuss the theoretical set up of the nmUED model in detail.

2.6 Theoretical Framework

2.6.1 The QCD sector

We consider QCD in $5D$ with brane-localized kinetic terms for quark and gluon fields at the orbifold fixed points. Under S^1/Z_2 orbifolding, there appear two fixed points which we consider at $L = \pm\pi R/2$, for simplicity. We write down the complete QCD action where $S_{\text{gluon (quark)}}$ is the action for the gluon (quark) fields including the gauge-fixing term [82].

$$S_{\text{nmQCD}} = S_{\text{gluon}} + S_{\text{gluon,gf}} + S_{\text{quark}}, \tag{2.20}$$

$$S_{\text{gluon}} = \int d^4x \int_{-L}^{L} dy \Bigg\{ -\frac{1}{4} G^a_{MN} G^{aMN} + \Big(\delta(y-L) + \delta(y+L)\Big)\Big[-\frac{r_G}{4} G^a_{\mu\nu} G^{a\mu\nu}\Big]\Bigg\}, \tag{2.21}$$

$$\begin{aligned} S_{\text{gluon,gf}} = \int d^4x \int_{-L}^{L} dy \Bigg\{ & -\frac{1}{2\xi_G}(\partial_\mu G^{a\mu} - \xi_G \partial_y G^a_y)^2 - \frac{1}{2\xi_{G,b}}\Big[(\partial_\mu G^{a\mu} + \xi_{G,b} G^a_y)^2 \delta(y-L) \\ & + (\partial_\mu G^{a\mu} - \xi_{G,b} G^a_y)^2 \delta(y+L)\Big]\Bigg\}, \end{aligned} \tag{2.22}$$

$$\begin{aligned} S_{\text{quark}} = \int d^4x \int_{-L}^{L} dy \sum_{i=1}^{3} \Bigg\{ & i\overline{U}_i \Gamma^M \mathcal{D}_M U_i + r_Q \Big(\delta(y-L) + \delta(y+L)\Big)\Big[i\overline{U}_i \gamma^\mu \mathcal{D}_\mu P_L U_i\Big] \\ & + i\overline{D}_i \Gamma^M \mathcal{D}_M D_i + r_Q \Big(\delta(y-L) + \delta(y+L)\Big)\Big[i\overline{D}_i \gamma^\mu \mathcal{D}_\mu P_L D_i\Big] \\ & + i\overline{u}_i \Gamma^M \mathcal{D}_M u_i + r_Q \Big(\delta(y-L) + \delta(y+L)\Big)\Big[i\overline{u}_i \gamma^\mu \mathcal{D}_\mu P_R u_i\Big] \\ & + i\overline{d}_i \Gamma^M \mathcal{D}_M d_i + r_Q \Big(\delta(y-L) + \delta(y+L)\Big)\Big[i\overline{d}_i \gamma^\mu \mathcal{D}_\mu P_R d_i\Big]\Bigg\}. \end{aligned} \tag{2.23}$$

The descriptions of the fields are same as we mentioned earlier. ξ_G and $\xi_{G,b}$ are the bulk and the boundary gauge fixing parameters respectively. r_G, r_Q are the coefficients of BLKTs for the gluon and quark fields, respectively. We consider equal boundary parameter at the fixed points which ensures the conservation of KK parity.

The forms of the bulk equations of motion and the boundary conditions at the two orbifold fixed points are determined using the variational principle. In this thesis we use the unitary gauge with ξ_G, $\xi_{G,b} \to \infty$ which sets $G^a_y \to 0$ where G^a_y is the 5th component

of the gluon field. Here, U_i, D_i (u_i, d_i) represents the 'up' and 'down'-type $SU(2)$ doublet (singlet) quark fields. $i = 1, 2, 3$ stands for the three generations of quarks.

In the unitary gauge, the $5D$ fields of G^a_μ, $Q_{L,R}$, $u_{L,R}$ and $d_{L,R}$ are KK decomposed as follows:

$$G^a_\mu(x,y) = \sum_{n=0}^{\infty} G^{a(n)}_\mu(x) f_{G^{(n)}}(y), \tag{2.24}$$

$$Q_L(x,y) = Q^{(0)}_L(x) f_{Q^{(0)}_L}(y) + \sum_{n>0:\text{even}} Q^{(n)}_L(x) f_{Q^{(n)}_L}(y) + \sum_{n>0:\text{odd}} Q^{(n)}_L(x) f_{Q^{(n)}_L}(y), \tag{2.25}$$

$$Q_R(x,y) = \sum_{n>0:\text{even}} Q^{(n)}_R(x) f_{Q^{(n)}_R}(y) + \sum_{n>0:\text{odd}} Q^{(n)}_R(x) f_{Q^{(n)}_R}(y), \tag{2.26}$$

$$u_R(x,y) = u^{(0)}_R(x) f_{u^{(0)}_R}(y) + \sum_{n>0:\text{even}} u^{(n)}_R(x) f_{u^{(n)}_R}(y) + \sum_{n>0:\text{odd}} u^{(n)}_R(x) f_{u^{(n)}_R}(y), \tag{2.27}$$

$$u_L(x,y) = \sum_{n>0:\text{even}} u^{(n)}_L(x) f_{u^{(n)}_L}(y) + \sum_{n>0:\text{odd}} u^{(n)}_L(x) f_{u^{(n)}_L}(y), \tag{2.28}$$

$$d_R(x,y) = d^{(0)}_R(x) f_{d^{(0)}_R}(y) + \sum_{n>0:\text{even}} d^{(n)}_R(x) f_{d^{(n)}_R}(y) + \sum_{n>0:\text{odd}} d^{(n)}_R(x) f_{d^{(n)}_R}(y), \tag{2.29}$$

$$d_L(x,y) = \sum_{n>0:\text{even}} d^{(n)}_L(x) f_{d^{(n)}_L}(y) + \sum_{n>0:\text{odd}} d^{(n)}_L(x) f_{d^{(n)}_L}(y), \tag{2.30}$$

where the mode functions of level-n can be categorized as

$$f_{G^{(n)}}(y) = N_{G^{(n)}} \times \begin{cases} \dfrac{\cos(M_{G^{(n)}} y)}{C_{G^{(n)}}} & \text{for } n \text{ even} \\ -\dfrac{\sin(M_{G^{(n)}} y)}{S_{G^{(n)}}} & \text{for } n \text{ odd} \end{cases}, \tag{2.31}$$

$$f_{Q^{(n)}} \equiv f_{Q^{(n)}_{iL}} = f_{u^{(n)}_{iR}} = f_{d^{(n)}_{iR}} = N_{Q^{(n)}} \times \begin{cases} \dfrac{\cos(M_{Q^{(n)}} y)}{C_{Q^{(n)}}} & \text{for } n \text{ even} \\ -\dfrac{\sin(M_{Q^{(n)}} y)}{S_{Q^{(n)}}} & \text{for } n \text{ odd} \end{cases}, \tag{2.32}$$

$$g_{Q^{(n)}} \equiv f_{Q^{(n)}_{iR}} = -f_{u^{(n)}_{iL}} = -f_{d^{(n)}_{iL}} = N_{Q^{(n)}} \times \begin{cases} \dfrac{\sin(M_{Q^{(n)}} y)}{C_{Q^{(n)}}} & \text{for } n \text{ even} \\ \dfrac{\cos(M_{Q^{(n)}} y)}{S_{Q^{(n)}}} & \text{for } n \text{ odd} \end{cases}, \tag{2.33}$$

with the normalization factors $N_{G^{(n)}}$, $N_{Q^{(n)}}$. Hereafter, we will use the following shorthand notations,

$$C_{X^{(n)}} = \cos\left(\frac{M_{X^{(n)}}\pi R}{2}\right), \quad S_{X^{(n)}} = \sin\left(\frac{M_{X^{(n)}}\pi R}{2}\right), \quad T_{X^{(n)}} = \tan\left(\frac{M_{X^{(n)}}\pi R}{2}\right), \tag{2.34}$$

where X stands for G (gluon) and Q (quark) [5] and $M_{X^{(n)}}$ is the corresponding KK mass at the n-th level determined through the transcendental equations

$$r_X M_{X^{(n)}} = \begin{cases} -T_{X^{(n)}} & \text{for } n \text{ even} \\ 1/T_{X^{(n)}} & \text{for } n \text{ odd} \end{cases}. \tag{2.35}$$

The generalized orthonormal conditions for $\{f_{Q^{(n)}}\}$ and $\{g_{Q^{(n)}}\}$ take the forms

$$\begin{aligned} \int_{-L}^{L} dy \Big[1 + r_X\left(\delta(y-L) + \delta(y+L)\right)\Big] f_{X^{(m)}} f_{X^{(n)}} &= \delta_{m,n}, \\ \int_{-L}^{L} dy g_{Q^{(m)}} g_{Q^{(n)}} &= \delta_{m,n}, \end{aligned} \tag{2.36}$$

respectively, while the expressions for $N_{X^{(n)}}$ turn out to be as follows:

$$N_{X^{(n)}}^{-2} = \begin{cases} 2r_X + \dfrac{1}{C_{X^{(n)}}^2}\left[\dfrac{\pi R}{2} + \dfrac{1}{2M_{X^{(n)}}}\sin(M_{X^{(n)}}\pi R)\right] & \text{for } n \text{ even} \\ 2r_X + \dfrac{1}{S_{X^{(n)}}^2}\left[\dfrac{\pi R}{2} - \dfrac{1}{2M_{X^{(n)}}}\sin(M_{X^{(n)}}\pi R)\right] & \text{for } n \text{ odd} \end{cases}. \tag{2.37}$$

Note that, in the presence of BLTs, these normalization factors $N_{X^{(n)}}$ have rather non-trivial forms when compared to the simple forms like $\frac{1}{\sqrt{\pi R}}$ or $\frac{1}{\sqrt{2\pi R}}$ as in the case of mUED. Especially, the profile for the zero mode is normalized as

$$N_{X^{(0)}} = \frac{1}{\sqrt{2r_X + \pi R}}, \tag{2.38}$$

which results in the following theoretical lower bound on r_X in order to circumvent a tachyonic zero mode:

$$r_X > -\frac{\pi R}{2}. \tag{2.39}$$

[5] Here Q means all type of quarks in general.

2.6.2 The electroweak gauge boson and the Higgs sectors

The gauge boson and the Higgs sectors of the nmUED scenario have been discussed in ref. [83]. We consider the following 5D action describing the electroweak gauge boson and the Higgs sectors of the nmUED scenario under study:

$$S = \int d^4x \int_{-L}^{L} dy \Bigg\{ -\frac{1}{4} W^a_{MN} W^{aMN} - \frac{1}{4} B_{MN} B^{MN} + (D_M \Phi)^\dagger (D^M \Phi) + \hat{\mu}^2 \Phi^\dagger \Phi - \frac{\hat{\lambda}}{4} (\Phi^\dagger \Phi)^2 + \Big(\delta(y-L) + \delta(y+L)\Big) \Big[-\frac{r_W}{4} W^a_{\mu\nu} W^{a\mu\nu} - \frac{r_B}{4} B_{\mu\nu} B^{\mu\nu} + r_H (D_\mu \Phi)^\dagger (D^\mu \Phi) + \mu_b^2 \Phi^\dagger \Phi - \frac{\lambda_b}{4} (\Phi^\dagger \Phi)^2 \Big] \Bigg\}. \tag{2.40}$$

W_{MN} and B_{MN} are the $5D$ field strength tensors of the $SU(2)$ and $U(1)_Y$ gauge groups with the corresponding gauge bosons: W_M and B_M. The $5D$ Higgs doublet Φ is represented as,

$$\Phi = \begin{pmatrix} \phi^+ \\ \frac{1}{\sqrt{2}} \left(\hat{v}(y) + H + i\chi\right) \end{pmatrix} \tag{2.41}$$

where ϕ^+ is the charged component, H and χ are the neutral components and $\hat{v}(y)$ is the $5D$ bulk Higgs vacuum expectation value (vev). D_M stands for the $5D$ covariant derivatives and $\hat{\mu}$ and $\hat{\lambda}$ represent the $5D$ bulk Higgs mass and the Higgs self-coupling, respectively.

We take Z_2 eigenvalues for the fields W^a_μ, B_μ, H, χ, ϕ^+ to be even at both the fixed points to realize the zero modes (*i.e.,* the SM fields) have vanishing KK-masses from compactification. This automatically renders the eigenvalues of W^a_y, B_y to be odd because of $5D$ gauge symmetry for which there are no corresponding zero modes.

As can be seen in equation 2.40, the BLTs (proportional to the δ-functions) are introduced at the orbifold fixed points for both the gauge and the Higgs sectors. r_W, r_B, r_H are coefficients of the brane-local terms corresponding to the W_M, B_M and Φ fields. μ_b is the brane-local mass term (BLMT) parameter and λ_b is the brane-local self-coupling parameter for the Higgs field.

We again remind that KK parity ($y \to -y$ symmetry) is preserved. It ensures the existence of a stable dark matter which is the lightest KK particle (LKP) obtained on compactification. This is particularly relevant for the electroweak sector since the dark matter, in most cases, is an electroweak gauge boson.

In this work, for simplicity, we focus on the following situation:

$$\sqrt{\frac{4\hat{\mu}^2}{\hat{\lambda}}} = \sqrt{\frac{4{\mu_b}^2}{\lambda_b}} \quad \text{and} \quad r_W = r_B \equiv r_{\text{EW}}. \tag{2.42}$$

The first condition ensures a constant profile of the Higgs VEV over the whole space, *i.e.*,

$$\hat{v}(y) \to \sqrt{\frac{4\hat{\mu}^2}{\hat{\lambda}}} = \sqrt{\frac{4{\mu_b}^2}{\lambda_b}} \equiv \hat{v}, \tag{2.43}$$

while with the second condition we can continue to relate the $5D$ W, Z and the photon (γ) states (at tree level) via the usual Weinberg angle θ_W at all KK levels, *i.e.*,

$$W_M^{\pm} = \frac{W_M^1 \mp iW_M^2}{\sqrt{2}}, \quad \begin{pmatrix} Z_M \\ \gamma_M \end{pmatrix} = \begin{pmatrix} \cos\theta_W & \sin\theta_W \\ -\sin\theta_W & \cos\theta_W \end{pmatrix} \begin{pmatrix} W_M^3 \\ B_M \end{pmatrix}. \tag{2.44}$$

The gauge-fixing conditions along with their consequences are discussed briefly in appendix B.1. We choose the unitary gauge. For the fields W_μ^+, Z_μ, H, χ, ϕ^+ and for the ones like $\partial_y W_y^+$, $\partial_y Z_y$, the mode functions for KK decomposition and the conditions that determine their KK-masses are summarized below.

$$f_{F_{(n)}}(y) = N_{F_{(n)}} \times \begin{cases} \dfrac{\cos(M_{F_{(n)}} y)}{C_{F_{(n)}}} & \text{for even } n, \\ -\dfrac{\sin(M_{F_{(n)}} y)}{S_{F_{(n)}}} & \text{for odd } n, \end{cases} \tag{2.45}$$

$$m_{F_{(n)}}^2 = m_F^2 + M_{F_{(n)}}^2, \tag{2.46}$$

$$\frac{(r_F m_{F_{(n)}}^2 - m_{F,b}^2)}{M_{F_{(n)}}} = \begin{cases} -T_{F_{(n)}} & \text{for even } n, \\ +1/T_{F_{(n)}} & \text{for odd } n \end{cases} \tag{2.47}$$

with the following short-hand notations:

$$C_{F^{(n)}} = \cos\left(\frac{M_{F^{(n)}}\pi R}{2}\right), \quad S_{F^{(n)}} = \sin\left(\frac{M_{F^{(n)}}\pi R}{2}\right), \quad T_{F^{(n)}} = \tan\left(\frac{M_{F^{(n)}}\pi R}{2}\right). \tag{2.48}$$

The normalization factors $N_{F^{(n)}}$ for the mode functions $f_{F^{(n)}}(y)$ are given by

$$N_{F^{(n)}}^{-2} = \begin{cases} 2r_F + \dfrac{1}{C_{F^{(n)}}^2}\left[\dfrac{\pi R}{2} + \dfrac{1}{2M_{F^{(n)}}}\sin(M_{F^{(n)}}\pi R)\right] & \text{for even } n, \\ 2r_F + \dfrac{1}{S_{F^{(n)}}^2}\left[\dfrac{\pi R}{2} - \dfrac{1}{2M_{F^{(n)}}}\sin(M_{F^{(n)}}\pi R)\right] & \text{for odd } n. \end{cases} \tag{2.49}$$

Here $m_{F^{(n)}}$, m_F, $M_{F^{(n)}}$, r_F and $m_{F,b}$ stand for the physical mass, the bulk mass, the KK mass, the coefficient of the corresponding brane-local kinetic term (BLKT) and brane mass term of the field F, respectively. Inputs for the mass-determining conditions for all these fields are presented in appendix B.1. Further, following conditions must hold to ensure the zero-mode (SM) profiles to be flat which help evade severe constraints from electroweak observables like the Z boson mass, $\sin^2\theta_W$ etc.

$$\begin{aligned} r_{\text{EW}} &= r_H \qquad \text{for } W_\mu^+,\ Z_\mu, \\ r_H(2\hat{\mu}^2) &= 2\mu_b^2 \qquad \text{for } H. \end{aligned} \tag{2.50}$$

Non-compliance of the above relations could result in unacceptable modifications in the level-0 (SM) Lagrangian [83].

Also, with the above two conditions, equation 3.2 reduces to the following simple form:

$$r_F M_{F^{(n)}} = \begin{cases} -T_{F^{(n)}} & \text{for } n \text{ even}, \\ 1/T_{F^{(n)}} & \text{for } n \text{ odd} \end{cases} \tag{2.51}$$

where $M_{F^{(0)}} = 0$ (thus ensuring vanishing KK masses for the level-0 (SM) fields). A theoretical lower bound of $r_F > -\frac{\pi R}{2}$ must hold to circumvent tachyonic zero modes. On the other hand, vanishing KK masses at level-0 are always realized for ϕ^+ and χ which are eventually "eaten up" by the massless level-0 W_μ^+, Z_μ states respectively as they become massive. However, no zero mode appears for W_y^+, Z_y since they are projected out by the Z_2-odd condition. The mode functions for the fields W_y^+, Z_y are given by

$$f_{F^{(n)}}(y) = N_{F^{(n)}} \times \begin{cases} \dfrac{\sin(M_{F^{(n)}} y)}{C_{F^{(n)}}} & \text{for even } n, \\ \dfrac{\cos(M_{F^{(n)}} y)}{S_{F^{(n)}}} & \text{for odd } n \end{cases} \tag{2.52}$$

with the mass-determination condition as given in equation 3.2. Use of equation B.4 allows one to eliminate χ in favor of Z_y and ϕ^+ in favor of W_y^+. Correct normalization of the kinetic terms requires Z_y and W_y^+ to be renormalized in the following way:

$$Z_y^{(n)} \to \left(1 + \frac{M_{Z_{y(n)}}^2}{M_Z^2}\right)^{-1/2} Z_y^{(n)}, \qquad W_y^{(n)+} \to \left(1 + \frac{M_{W_{y(n)}}^2}{M_W^2}\right)^{-1/2} W_y^{(n)+}. \tag{2.53}$$

Note that $Z_y^{(n)}$ is the pseudoscalar Higgs state and $W_y^{(n)+}$ is the charged Higgs boson from the n-th KK level which has no level-0 counterpart. Thus, up to KK level-1, the Higgs

spectrum consists of the following five Higgs bosons: the SM (level-0) Higgs boson (H) and four Higgs states from level-1, *i.e.*, the neutral CP-even Higgs boson ($H^{(1)^0}$) which is the level-1 excitation of the SM Higgs boson, the neutral CP-odd Higgs boson ($A^{(1)^0}$) and the two charged Higgs bosons $H^{(1)^\pm}$.

2.6.3 The Yukawa sector and the quark mass matrix

We now incorporate the brane-local Yukawa terms (BLYTs) in the nmuED scenario. The action in the Yukawa sector with BLYT is given by

$$S_{\text{Yukawa}} = \int d^4x \int_{-L}^{L} dy \sum_{i,j=1}^{3} \Bigg\{ -\Big(1 + r_Y \delta(y-L) + \delta(y+L)\Big)\Big[Y^u_{ij}\overline{Q}_i u_j \tilde{\Phi} + Y^d_{ij}\overline{Q}_i d_j \Phi + \text{h.c.}\Big] \Bigg\} \tag{2.54}$$

where r_Y is the corresponding brane-local Yukawa parameter. On EWSB via the ordinary Higgs mechanism, the Higgs doublet Φ acquires the vev $\langle\Phi\rangle = (0, v/\sqrt{2})^{\text{T}}$ with $v = 246$ GeV. We assume that the brane-localized Yukawa terms are flavour-blind thereby allowing us to diagonalize the Yukawa matrices $\mathcal{Y}^u_{ij}$ and $\mathcal{Y}^d_{ij}$ in a way similar to that for the SM and which can be expressed as

$$\int d^4x \int_{-L}^{L} dy \Bigg\{ -\Big(1 + r_Y\left(\delta(y-L) + \delta(y+L)\right)\Big) \sum_{i=1}^{3} \Big[\Big(\mathcal{Y}^u_{ii}\frac{v}{\sqrt{2}}\Big)\overline{U}_i u_i + \Big(\mathcal{Y}^d_{ii}\frac{v}{\sqrt{2}}\Big)\overline{D}_i d_i + \text{h.c.}\Big] \Bigg\}. \tag{2.55}$$

Using the KK mode expansions of quarks in eqn. 2.30 and mode functions 2.32 and 2.33, we obtain

$$-\Big(\mathcal{Y}^q_{ii}\frac{v}{\sqrt{2}}\Big) \int d^4x \Bigg\{ R_{Q00}\overline{q}^{(0)}_{iL} q^{(0)}_{iR} + r_{Q11}\overline{Q}^{(1)}_{iL} q^{(1)}_{iR} - R_{Q11}\overline{q}^{(1)}_{iL} Q^{(1)}_{iR} + \text{h.c.} \Bigg\}, \tag{2.56}$$

where we make a redefinition of $u^{(0)}_{iL} = U^{(0)}_{iL}$. $R_{Q00}, r_{Q11}, R_{Q11}$ result from the overlap integrals and are given by

$$R_{Q00} = \int_{-L}^{L} dy \Big(1 + r_Y\Big(\delta(y-L) + \delta(y+L)\Big)\Big) f^2_{Q^{(0)}} = \frac{2r_Y + \pi R}{2r_Q + \pi R}, \tag{2.57}$$

$$\begin{aligned} r_{Q11} &= \int_{-L}^{L} dy \Big(1 + r_Y\Big(\delta(y-L) + \delta(y+L)\Big)\Big) f^2_{Q^{(1)}} \\ &= \frac{2r_Y + \frac{1}{S^2_{Q^{(1)}}}\left[\frac{\pi R}{2} - \frac{1}{2M_{Q^{(1)}}}\sin(M_{Q^{(1)}}\pi R)\right]}{2r_Q + \frac{1}{S^2_{Q^{(1)}}}\left[\frac{\pi R}{2} - \frac{1}{2M_{Q^{(1)}}}\sin(M_{Q^{(1)}}\pi R)\right]}, \end{aligned} \tag{2.58}$$

$$R_{Q11} = \int_{-L}^{L} dy \Big(1 + r_Y \Big(\delta(y-L) + \delta(y+L)\Big)\Big) g^2_{Q^{(1)}}$$
$$= \frac{2r_Y (C_{Q^{(1)}}/S_{Q^{(1)}})^2 + \frac{1}{S^2_{Q^{(1)}}} \left[\frac{\pi R}{2} + \frac{1}{2M_{Q^{(1)}}} \sin(M_{Q^{(1)}}\pi R)\right]}{\frac{1}{S^2_{Q^{(1)}}} \left[\frac{\pi R}{2} + \frac{1}{2M_{Q^{(1)}}} \sin(M_{Q^{(1)}}\pi R)\right]}. \tag{2.59}$$

The zero mode masses (*i.e.*, the masses of the SM quarks) get fixed as

$$m_{q_i} = \Big(\mathcal{Y}^q_{ii} \frac{v}{\sqrt{2}}\Big) R_{Q00}. \tag{2.60}$$

It is noted that when $r_Y = -\pi R/2$, the value of R_{Q00} becomes zero and the SM quarks become massless. Obviously, this limit is meaningless in phenomenology and we should ignore this possibility. On the other hand, in the limit $r_Q = r_Y$, values of both R_{Q00} and r_{Q11} become 1 while R_{Q11} is still away from 1. This implies that deviations from the mUED case may still be present in the physical mass spectrum of the level-1 KK quarks. The mUED limit is recovered with $r_G = r_Q = 0$ when all of $R_{Q00}, r_{Q11}, R_{Q11}$ become equal to 1. This, in turn, implies that non-vanishing r_Y may play some role in determining even the spectrum of the KK quarks that correspond to the lighter flavours of the SM. The effect is generally miniscule for their mass-eigenvalues since equation (2.56) has an overall factor which amounts to the mass of the SM quark of i-th light flavour. However, as we will find later, the Yukawa sector has an important implication for the mixing between the weak eigenstates of the KK quarks of lighter SM flavours.

There is another interesting phenomenon known as *level-mixing* that can take place between similar states from two different KK levels. This explicitly violates KK number. This is theoretically possible since the translational invariance in $5D$ is broken by the orbifold fixed points. However, to conserve KK-parity, the mixings would be limited to those between even or odd states only. The phenomenological implications of such *level-mixing* is found to be negligible for the first two generations but is not always so for the top quark. We will discuss this topic in the next chapter. In the case of mUED, such effects can only be induced at a higher order. However, presence of BLTs ensures overlap integrals of the following form:

$$-m_{q_i} \int d^4x \Big\{ \overline{q}^{(0)}_{iL} q^{(0)}_{iR} + r'_{Q11} \overline{Q}^{(1)}_{iL} q^{(1)}_{iR} - R'_{Q11} \overline{q}^{(1)}_{iL} Q^{(1)}_{iR} + \text{h.c.} \Big\}, \tag{2.61}$$

where r'_{Q11}, R'_{Q11} are defined as

$$r'_{Q11} = \frac{r_{Q11}}{R_{Q00}}, \quad R'_{Q11} = \frac{R_{Q11}}{R_{Q00}}. \tag{2.62}$$

Now we can obtain the mass matrix for the level-1 KK quarks as

$$-\int d^4x\Bigg\{\left[\overline{Q}_i^{(1)},\ \overline{q}_i^{(1)}\right]_L \underbrace{\begin{bmatrix} M_{Q^{(1)}} & r'_{Q11}m_{q_i} \\ -R'_{Q11}m_{q_i} & M_{Q^{(1)}} \end{bmatrix}}_{\equiv \mathcal{M}_{q_i}^{(1)}} \begin{bmatrix} Q_i^{(1)} \\ q_i^{(1)} \end{bmatrix}_R + \text{h.c.}\Bigg\}. \tag{2.63}$$

By choosing same mass for the diagonal entries we implicitly assume that the BLKTs for the quarks are blind to $SU(2)$ quantum numbers (singlet or doublet) they possess. By use of the following bi-unitary transformations

$$\begin{bmatrix} Q_i^{(1)} \\ q_i^{(1)} \end{bmatrix}_L = V_{q_iL}^{(1)} \begin{bmatrix} \mathcal{Q}_{i2}^{(1)} \\ \mathcal{Q}_{i1}^{(1)} \end{bmatrix}_L, \quad \begin{bmatrix} Q_i^{(1)} \\ q_i^{(1)} \end{bmatrix}_R = V_{q_iR}^{(1)} \begin{bmatrix} \mathcal{Q}_{i2}^{(1)} \\ \mathcal{Q}_{i1}^{(1)} \end{bmatrix}_R, \tag{2.64}$$

we can diagonalize equation (2.63) as follows:

$$-\int d^4x \left[\overline{\mathcal{Q}}_{i2}^{(1)},\ \overline{\mathcal{Q}}_{i1}^{(1)}\right] \begin{bmatrix} m_{q_i2}^{(1)} & \\ & m_{q_i1}^{(1)} \end{bmatrix} \begin{bmatrix} \mathcal{Q}_{i2}^{(1)} \\ \mathcal{Q}_{i1}^{(1)} \end{bmatrix}, \tag{2.65}$$

where $\mathcal{Q}_{i1}^{(1)}, \mathcal{Q}_{i2}^{(1)}$ are the mass eigenstates of level-1 KK quarks. The set of eigenvalues, $\left(m_{q_i1}^{(1)}\right)^2, \left(m_{q_i2}^{(1)}\right)^2$, of the mass matrix squared $\mathcal{M}_{q_i}^{(1)}\mathcal{M}_{q_i}^{(1)\dagger}$ are assumed with $m_{q_i2}^{(1)} > m_{q_i1}^{(1)}$. The forms of the matrices $V_{q_iL}^{(1)}, V_{q_iR}^{(1)}$ are fixed by the eigenvectors of $\mathcal{M}_{q_i}^{(1)}\mathcal{M}_{q_i}^{(1)\dagger}$ simultaneously.

To conclude this chapter, we like to point out that the effects of brane local terms are manifested via altered form of the KK mode functions and their normalizations. KK Mass determining condition is drastically modified and non-trivial mixing effects are introduced. We expect that this may have implications at the LHC. In the following chapters we are going to address such issues systematically.

Chapter 3

The strongly interacting sector of the nmUED scenario

3.1 Introduction

In this chapter, we concentrate on the effects of the boundary localized kinetic terms (BLKTs) and the Yukawa terms (BLYTs) on the strongly interacting sector comprising of KK gluon and KK quarks and their basic phenomenology at the LHC. We confine ourselves only to the first KK level except for the top quark sector for which we briefly discuss some interesting aspects involving the second KK level. We also restrict our analysis to a common BLT term at the two orbifold fixed points for both gluon and the quarks thus preserving the KK-parity. The BLTs for these two sectors are expressed in terms of two (three, including BLYT which is important for the top quark sector) mutually independent parameters that serve as the only two (three) additional ones when compared to the mUED case. Our goal is to study the strong production of these KK excitations quantitatively, followed by a parton-level study of the final states with jets+leptons+$\not{E}_T$ arising from cascade decays. For this, we incorporate an electroweak sector which is mUED-like.

In order to carry out a parton-level study of the final states with jets+leptons+$\not{E}_T$ we incorporate an electroweak sector which is mUED-like.

Further, we do not consider the effect of radiative corrections to the KK masses thus leaving out Λ as a parameter. As we would see later in this chapter, BLTs can indeed generate much larger splitting among gluon and quarks at the first KK level than what radiative corrections could inflict in mUED, for a given value of R^{-1}. In that sense and in the spirit of ref. [83], this analysis has a complementary aspect to that in mUED. Hence, the scenario we work in has three relevant parameters: R^{-1}, r_G and r_Q, the latter two being the BLT parameters for the KK gluon and the quarks respectively (along with the

mass of the Higgs boson).

We observe that BLTs can indeed inflict major distortions in the mUED spectrum beyond recognition [64, 65]. On top of that, some of the crucial couplings involving the KK quarks, gluons and the electroweak gauge bosons are modified in a nontrivial way. This can not only alter the (mUED) expectations at the LHC in a characteristic way, but also could open up new possibilities. Thus, such a framework would provide a rather relaxed framework which can make the confusion among mUED, nmUED, and SUSY (and also possibly, T-parity conserving little Higgs models (see refs. [84, 85] and references therein) get more complete.

The chapter is organized as follows. In section 3.2 we derive the mass spectrum and the couplings and highlight their features by contrasting them with those in the mUED framework. The resulting phenomenology at the LHC is taken up in section 3.3 where we discuss in detail the production rates of the level-1 KK gluon and quarks and the decay branching fractions of the KK particles involved in the cascades as functions of the fundamental parameters of the framework. Situations in nmUED are studied with concrete examples to demonstrate the possibility of a near-complete faking from mUED and SUSY scenarios. Some characteristic discriminators that could partially alleviate the confusion under favourable conditions are also discussed with reference to various different final states at the LHC. In section 3.4 we conclude.

3.2 Mass spectrum and couplings

In this section we discuss the variations of the masses of the level-1 KK quarks and the KK gluon and the dependence of the strength of the interaction between them as a function of R^{-1} and parameters like r_G, r_Q and r_Y. For convenience, the latter three dimensionful parameters are rescaled in terms of R as shown below.

$$r'_G = r_G R^{-1}, \quad r'_Q = r_Q R^{-1}, \quad r'_Y = r_Y R^{-1}, \tag{3.1}$$

It is to be noted that, with this redefinition, the variables C, S and T in equations (2.34) now become functions of scaled mass parameters $M'_{G^{(n)}}$ ($M'_{Q^{(n)}}$) instead of $M_{G^{(n)}}$ ($M_{Q^{(n)}}$), respectively. We define and use these modified mass parameters in the subsections to follow.

3.2.1 Masses of level-1 KK gluon and quarks

From equations (2.35) one finds that KK masses of both level-1 gluon and quarks (from the first two generations) are governed by identical set of transcendental equations involving r'_G (for the KK gluon) and r'_Q (for the KK quarks). However, this statement is true only at the lowest order. Radiative corrections to various masses would be different but we will not consider such corrections in this thesis. The transcendental equations for the odd 'n' (for level-1 KK-gluon and quark) from expressions (2.35) and can be rewritten in terms of the scaled variables r'_G (r'_Q) and $M'_{G^{(1)}}$ ($M'_{Q^{(1)}}$) as follows

$$r'_X M'_{X^{(1)}} = 1/T_{X^{(1)}}, \tag{3.2}$$

where $M'_{X^{(1)}} = M_{X^{(1)}}/R^{-1}$ and X stands for G (gluon) and Q (quark). These transcendental equations are solved numerically for the KK masses of the level-1 KK gluon and quarks. The variations of the masses are plotted in figure 3.1 as a function of r'_X.

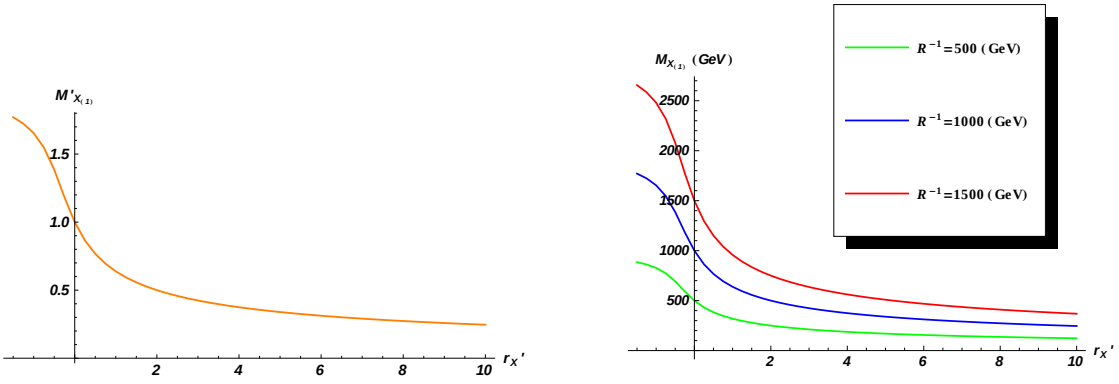

Figure 3.1: Ratio of actual KK mass of level-1 KK gluon/quark and R^{-1} (left panel) and the corresponding actual masses (right panel; for different values of R^{-1}) plotted against the parameter r'_X characterizing the brane-localized term. The trivial case of $M'_{X^{(1)}} = 1$ (left panel) or $M_{X^{(1)}} = R^{-1}$ (right panel) is retrieved when $r'_X = 0$.

By virtue of equation (3.2), this dependence is blind to R^{-1}. It is interesting to note that for $r'_X < 0$, $M'_{X^{(1)}} > 1$ signifying the actual KK mass to be larger than R^{-1}. The reverse is true for $r'_X > 0$. As we can see from this panel that the variation flattens up quickly with increasing r'_X. In the right panel of figure 3.1 we show the actual variations of KK masses (*i.e.*, of $M_{X^{(1)}}$) for level-1 KK gluon/quark for three given values of R^{-1}. This plot readily follows from the one in the left panel using the relation between $M_{X^{(1)}}$ and $M'_{X^{(1)}}$ as indicated above. This also reveals that a particular mass-value for the KK gluon (quark) could arise from different combinations of R^{-1} and r'_G (r'_Q) which is further

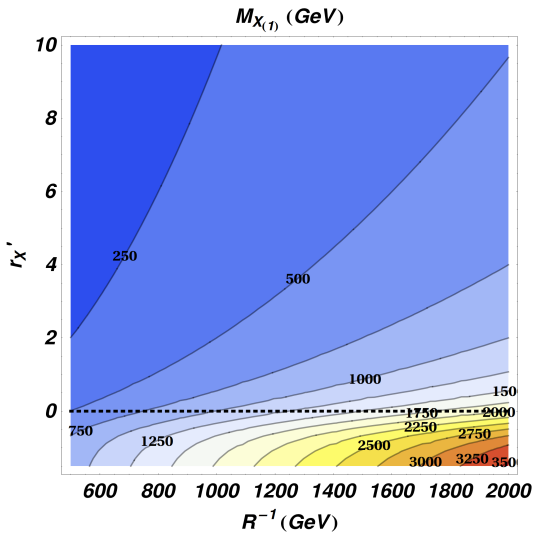

Figure 3.2: *IsoKKmass* (in GeV) contours for level-1 KK gluon/quark in the $R^{-1} - r'_X$ plane.

illustrated in figure 3.2 for a continuous range of R^{-1}. This leads us to explore the *isomass* contours in the $R^{-1} - r'_X$ plane as illustrated in figure 3.2. This shows clearly how similar values of KK masses can be obtained for different combinations of R^{-1} and r'_X. Note that the straight line represented by $r'_G, r'_Q = 0$ (parallel to the R^{-1}-axis) cuts the mass contours at values of R^{-1} equal to the mass-value of the contour. This is in conformity with figure 3.1.

We give a quantitative summary for the KK masses of level-1 KK gluon/quark in table 3.1 by providing some concrete numbers. $M'_{X^{(1)}}$ represents the solutions of equation (3.2) for reference input values of r'_X which are independent of R^{-1} (as discussed earlier in this subsection). The actual KK masses are simple products of $M'_{X^{(1)}}$ and R^{-1}. One such set of actual masses is shown for $R^{-1} = 1000$ GeV in table 3.1. In the above discussion we have taken a simplistic approach as far as the masses of the level-1 KK quarks are concerned. It should be kept in mind that the mass-eigenvalues of the KK quarks would be evaluated from $\mathcal{M}^{(1)}_{q_i}\mathcal{M}^{(1)\dagger}_{q_i}$ in equation (2.63). In general, the two eigenvalues are not degenerate because of the presence of non-vanishing overlap integrals like r'_{Q11}, R'_{Q11} *etc.* which are by themselves dimensionless and are also governed by dimensionless parameters like r'_Q, r'_Y, $M'_{Q^{(1)}}$ *etc.* When contrasted with mUED, this is a clear new feature appearing in the framework of UED with brane-localized terms. However, as can be seen from equation (2.63), the mass-splitting is proportional to the value of the corresponding zero-mode quark mass and thus negligible for the level-1 KK quarks from the first two generations. In this limit, the mass eigenvalues ($m^{(1)}_{q_{i(1,2)}}$) becomes identical to the KK mass

($M_{Q^{(1)}}$). On the contrary, $M_{G^{(1)}}$ corresponds to the physical mass of $G^{(1)}$.

r'_X	$M'_{X^{(1)}}$	$M_{X^{(1)}}$ (GeV) (for $R^{-1} = 1000$ GeV)
-1.5	1.771	1771
-1.0	1.654	1654
-0.5	1.386	1386
0.0	1.000	1000
0.5	0.767	767
1.0	0.638	638
2.0	0.500	500
5.0	0.339	339
10.0	0.246	246

Table 3.1: KK masses for level-1 KK gluon/quarks for varying r'_X and for $R^{-1} = 1000$ GeV.

The phenomenon is not quite unexpected though since the effect under consideration originates in the Yukawa sector of the theory. Thus, such an effect will be appreciable for only the KK top quarks and to a far lesser extent for the KK bottom quarks. In the left plot of figure 3.3 we illustrate the effect for the lighter top quark with the help of *isomass* contours that show significant, nontrivial dependence of the mass on r'_Y in addition to that on r'_Q for a given value of R^{-1} (= 1000 GeV). The right panel of figure 3.3 is for the case of lighter level-1 KK bottom quark. This one clearly reveals that for level-1 KK quarks corresponding to the lighter SM quarks, the dependence of their masses on r'_Y is small. Thus, these two plots collectively help one estimate the quantitative role of r'_Y in the phenomenon.

As discussed in the beginning of section 2.6.3, at around $r'_Y = -\pi/2$ the values of r'_{Q11}, R'_{Q11} rise sharply and get divergent. In both plots of figure 3.3, this results in a thin strip of region about this value of r'_Y over which there is no physical solution. Further, as mentioned at the end of section 2.6.3, because of the extremal situation it can lead to, r'_Y close to its limiting value of $-\pi/2$ can have non-trivial bearing even on the properties of the KK quarks of light flavours, at least, in principle.

Further, the possibility of level-mixing between similar KK-parity states driven by the brane-localized Yukawa term emerges as an interesting feature of the top quark sector whose phenomenology could be rather rich in such a scenario. Our preliminary inves-

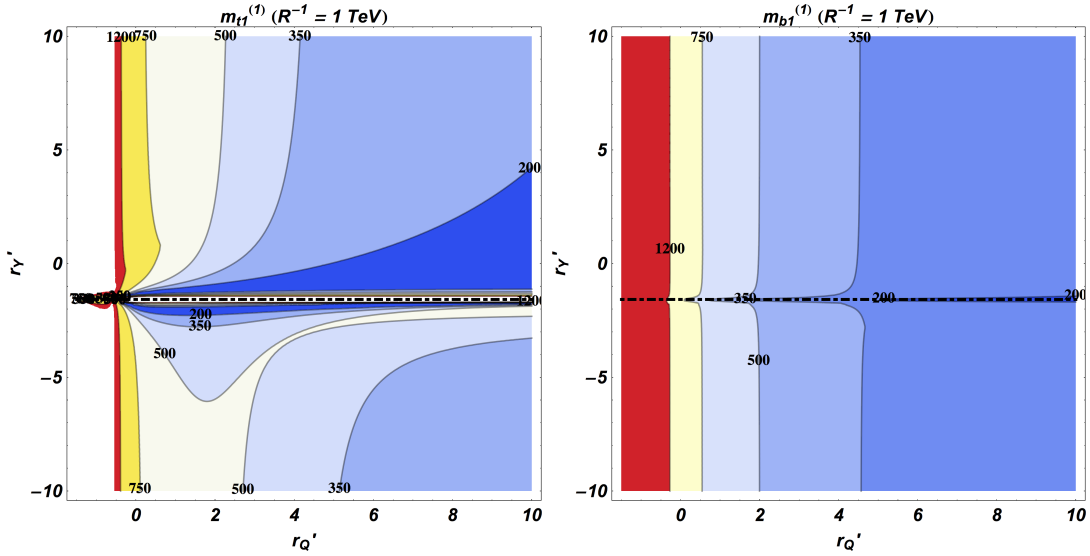

Figure 3.3: Isomass contours for the light level-1 top quark (left) and the light level-1 bottom quark (right) for $R^{-1} = 1000\,\text{GeV}$ in the $r_Q' - r_Y'$ plane.

tigation into the subject reveals that mixing between level-0 and level-2 top quarks can be *a priori* significant. Such a mixing could potentially trigger an appreciable shift in the mass of the level-2 top quark and make the same phenomenologically interesting at the LHC. Moreover, as could be expected, the SM top mass receives contribution from such a mixing. Thus, refined experimental estimates of the mass of the SM top quark from Tevatron [86] and the LHC [87] would inevitably constrain the parameters of the nmUED scenario we are considering here. We will study the KK top quark sector including the role of level mixing in the next chapter 4.

3.2.2 Interactions involving level-1 KK gluons and quarks

In this subsection we discuss the other important aspect of the framework, *viz.*, the couplings involving the KK gluon and KK quarks. Here again, we limit ourselves only to the first KK level.

$4D$ QCD coupling g_{4s} is defined as

$$g_{4s} \equiv N_{G_{(0)}} g_{5s} = \frac{g_{5s}}{\sqrt{2r_G + \pi R}}. \tag{3.3}$$

Quartic interaction involving four level-1 KK gluons is somewhat non-trivial and gets modified by the presence of brane-localized terms. However, it is rather inconsequential for LHC phenomenology and hence we do not discuss this any further. All other self-

coupling terms involving level-1 KK gluon and SM gluon (both 3-point and 4-point ones) remain the same as in mUED.

Next, we turn to the case of the interaction involving a level-1 KK gluon and a level-1 KK quark along with an (level-0) SM quark. Here we comment on the forms of the bi-unitary matrices $V^{(1)}_{q_iL}$ and $V^{(1)}_{q_iR}$ that diagonalize the mass matrix for level-1 KK quarks where 'i' refers to the quark-flavour. For (almost) mass-degenerate KK quarks (in the limit of $r'_Q = r'_Y$ which we adopt for studying the KK quarks corresponding to lighter SM flavours), $V^{(1)}_{q_iL}$ and $V^{(1)}_{q_iR}$ can be shown, to a very good approximation, to have the following form that reflects maximal mixing:

$$V^{(1)}_{q_iL} = V^{(1)}_{q_iR} \approx \begin{bmatrix} -\text{sgn}(r'_Q)\cos\left(\frac{\pi}{4}\right) & \sin\left(\frac{\pi}{4}\right) \\ -\text{sgn}(r'_Q)\sin\left(\frac{\pi}{4}\right) & -\cos\left(\frac{\pi}{4}\right) \end{bmatrix}, \tag{3.4}$$

except for the case of $r'_Q = 0$.[1] In the case of conventional UED scenarios without brane-localized terms, one finds the mass-eigenvalues to be exactly degenerate (before radiative correction to the masses) and these matrices look like:

$$V^{(1)}_{q_iL}|_{\text{mUED}} = \begin{bmatrix} \cos(\theta^{(1)}_{q_i}) & \sin(\theta^{(1)}_{q_i}) \\ -\sin(\theta^{(1)}_{q_i}) & \cos(\theta^{(1)}_{q_i}) \end{bmatrix}, \quad V^{(1)}_{q_iR}|_{\text{mUED}} = \begin{bmatrix} \cos(\theta^{(1)}_{q_i}) & -\sin(\theta^{(1)}_{q_i}) \\ \sin(\theta^{(1)}_{q_i}) & \cos(\theta^{(1)}_{q_i}) \end{bmatrix}, \tag{3.5}$$

which include chiral rotation and the mixing angle $\theta^{(1)}_{q_i}$ is fixed by

$$\sin(2\theta^{(1)}_{q_i}) = \frac{m_{q_i}}{\sqrt{M^2_{Q_{(1)}} + m^2_{q_i}}}, \quad \cos(2\theta^{(1)}_{q_i}) = \frac{M_{Q_{(1)}}}{\sqrt{M^2_{Q_{(1)}} + m^2_{q_i}}}, \tag{3.6}$$

where m_{q_i} is the mass of the 'i' th flavour SM quark. The difference in form of the matrices presented in equations (3.4) and (3.5) owes its origin to the difference between 'approximate degeneracy' and 'exact degeneracy' of the mass-eigenvalues of the quarks. Further, it may be noted that for the five light flavours, $M_{Q^{(1)}} \gg m_{q_i}$. Thus, use of equation (3.6) reduces equation (3.5) to the following trivial form:

$$V^{(1)}_{q_iL}|_{\text{mUED}} = V^{(1)}_{q_iR}|_{\text{mUED}} = \begin{bmatrix} 1 & 0 \\ 0 & 1 \end{bmatrix} \quad (\textit{i.e.}, \theta^{(1)}_{q_i} = 0), \tag{3.7}$$

whose form is different from that of equation (3.4).

[1] This general form of the matrix is used in our subsequent analysis. It should be noted that this expression is qualitatively different from its mUED counterpart for which it is an unit matrix (see equation (3.7)) and this cannot be seen as a limiting case (*i.e.*, $r'_G = r'_Q = 0$) of the former.

Using equation (2.23), the 4D effective action depicting the quark-gluon interaction up to the first KK level can be written down as follows:

$$S_{\text{quark}|\text{int}} = \int d^4x \sum_i \Bigg\{ g_{4s} T^a \Bigg[G_\mu^{a(0)} \Big(\overline{q}_i^{(0)} \gamma^\mu q_i^{(0)} + \overline{\mathcal{Q}}_{i1}^{(1)} \gamma^\mu \mathcal{Q}_{i1}^{(1)} + \overline{\mathcal{Q}}_{i2}^{(1)} \gamma^\mu \mathcal{Q}_{i2}^{(1)} \Big)$$
$$+ G_\mu^{a(1)} (g'_{G_1 Q_1 Q_0}) \Bigg(\overline{q}_i^{(0)} \gamma^\mu \left(v^{(1)}_{q_i R(21)} P_R + v^{(1)}_{q_i L(11)} P_L \right) \mathcal{Q}_{i2}^{(1)} + \overline{q}_i^{(0)} \gamma^\mu \left(v^{(1)}_{q_i R(22)} P_R + v^{(1)}_{q_i L(12)} P_L \right) \mathcal{Q}_{i1}^{(1)}$$
$$+ \overline{\mathcal{Q}}_{i2}^{(1)} \gamma^\mu \left(v^{(1)}_{q_i R(21)} P_R + v^{(1)}_{q_i L(11)} P_L \right) q_i^{(0)} + \overline{\mathcal{Q}}_{i1}^{(1)} \gamma^\mu \left(v^{(1)}_{q_i R(22)} P_R + v^{(1)}_{q_i L(12)} P_L \right) q_i^{(0)} \Bigg) \Bigg] \Bigg\}, \tag{3.8}$$

where the superscripts $0, 1$ in parenthesis indicate the KK level. $\mathcal{Q}_{1,2}$ represent the quark mass-eigenstates at the first KK level, i is the generic flavour-index and v_q-s are the elements of the V_q matrices in equations (2.64), (3.4). The latter can now be rewritten in the following general form:

$$V_{q_i L}^{(1)} = \begin{bmatrix} v^{(1)}_{q_i L(11)} & v^{(1)}_{q_i L(12)} \\ v^{(1)}_{q_i L(21)} & v^{(1)}_{q_i L(22)} \end{bmatrix}, \quad V_{q_i R}^{(1)} = \begin{bmatrix} v^{(1)}_{q_i R(11)} & v^{(1)}_{q_i R(12)} \\ v^{(1)}_{q_i R(21)} & v^{(1)}_{q_i R(22)} \end{bmatrix}. \tag{3.9}$$

The first term in equation (3.8) gives the usual interaction of the SM gluon with a pair of SM quarks. The next two terms give the interactions of the SM gluon with two different pairs of mass-eigenstates of level-1 KK quarks and these are identical to their mUED counterparts. This is because they are governed by the overlap integral

$$\int_{-L}^{L} dy \Big(1 + r_Q \left(\delta(y - L) + \delta(y + L) \right) \Big) f_{G^{(0)}} f_{Q^{(1)}} f_{Q^{(1)}}, \tag{3.10}$$

which reduces to $f_{G^{(0)}} (= N_{G^{(0)}}$, the normalization factor in equation (3.3)) by virtue of the manifest identity in equation (2.36). The only deviation that occurs is in the case of an SM quark interacting with a level-1 KK quark and a level-1 KK gluon. The concrete form of the deviation (with respect to the mUED case) can be shown to be as in equation (3.11).

$$g'_{G_1 Q_1 Q_0} \equiv \frac{1}{N_{G(0)}} \int_{-L}^{L} dy \Big(1 + r_Q \left(\delta(y - L) + \delta(y + L) \right) \Big) f_{G^{(1)}} f_{Q^{(1)}} f_{Q^{(0)}}$$
$$= \frac{N_{Q^{(0)}}}{N_{G^{(0)}}} \frac{N_{G^{(1)}} N_{Q^{(1)}}}{S_{G^{(1)}} S_{Q^{(1)}}} \Big[2 r_Q S_{G^{(1)}} S_{Q^{(1)}} - \frac{\sin((M_{Q^{(1)}} + M_{G^{(1)}}) \frac{\pi R}{2})}{M_{Q^{(1)}} + M_{G^{(1)}}} + \frac{\sin((M_{Q^{(1)}} - M_{G^{(1)}}) \frac{\pi R}{2})}{M_{Q^{(1)}} - M_{G^{(1)}}} \Big]. \tag{3.11}$$

The factor $g'_{G_1 Q_1 Q_0}$ is dimensionless and hence does not depend upon R^{-1} which is a dimensionful parameter. In fact, $g'_{G_1 Q_1 Q_0}$ is implicitly governed by the dimensionless parameters r'_G and r'_Q through the variables appearing in equation (3.11). This is a rather

complicated dependence and its concrete profile has a rich structure as shown in figure 3.4. In the limit $r_G = r_Q$, it can be shown that $g'_{G_1Q_1Q_0} = 1$ which is the mUED.

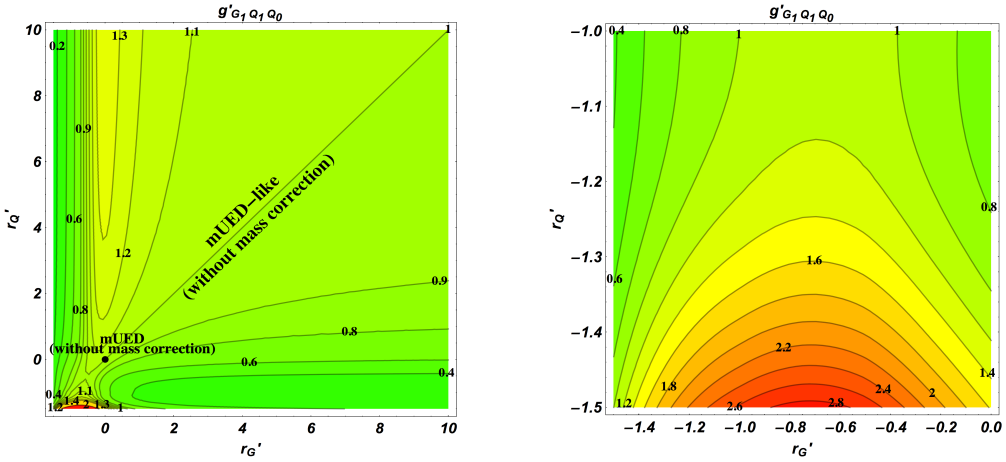

Figure 3.4: Contours of deviation in $G_1Q_1Q_0$ coupling in nmUED with respect to the mUED case: over larger ranges of values for r'_G and r'_Q (left) and a zoomed up view over ranges of negative values for both (right) with interesting variations. Note that $r'_{G_{min}} = r'_{Q_{min}} = -1.5$ for these plots. This is somewhat above the theoretical minimum of $-\frac{\pi}{2}$ for both the parameters for which the scenario becomes unphysical (see text for details).

In figure 3.4 we present the contours of the deviation factor $g'_{G_1Q_1Q_0}$ presented in equation (3.11) in the $r'_G - r'_Q$ plane. The figure on left illustrates the contours over larger ranges of values for r'_G and r'_Q. It is to be noted that along its diagonal ($r'_G = r'_Q$) the deviation is exactly equal to 1 implying the coupling to be equal to that in the mUED.[2] The coupling has a much richer structure at very low values of r'_G and r'_Q close to the origin of the figure (indicated by blots in red and yellow) as both parameters approach their limiting value of $-\frac{\pi}{2}(\simeq -1.56)$. This is perhaps best understood if we just look at the form $\frac{N_{Q^{(0)}}}{N_{G^{(0)}}}$ in equation (3.11) for which both $N_{Q^{(0)}}$ and $N_{G^{(0)}}$ blow up at the said value. A closer look into this region is offered by a zoomed-up view in the right frame of figure 3.4.

To probe further into the generic aspects of correlated variations of the KK masses and the deviations in coupling from the mUED value, it would be useful to follow up with a study showing their mutual variation. This is pertinent since, as indicated above, the masses of the KK-quark and KK-gluon (we restrict ourselves to level-1 KK excitations only) are also functions of r'_G and r'_Q as does the deviation-factor. The only difference is

[2]The scenarios residing on the diagonal thus have degenerate KK masses which are different from those expected in a UED scenario without BLT (loosely indicated as mUED in the plot) for any given value of R^{-1}. We already assumed that in general, BLTs contribute dominantly to the KK masses when compared to the radiative corrections. The mUED scenario is defined only with the latter ones. Hence, on the diagonal, the scenarios are "mUED-like".

that while the masses do vary with R^{-1}, the deviation-factor does not.

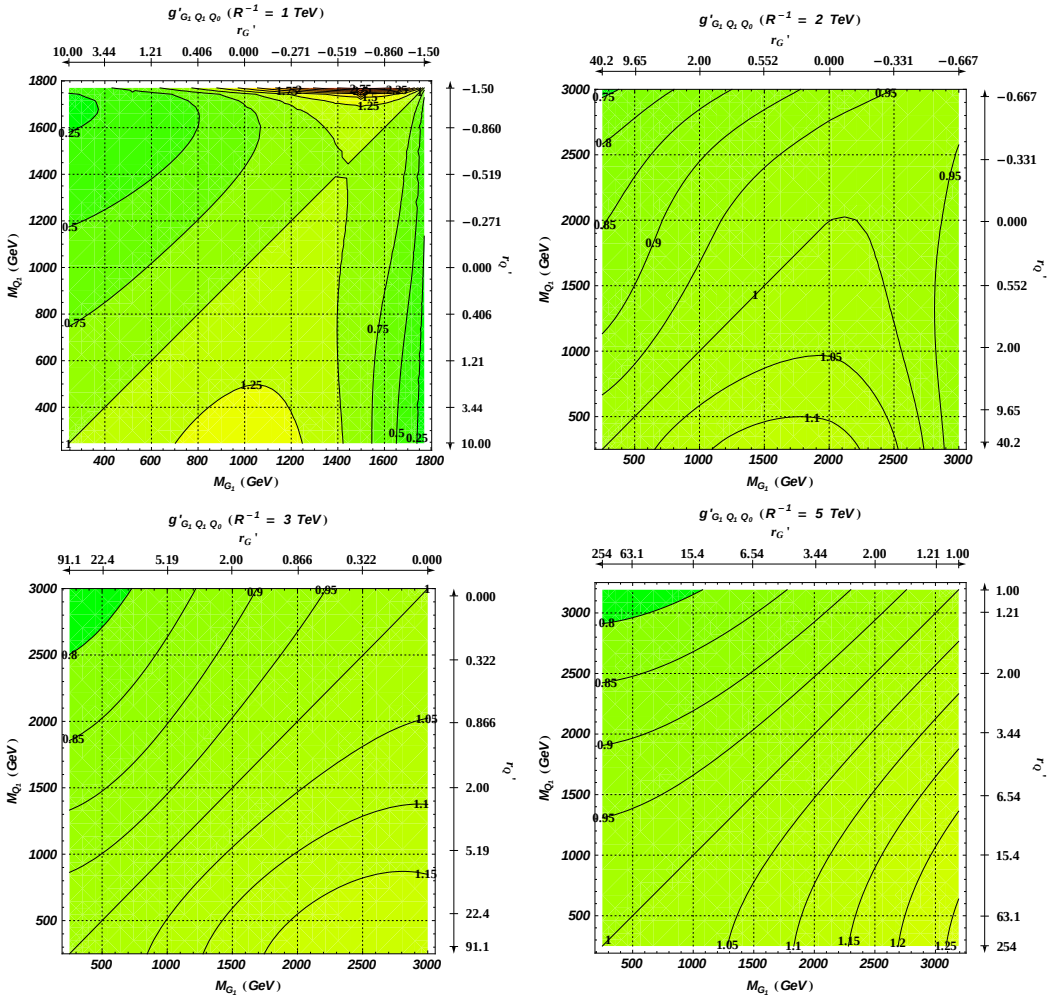

Figure 3.5: Contours of the coupling deviation-factor $g'_{G_1Q_1Q_0}$ in the $M_{G^{(1)}} - M_{Q^{(1)}}$ (KK) mass-plane for $R^{-1} = 1$ TeV (top, left), $R^{-1} = 2$ TeV (top, right), $R^{-1} = 3$ TeV (bottom, left) and $R^{-1} = 5$ TeV (bottom, right).

Thus, analogous to figure 3.4, contours of fixed deviations in the couplings can be drawn but this time in the $M_{G^{(1)}} - M_{Q^{(1)}}$ plane with R^{-1} as a parameter. Such variations are shown in figure 3.5. In the top panel of figure 3.5, from left to right, we present the case of $R^{-1} = 1$ TeV and 2 TeV while in the bottom panel the corresponding ones illustrate the cases for $R^{-1} = 3$ TeV and 5 TeV, respectively. In order to facilitate the correspondences between the brane parameters and the masses of the respective excitations for different values of R^{-1}, the ranges of r'_G (along the abscissa) and r'_Q (along the ordinate) are indicated on the top and the right of each of these plots. In both cases, the diagonal represents the contour for $g'_{G_1Q_1Q_0} = 1$. Under the hood, the geometrical origin of the diagonal has a

common thread to that in the left panel of figure 3.4, *i.e.*, for $r'_G = r'_Q$, although the ranges considered for them are different from the earlier case. The small region in yellow and red close to the top-right corner of the top-left plot in figure 3.5 corresponds to the bottom-left corner of the left plot in figure 3.4.

For figure 3.5, the criteria for choosing the mass-ranges for the level-1 gluon and quarks are, in turn, primarily based on the tentative reach of LHC ($\sim$ 3 TeV) running at the center of mass energy of 14 TeV and then, choosing not too large values of r'_G and r'_Q for different values of R^{-1} considered for these plots. Recall that, in this scenario, equal values of $M_{G^{(1)}}$ and $M_{Q^{(1)}}$, for a given R^{-1} result from equal values of r'_G and r'_Q, respectively. Thus, as is clearly seen from figure 3.5, degenerate masses occur along the diagonal. As pointed out in the context of figure 3.4, here also, by the same token, mUED-like scenarios live close along the diagonals.

Figure 3.5 tells us that different combinations of masses for level-1 gluon and level-1 quarks would correspond to very specific values of the deviation-factor for the modified coupling. The deviation can go either way, *i.e.*, $g'_{G_1Q_1Q_0} \gtrless 1$. However, the correspondence between masses and the deviation in coupling is specific to the value of R^{-1}, as can be understood by comparing the plots presented in figure 3.5. We like to emphasize that this correspondence, in principle, could be exploited at the LHC to extract information on the parameters of the scenario. For example, if the masses in context can be known and the relevant cross sections can be estimated from the data, these could be used to determine the deviation in coupling.[3] Since this deviation, when combined, with the information on the masses, has a unique relationship to R^{-1} in the current scenario, the latter can also be determined subsequently. The information thus obtained on R^{-1}, in turn, can be employed to determine the values of r'_G and r'_Q since these determine the masses which are, by now, known.

To be convinced that such an approach would work, one has to demonstrate quantitatively that the value of R^{-1} can be estimated reasonably correctly. There are *prima facie* evidence that such an estimate would be unambiguous. This follows from the observation that neither the $g'_{G_1Q_1Q_0}$ contours in figure 3.4 nor the same in figure 3.5 intersect each

[3]Extracting a somewhat precise information about the deviation in coupling could be a challenging task at a hadron collider. This is because any attempt to understand this from a total yield (where all production processes contribute) would inevitably involve the decay-patterns of the originally produced new-physics excitations. Extracting some concrete information from within such a milieu requires further assumptions over the scenario and thus, the exercise may become heavily 'model-dependent'. However, the situation is expected to be much under control in an extremely constrained scenario like the mUED where the production cross sections could very well be related to the decay-patterns of the produced particles. This is the case with us since we are trying to measure a deviation of the coupling from its mUED value.

other.

$g'_{G_1Q_1Q_0}$	R^{-1} (TeV)	$M_{G_{(1)}}$ (GeV)	$M_{Q_{(1)}}$ (GeV)
0.85	2	835.1	2724.3
	3	840.9	2407.6
	5	1246.1	2819.1
1.1	2	1820.0	500.0
	3	2019.5	1036.0
	5	2121.7	989.6

Table 3.2: (KK)-mass-values for level-1 KK gluon/quark in nmUED for varying two representative values of $g'_{G_1Q_1Q_0}$ and for varying R^{-1}. The choice of values for $g'_{G_1Q_1Q_0}$ is motivated by figure 3.5.

In table 3.2 we demonstrate the situation with some actual numbers for two different values of $g'_{G_1Q_1Q_0}$ which one might be able to extract from experiments. The number presented in the table are picked up directly from the contour-plots in figure 3.5. Note that the values 0.85 and 1.1 that are chosen for $g'_{G_1Q_1Q_0}$ in table 3.2 could result in $\sim 50\%$ deviations from the nominal values of the cross sections (which go as $g'^4_{G_1Q_1Q_0}$) for the strong production modes at the LHC. This kind of a departure can be expected to be measured efficiently enough and thus can be used for further inferences. It is then informative to find from table 3.2 that for an experimentally estimated value of $g'_{G_1Q_1Q_0}$ and for a known set of masses for the KK gluon and KK quarks, the value of R^{-1} is pretty distinct and thus can be estimated unambiguously.

3.3 Phenomenology at the LHC

In this section we discuss the cross sections of the level-1 KK gluon ($G^{(1)}$) and quarks ($Q^{(1)}$) of the nmUED scenario produced via strong interaction at the LHC. Hereafter, we use simplified notations, m_{G^1} and m_{Q^1}, to denote the physical masses of the level-1 KK gluon and quarks, respectively. The patterns are explained by relating them to the features of the scenario as discussed in detail in sections 3.2.1 and 3.2.2. We then proceed to contrast the production-rates with the corresponding ones from mUED and SUSY. We also discuss at length the overall implications of such an nmUED scenario whose signals can be faked by the latter two.

3.3.1 Production cross sections for level-1 KK gluon and quarks

In figures 3.6 and 3.7 we present the cross sections for different final states for the 8 TeV and 14 TeV runs of the LHC, respectively, in the $r'_G - r'_Q$ plane. Results for generic final states like G_1G_1, G_1Q_1 and Q_1Q_1 are laid out in separate columns (from left to right) while separate rows are used to present the results for $R^{-1} = 1$ TeV, 3 TeV and 5 TeV (from the top to the bottom). The final state indicated by G_1Q_1 includes contributions from both G_1Q_1 and $G_1\bar{Q}_1$ while under Q_1Q_1 we combine the rates from Q_1Q_1, $Q_1\bar{Q}_1$ and $\bar{Q}_1\bar{Q}_1$. The rates include contributions from five flavours of level-1 KK quarks that correspond to five light SM quarks. For these states, as pointed out in sections 3.2.1 and 3.2.2, the role of r'_Y is not significant except for some extremal cases, *e.g.*, when $r'_Y \gg 1$, for smaller R^{-1}. Hence, we adopt a simplifying scheme where we set $r'_Q = r'_Y$ while analyzing these excitations at the LHC. Also, the contributions from both $SU(2)$-doublet and $SU(2)$-singlet varieties of KK quarks are included.

The cross sections are calculated using MadGraph-5 [88] in which the strongly interacting sector of the scenario is implemented through FeynRules [89] via its UFO (Universal FeynRules Output) [90, 91] interface. The mUED implementation [61] of CalcHEP [92] has been used for cross checks in appropriate limits and for some actual computation of cross sections in mUED. We used CTEQ6L [93] parametrization for the parton distribution function. The factorization/renormalization scale is fixed at the sum of the masses of the final-state particles. In the remaining part of this chapter, we refer only to the physical masses m_{Q^1}. These are the degenerate mass-eigenvalues obtained by diagonalizing the KK quark mass-matrix in the presence of brane-localized Yukawa terms and practically same as the KK masses for the light quark flavours.

Some features common to both figures 3.6 and 3.7 are as follows:

- the maximum value of the mass for the level-1 KK gluon and quarks considered for $\sqrt{s} = 8$ TeV (14 TeV) run of the LHC is 2 TeV (3 TeV) which happens to be the tentative (perhaps, optimistic) reach of LHC running at this center of mass energy. The conservative lower limit of the masses that has gone into the analysis is 500 GeV,

- for given values of R^{-1}, the various ranges of r'_G and r'_Q in different rows ensure m_{G^1} and m_{Q^1} in the above-mentioned ranges,

- to capture cross-sections varying over orders of magnitude, the contours are drawn after taking the logarithm (to base 10) of the cross sections. We, thus, encounter

negative-valued contours in these figures,

- for final states containing one or more level-1 KK quark (the second and the third columns), the contour values, (*i.e.*, the cross sections) rise along the diagonal connecting the bottom-left and the top-right corners of the plots. This can be understood in terms of decreasing m_{G_1} and m_{Q_1} as both r'_G and r'_Q increase in that direction,

- the variation in the G_1G_1 production (the first column) has a curious trend when compared with the final-states having Q_1. The parallel, vertical stripes (except in some region with $r'_G,\, r'_Q < 0$ only for low R^{-1} ($\sim$ 1 TeV)) imply that the cross-sections almost do not vary with r'_Q. This means they are insensitive to variations in m_{Q_1}. This is because the event rate for this final state is dominated by the s-channel (gluon-fusion) subprocess where Q_1 plays no role unlike in the t-channel where the latter can appear as a propagator. Hence, we see a gradual, steady increase in rates only with increasing r'_G, *i.e.*, with decreasing m_{G_1} which is quite expected.

- the local dependence of the G_1G_1 rate on r'_Q, for $r'_G,\, r'_Q < 0$ and $R^{-1} \sim 1$ TeV, shows a different trend. In this region (from the deep blue to the white passing through the light blue region), the rate grows in a direction of increasing m_{Q_1} which is somewhat not so intuitive. It is instructive to observe that for such a region, m_{G_1} also turns out to be relatively heavy (since, $r'_G < 0$). Our probe into the phenomenon revealed that over this region the t-channel contribution becomes important[4] and the relative values of m_{G_1} and m_{Q_1} are such that a perceptible destructive interference takes place between s and t channels. Note also that with $g'_{G_1Q_1Q_0}$ getting extremally large over this region (see figure 3.4) of the parameter space, the overall situation gets further compounded,

- the explanation holds for any final state that receives significant contributions from subprocesses initiated by gluon(s). Thus, it is not unexpected that rates for G_1Q_1 final state show a similar behaviour in the said region of the parameter space while the same for the level-1 quark-pair final state, dominated by Q_1Q_1 (which is not gluon-induced), though rich in feature, do not show such a trend very clearly,

- for the Q_1-pair final state, one finds that in the region of low r'_Q (< 0) the contours of larger cross sections reappear as one goes further down in r'_Q. This seems to

[4]Presumably, this happens since a larger m_{G_1} requires a larger $\sqrt{\hat{s}}$, in turn resulting in a lower partonic flux for the gluon in the protons that ultimately results in a suppressed contribution from the s-channel.

be a result of extremally large value of $g'_{G_1Q_1Q_0}$ which can be understood from the region shaded in red in the right plot of figure 3.4. Closer inspection reveals that the small, yellow contour at the bottom of these plots exactly correspond to the region of parameter space shaded in red in figure 3.4. In this region, naively, the boost in cross section can be up to a factor $g'^4_{G_1Q_1Q_0}$ which turns out to be ≈ 30,

- as we go from G_1G_1 production to Q_1Q_1 production passing through G_1Q_1 production the contours get flattened up in an anti-clockwise direction. This is easy to understand in terms of an increased dependence of the rates on m_{Q_1} and hence, on r'_Q,

- it may be noted that in the top panel of both figures 3.6 and 3.7 (with $R^{-1} = 1$ TeV) the cross sections are not actually defined along the straight line with $r'_Q = 0$. This is because some elements of the matrix in equation (3.4) which enter the involved couplings for these final states are not defined at $r'_Q = 0$,

- negative values of r'_G and r'_Q are not considered for R^{-1}=3 TeV and 5 TeV cases since these take m_{G_1} and m_{Q_1} far above the LHC reach. Thus, as we do not enter the "exotic" part of the parameter space (with both r'_G, $r'_Q < 0$), we do not see any special variation in the contour-patterns at lower values of r'_G and r'_Q.

The only major difference of a generic nature that we see between the results presented in figures 3.6 ($\sqrt{s} = 8$ TeV) and 3.7 ($\sqrt{s} = 14$ TeV) is that for similar values of r'_G and r'_Q, *i.e.*, for similar values of m_{G_1} and m_{Q_1} for a given R^{-1}, the rates are higher for the 14 TeV run, as expected.

mUED Parameters		$R^{-1} = 1000$ GeV, $\Lambda R = 10$					
mUED/SUSY Mass (in GeV)		$m_{G_1/\tilde{g}}$= 1220 $m_{Q_1^D,\tilde{q}_L}$= 1154 $m_{Q_1^S,\tilde{q}_R}$= 1133					
		Cross sections (in pb)					
Final states		G_1G_1	G_1Q_1	$G_1\bar{Q}_1$	Q_1Q_1	$\bar{Q}_1\bar{Q}_1$	$Q_1\bar{Q}_1$
mUED		0.216	1.250	0.082	1.132	0.009	0.403
nmUED	R^{-1}=700 GeV r'_G =-1.34 $r'_Q = r'_Y$ =-0.90 $g'_{G_1Q_1Q_0}$=0.627	0.178	0.503	0.032	0.177	0.001	0.173
	R^{-1}=1000 GeV r'_G =-0.30 $r'_Q = r'_Y$ =-0.19 $g'_{G_1Q_1Q_0}$=1.035	0.172	1.349	0.085	1.277	0.009	0.432
	R^{-1}=1500 GeV r'_G=0.37 $r'_Q = r'_Y$ =0.54 $g'_{G_1Q_1Q_0}$=1.033	0.173	1.364	0.086	1.303	0.010	0.438
	R^{-1}=2000 GeV r'_G=1.15 $r'_Q = r'_Y$ =1.43 $g'_{G_1Q_1Q_0}$=1.026	0.171	1.336	0.084	1.262	0.009	0.427
	R^{-1}=2500 GeV r'_G=2.13 r'_Q=r'_Y =2.56 $g'_{G_1Q_1Q_0}$=1.019	0.172	1.326	0.083	1.233	0.009	0.421
SUSY (MSSM)		0.019	0.181	0.012	0.153	0.001	0.054

Table 3.3: Comparison of the cross sections in mUED, nmUED and SUSY (MSSM) scenarios for similar spectra at the LHC with $\sqrt{s} = 14$ TeV. In mUED the spectrum is generated for a given R^{-1} (1 TeV). In nmUED matching spectra are generated by varying R^{-1} and tuning the values of r'_G and r'_Q simultaneously while keeping $r'_Y = r'_Q$. For SUSY, the masses of the corresponding excitations (indicated clearly against the mass variables) are tuned to similar values by varying the soft SUSY breaking parameters appropriately. CTEQ6L parton distribution functions are used and the renormalization/factorization scale is set at the sum of two final state masses.

3.3.2 mUED vs nmUED vs SUSY

In this subsection we take up the interesting possibility of mUED and nmUED faking each other and faking SUSY as well. This is reminiscent of the possibility of UED faking SUSY [94] where one talks about a situation in which the final state masses happen to be consistent with a mUED-like spectrum [65, 95]. There, SUSY being a less constrained scenario, this is the natural set up to study its faking by mUED. Thus, with more free parameters in the scenario, nmUED may enjoy a more direct parallel to SUSY when being compared with mUED.[5]

In table 3.3 we compare the cross sections for the production of level-1 KK gluon and quarks for the $\sqrt{s} = 14$ TeV LHC run in the mUED and nmUED scenarios. Assuming that the ballpark values of the masses of these excitations could be anticipated once a positive signal is found at the LHC, we fix these masses to carry out the analysis.

The reference values for the masses employed in table 3.3 are $m_{G_1} = 1220$ GeV, $m_{Q_1^D} = 1154$ GeV and $m_{Q_1^S} = 1133$ GeV. These are obtained in the mUED scenario by setting $R^{-1} = 1000$ GeV and $\Lambda R = 10$. For the nmUED scenario, we require the level-1 gluon mass to be the same as in the case of mUED while for the doublet and singlet KK quarks we take a common value which is almost equal to the singlet one in mUED. Note that, in the absence of radiative corrections, the masses of the doublet and singlet KK quarks are the same in the nmUED scenario under consideration and both are determined by the brane-localized parameter r'_Q. Such an nmUED spectrum is generated for different R^{-1} by suitably tuning the brane-localized parameters r'_G and r'_Q.

A priori, a comparison of cross sections from the two scenarios having similar spectrum assumes a special significance since the brane-localized parameters, r'_G and r'_Q, not only control the KK masses but also affect their couplings. These are discussed in sections 3.2.1 and 3.2.2 with illustrations (see figures 3.4 and 3.5). It can be gleaned from table 3.3 that except for the case where $R^{-1}_{mUED} > R^{-1}_{nmUED}$ with $R^{-1}_{nmUED} = 700$ GeV and leaving out the G_1-pair final state, the cross sections for the rest are within $\sim 10\%$ of the corresponding mUED values. For these cases, the reason of such a closeness in cross sections can be understood in terms of the small deviation of the strong coupling from the mUED case which is quantified by $g'_{G_1Q_1Q_0}$ and indicated in column 2. The smallness of the deviation

[5] Going one step further, it may be said that faking between UED and SUSY tend to get more complete [64,65] with an nmUED-type scenario for which the masses of the KK excitations may take almost any arbitrary values. In this sense, it may be interesting to note the apparent contrast in the naming schemes for scenarios in SUSY and those involving a UED framework. In the case of SUSY, the minimal version is the least constrained one (with too many free parameters) while the same for UED is the one which is its most constrained incarnation with only two (three, with level-0 Higgs mass parameter) parameters.

in $g'_{G_1Q_1Q_0}$ is ensured by the requirement of near-identical values of r'_G and r'_Q in nmUED that reproduce the characteristic splitting between the masses of the KK gluon and the quarks in mUED.

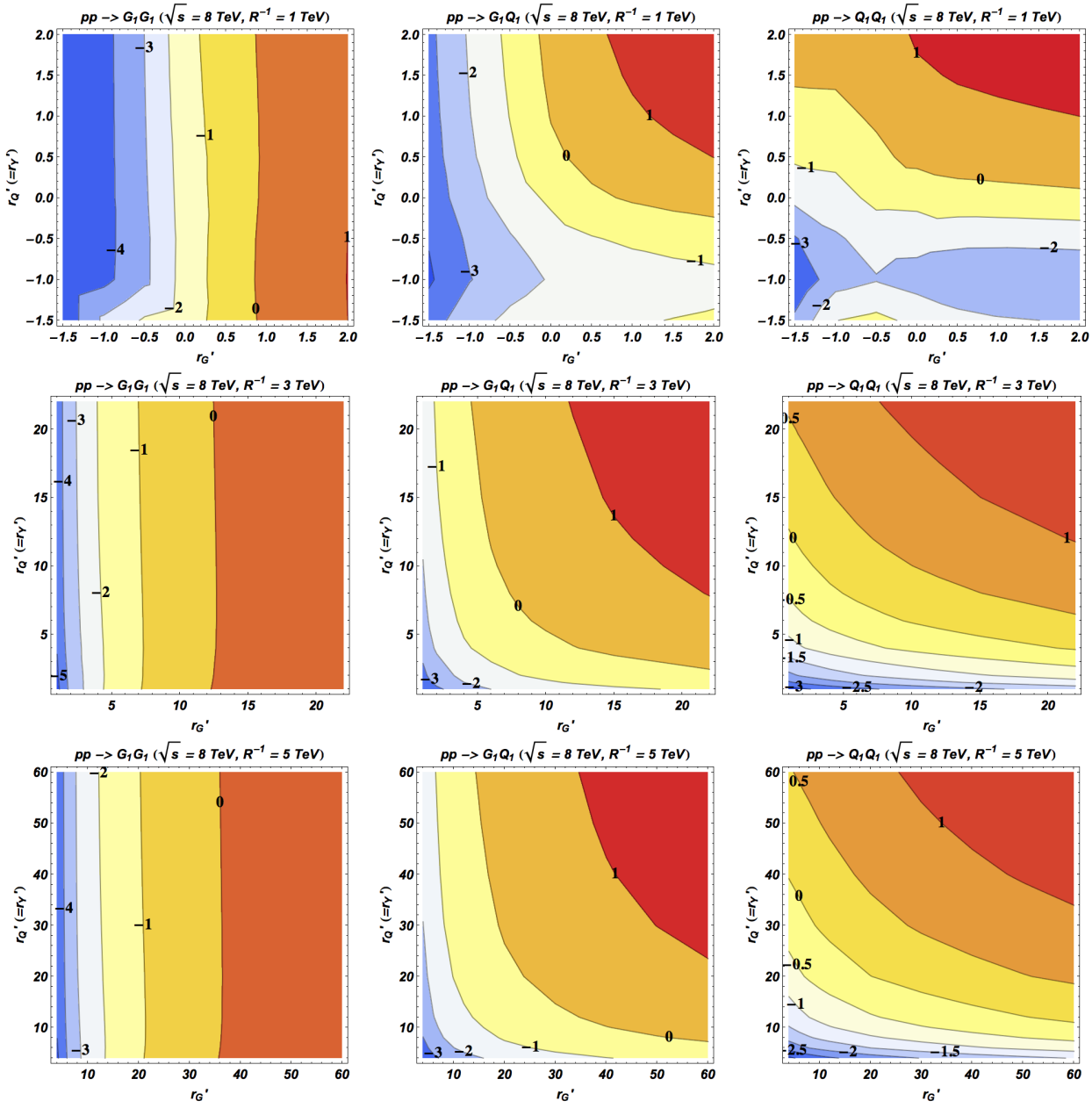

Figure 3.6: Log-valued (to base 10) cross section (in pb) contours for different final states at the LHC for $\sqrt{s} = 8$ TeV in the $r'_G - r'_Q$ plane with R^{-1} as a parameter. R^{-1} varies across the rows while each column specifies a particular final state. CTEQ6L parametrization is used for the parton distribution function. The factorization/renormalization scale is fixed at the sum of the masses of the two final-state particles. To find the conventions adopted in clubbing individual final states into generic ones, please refer to the text.

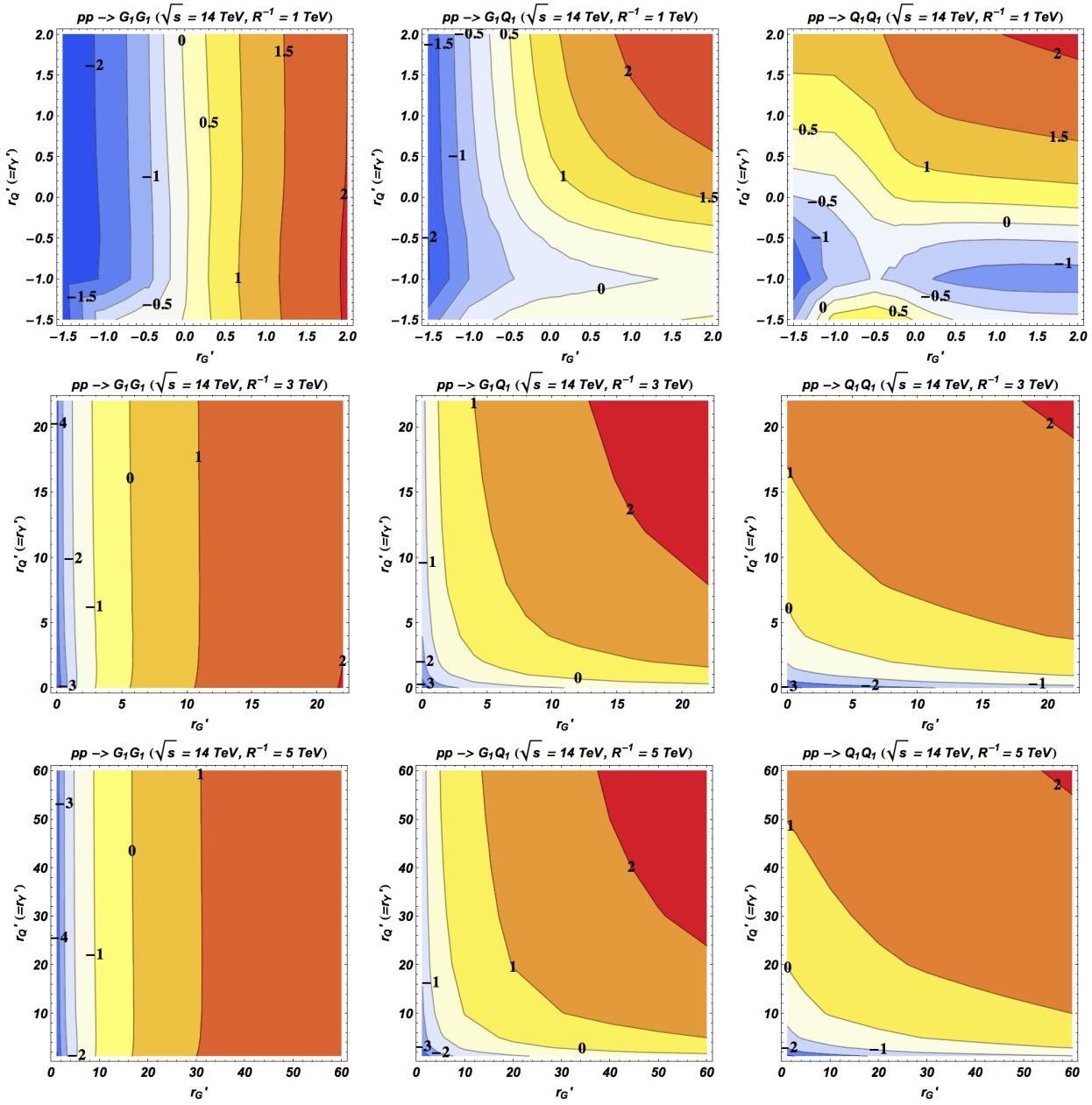

Figure 3.7: Same as in figure 3.6 but for $\sqrt{s} = 14$ TeV.

On the other hand, the case for the G_1-pair production is somewhat interesting. There, the cross sections are insensitive to variation in $g'_{G_1Q_1Q_0}$ in contrast to what we see in case of other final states as we move on from $R^{-1} = 700$ GeV. This may be attributed to the fact that the modified coupling given by $g'_{G_1Q_1Q_0}$ only appears in the t-channel while the process $pp \to G_1G_1$ gets dominant contribution from the s-channel. Moreover, unlike the previous cases, here, a marked difference is noticed between the cross sections for

the mUED and the nmUED scenarios with the nmUED cross section (~ 0.17 pb) being $\sim 20\%$ smaller than the corresponding mUED value (~ 0.22 pb). The reason for this can be traced back to the particular chiral structure of the interaction vertex originating from the action in equation (3.8) that contains the elements v-s of the V matrices (see equations (3.4), (3.7) and (3.9)).

The differences in the cross sections, as we see from table 3.3, for the mUED and the nmUED scenarios, are not big enough for the LHC to signal a clear departure from one or the other of the two competing scenarios. Thus, it turns out that if a spectrum is compatible with the mUED scenario, it would not be easy to rule out a non-minimal version of the UED solely based on such a study. Of course, it may happen that other simultaneous studies involving the electroweak sector could help distinguish between the two.

The last line in table 3.3 shows the corresponding cross sections in a SUSY scenario (based on Minimal Supersymmetric Standard Model (MSSM)). The level-1 KK excitations of the UED scenarios are substituted by their counterparts in SUSY: the KK gluon by the gluino, the $SU(2)$-doublet quark by the left handed squark and the $SU(2)$-singlet quark by the right handed squark. It is well known that, for identical mass spectra, UED production cross sections are generically larger than that for the analogous SUSY processes (by roughly a factor between 7 and 10). This is partly related to the structure of the UED matrix elements and the extra helicity states that UED excitations possess when compared to an analogous final state in SUSY. Even then, it is interesting to find that for $g'_{G_1Q_1Q_0} < 1$ (the first entry for the nmUED case in table 3.3), cross sections in some of the final states could approach the SUSY values. Thus, the total rate for strongly produced particles ceases to be a good enough indicator for the underlying scenario. This brings the alleged faking to an almost complete level. Note that this kind of a possibility does not arise in mUED. This again highlights how the correlation between masses and the couplings of the KK excitations in the nmUED scenario could shape the phenomenological situation in an interesting and involved way.

3.3.3 Decays of level-1 KK gluon, quarks and electroweak gauge bosons

In this section we discuss in brief the decay patterns of the level-1 KK gluon and quarks. When the KK gluon is heavier than the KK quarks (mutually degenerate for the lighter generation of the quarks), it decays to qQ_1 final state with 100% branching fraction. Thus, cascades are governed by the decay of the level-1 KK quarks which, in turn, decay to

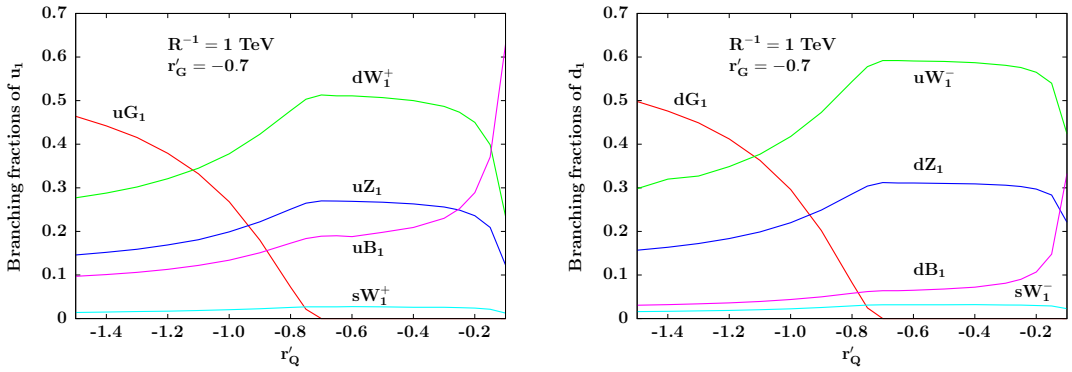

Figure 3.8: Branching fractions of level-1 *up* (left) and *down* (right) type KK quarks as functions of r'_Q for $R^{-1} = 1$ TeV. The level-1 gluon mass is taken to be 1.52 TeV which corresponds to $r'_G = -0.7$.

level-1 electroweak (EW) gauge bosons, $W_1^\pm$, Z_1 and B_1 in two-body modes. On the other hand, for $m_{Q_1} > m_{G_1}$, level-1 KK quark undergoes 2-body decays to KK gluon and $W_1^\pm$, Z_1 and B_1. The KK gluon, in turn, decays to SM quarks and the above set of electroweak KK gauge bosons via 3-body modes.

We work with an electroweak sector at the first KK level (comprising of the gauge bosons, the charged leptons and the neutrinos) which is reminiscent of mUED with corrected masses [60], that are essentially determined by R^{-1}. This can be seen as a limit of an electroweak sector in nmUED with vanishings BLTs. This is in line with the main goal of the present chapter as we focus on the role of BLKTs in the strongly interacting sector only. The resulting framework could thus be considered as a suitable benchmark (with only two BLKT parameters, r'_G and r'_Q) for initiating a phenomenological analysis of the nmUED at the LHC. The interaction vertex qQ'_1V_1 (V_1 being the level-1 electroweak gauge boson) that takes part in electroweak decays of the level-1 KK quarks gets modified and follows from equation (3.11) with $r'_G \to 0$. Of course, more involved studies in scenarios having BLTs for the electroweak sector are highly warranted since such scenarios could emerge as perfect imposters of their popular SUSY counterparts.

With this assumption, $W_1^\pm$ and Z_1 always decay to leptonic modes, *i.e.*, $W_1^\pm \to \ell_1\nu/\nu_1\ell$ and $Z_1 \to \ell_1\ell, \nu_1\nu$. B_1 is the lightest KK particle (LKP) and is stable. The only requirement to ensure these in nmUED is to set r'_G and r'_Q in a way such that m_{G_1} and m_{Q_1} do not become lighter than these electroweak bosons. This necessarily constrains the ranges of r'_G and r'_Q that such a framework can take.

In figure 3.8 we present the branching fractions of the up and down type KK quarks as functions of r'_Q and for fixed values of R^{-1} (1 TeV) and r'_G (-0.7). Each plot covers a

range in r'_Q for which both hierarchies between m_{G_1} and m_{Q_1} are realized. Note that the decay widths (and the branching fractions) of the two mass eigenstates for each type of KK quark are very similar since they result from nearly maximal mixings of the weak eigenstates (see equation 3.4). It is clear that for $m_{u_1/d_1} > m_{G_1}$, the KK quarks may dominantly decay into KK gluon with branching fractions reaching up to 50% before dropping quickly as quark mass increases. For a reverse hierarchy, the KK quarks only have 2-body electroweak decays. Among these, decays to Cabibbo-enhanced $W_1^\pm$ dominate followed by decays to Z_1, B_1 and Cabibbo-suppressed $W_1^\pm$ modes. The difference between electroweak branching fractions of the u and the d-type KK quarks stems solely from the difference in their hypercharges which only affects their decay widths to B_1. It can be seen from figure 3.8 that the peak branching fraction to $W_1^\pm$ could be between 50% and 60% for the u and the d-type KK quarks, respectively. The average branching fraction to Z_1 is found to be between 20% and 30% in the range of r'_Q where electroweak decays dominate for the two species of quarks. Branching to B_1 tends to remain at around 20% (10%) or less for the u-type (d-type) quark before it shoots up as the quarks become lighter (from left to right) and the splitting between them and $W_1^\pm$ and Z_1 become smaller. However, since the EW gauge boson masses are solely determined by R^{-1}, all three EW decay modes remain healthy over entire range of r'_Q.

Note that the branching fractions of the KK quarks to the stable LKP (B_1) is on the lower side and they hardly dominate (except in extreme corners of the parameter space). This is in stark contrast to mUED (or, for that matter, SUSY scenarios) where the right chiral level-1 KK quarks (right chiral squarks) decay almost 100% of the time to B_1 LKP (bino-like LSP) when their strong decays to level-1 KK gluon (gluino) are closed. Later, we will see that this can have major implications for the relative rates in different final states when compared to contending scenarios.

As mentioned earlier, for $m_{G_1} < m_{Q_1}$, KK gluon decays to level-1 EW gauge bosons ($W_1^\pm$, Z_1 and B_1) in three-body modes via off-shell KK quarks. The variations of these branching fractions with respect to r'_Q (or r'_G) are expected to be flat. This is because r'_Q (r'_G) appears in the primary vertex of these decays and in the propagator (through the KK quark mass) and these two affect all three body decay modes in a similar way. The branching ratios are governed by the secondary vertex and thus follow the same pattern as in the decay of KK quarks, *i.e.*, branching to $W_1^\pm$ dominates over the other two while the same to B_1 is the least favoured.[6]

[6]However, there may be a situation in nmUED when splitting between m_{G_1} and $m_{W_1^\pm/Z_1}$ drops critically resulting in an enhanced branching to B_1.

3.3.4 Exclusion limits

It is instructive to have a look at the current LHC data and understand to what extent they may constrain an nmUED scenario of the present kind. In absence of a complete implementation of the scenario in an event generator, we limit ourselves to a parton level analysis which would, for example, give a ballpark estimate of the exclusion limit for R^{-1} under a reasonable set of assumptions [7]. In principle, constraints can be derived on any subspace of the 3-dimensional space spanning over $R^{-1} - r'_G - r'_Q$.

Here, we take up a recent ATLAS analysis [96] of the final state with jets plus missing energy (with vetoed leptons) at $\sqrt{s} = 7$ TeV and integrated luminosity of 4.7 fb^{-1}. We refer to the exclusion they report for equal mass gluino and squarks in the CMSSM scenario which is 1360 GeV. It must be pointed out that a straight-forward comparison with the experimental data ultimately requires a thorough simulation (including the detector effects) of the nmUED scenario under consideration which should wait for a full implementation of the same in an event generator like MadEvent and/or others. Nonetheless, using the information we gathered in the last subsection, we can reasonably attempt to translate the above ATLAS bound to ballpark constraints on the nmUED scenario.

Towards this we find the value of cross section times branching fraction (before cuts) for $m_{\tilde{q}} = m_{\tilde{g}} = 1360$ GeV using the similar set of CMSSM parameters as in the ATLAS study. In the absence of a complete simulation (where one would be able to employ kinematic cuts), we rely on this number and treat the same as the upper bound on the cross section times branching fraction. The task is then to find the bound on the masses and/or the parameters of the nmUED scenario that satisfies this constraint.

To carry out the analysis, we break the same up in three distinct regions in the nmUED parameter space having $m_{Q_1} > m_{G_1}$, $m_{Q_1} = m_{G_1}$ and $m_{Q_1} < m_{G_1}$. Since we are not in a position to use kinematic cuts employed in the ATLAS analysis, the minimum requirement for being able to compare the nmUED results with the ATLAS study is to ensure the the kind of nmUED-spectra that result in hard enough jets and missing energy so that the ATLAS acceptances/efficiencies would hold safely [8]. Thus, the constraints we obtain for the nmUED scenario could only be conservative and can be improved with help of a dedicated simulation. It is found that $R^{-1} < 950$ GeV could be ruled out for $m_{Q_1} < m_{G_1}$

[7] Note that thorough simulation-studies for even the mUED scenario are not yet existing in the literature.

[8] The spectra for this analysis are so chosen that for unequal masses for Q_1 and G_1, the mutual splitting between them as well as the splitting between the lighter one between Q_1 and G_1 and the LKP is around 200 GeV. This would ensure (in absence of a full-fledged simulation with detector effects) jets from both primary and secondary cascades and the missing transverse energy to be hard enough to pass strong ATLAS cuts.

while, for $m_{G_1} < m_{Q_1}$, the exclusion could at best be up to 900 GeV [9]. For $m_{G_1} \simeq m_{Q_1}$, the lower bound can be as high as 1.1 TeV. However, in that case, sensitivity would be higher in the signal region with not too many hard jets since strong 2-body decays are phase-space suppressed.

In any case, we find that the bounds are degraded for nmUED when compared to CMSSM. This is not unexpected because of lower yield in $jets + \not{E}_T$ channel for nmUED. On the other hand, similar constraints on CMSSM are expected to be weaker from the analysis of leptonic final states while the same for nmUED would yield a more stringent bound.

3.3.5 The case for 14 TeV LHC

In this subsection we discuss in brief the pattern of yields in various multi-jet, multi-lepton final states accompanied by large amount of missing transverse energy. The reference values chosen for this discussion are $R^{-1} = 1$ TeV and $r'_G = -0.7$ which are the same as in section 3.3.3. In table 3.4 we present the expected uncut yields (in fb) for

these final states as r'_Q varies. For the second and the third columns, $m_{Q_1} < m_{G_1}$ while for the fifth and the sixth columns, $m_{Q_1} > m_{G_1}$. For the fourth column $r'_Q = r'_G$ and hence $m_{Q_1} = m_{G_1}$. To highlight the contrast, in the last three column we present the corresponding numbers for the mUED cases where the scenarios are solely determined by R^{-1}, for all practical purposes.

It is seen from table 3.4 that yields for all the final states decrease as r'_Q decreases except for $r'_Q = -1.5$ when the same increases suddenly. The latter can be understood in terms of an abrupt increase (up to three-fold) in the modified strong coupling close to the boundary of the theoretically allowed nmUED parameter space (see figure 3.4). The increase in the coupling strength, in fact, (over-)compensates for the lowering of the strong production cross sections as m_{Q_1} increases with decreasing r'_Q. The drop in the yields over the range $-0.1 > r'_Q > -1$ is attributed to the increase in m_{Q_1} when the increase in strong coupling strength is limited to around 20%. Note also the sharp variation of the yields for all the final states when going from $r'_Q = -0.1$ to $r'_Q = -0.5$. This is mainly due to a sharper rise in m_{Q_1} (by 300 GeV) when compared to the columns to follow (for

[9] Note that these bounds on R^{-1} are insensitive to the values of r'_Q and r'_G as long as the spectral splittings demanded are satisfied. Qualitatively, this can be termed as the most stringent constraint that could be put on the three-dimension nmUED parameter space considered here. One may like to take note of the anomalous region of a terminally large negative r'_Q with large m_{Q_1} for which the couplings become very strong and could over-compensate for the suppression in the cross section due to large m_{Q_1}. In this region, perhaps, a larger value of R^{-1} could be ruled out.

Scenario	nmUED $R^{-1} = 1$ TeV					mUED ($\Lambda R = 10$) R^{-1}/spectrum in TeV		
r'_Q	-0.1	-0.5	-0.7	-1.0	-1.5	R^{-1}=1.0	1.4	1.6
m_{Q_1} (TeV)	1.07	1.39	1.52	1.65	1.77	$m_{G_1} \approx 1.15$ $m_{Q_1} \approx 1.09$	≈ 1.60 ≈ 1.53	≈ 1.83 ≈ 1.75
$jets + \not{E}_T$	466	27	15	10	83	1396	158	50
$jets + 1\ell + \not{E}_T$	332	68	39	26	215	804	88	31
$jets + 2\ell + \not{E}_T$	143	62	35	22	205	371	42	15

Table 3.4: Parton level yields (in fb) for different final states for varying r'_Q with $r'_G = -0.7$ and $R^{-1} = 1$ TeV (leading to $m_{G_1} = 1.52$ TeV) at 14 TeV LHC. Also indicated are the corresponding numbers for mUED. Jets (inclusive) are comprised of four light flavours while the charged leptons contain only electrons and muons. QCD renormalization and factorization scales are set to the sum of the masses of the final state particles (level-1 KK quarks and/or gluon) produced in the strong scattering.

which the rises are by 125-135 GeV). On a closer look, the most drastic drop occurs for the $jets + \not{E}_T$ final state. This is explained by referring to figure 3.8 where one finds that the decay branching fraction for $Q_1 \to qB_1$ that contributes actively to the said final state suffers by a huge margin when r'_Q goes from -0.1 to -0.5. Another feature that emerges from table 3.4 is that the yields in the leptonic modes are more pronounced than that in the leptonically quiet mode. This can be understood from the fact that the branching fractions of the KK quarks and the gluon to $W_1^\pm$ and Z_1 are much larger than that to B_1 and that $W_1^\pm$ and Z_1 decay entirely into leptons and missing particles.

For the mUED part of figure 3.4 the chosen values of R^{-1} take care of the range of masses for KK quark/KK gluon that were used in the nmUED case. Note that the nmUED yields are computed for a fixed m_{G_1} while m_{Q_1} varies. For m_{G_1} (1.52 TeV) that we employ in nmUED, a similar R^{-1} in the two cases (1 TeV) gives larger yields for the mUED case. The reason is simple and as follows. The mUED spectrum is dominantly determined by R^{-1} and R^{-1}=1 TeV gives a much lighter ($\sim$ 1.15 TeV) KK gluon in comparison to the nmUED case in hand. Table 3.4 reveals that the masses are comparable in the two scenarios when $r'_Q = -0.7$ in nmUED and $R^{-1} = 1.4$ TeV in mUED. There also one finds that the rates are appreciably smaller for the nmUED case the most drastic difference

being in the $jets + \not{E}_T$ final state. The reason behind this has been discussed earlier. On the other hand, the closest possible faking in rates occur in some of the leptonic modes for $r'_Q = -0.7$ and $r'_Q = -1.0$ with $R^{-1} = 1.0$ TeV in nmUED and $R^{-1} = 1.6$ TeV in mUED. However, it is crucial to note that the rates in the all jets final state can be used as a robust discriminator between nmUED and mUED scenarios.

Thus, the pattern that exists among the yields in different final states could already disfavour mUED. When aided by a more thorough knowledge of their yields over the nmUED parameter space gathered through realistic simulations, such a study would constrain the nmUED parameter space as well. Further, crucial improvements, either in the form of exclusion or in pinning down the region of the parameter space is possible if some of the masses involved can be known, even if roughly. Under such a circumstance, the data can be simultaneously confronted by SUSY scenarios and the so-called SUSY-UED confusion could be addressed rather closely.

3.4 Conclusions and Outlook

In this chapter we discuss the role of non-vanishing BLTs (kinetic and Yukawa) in the strongly interacting sector of a scenario with one flat universal extra dimension and their impacts on the current and future runs at the LHC.

We solve for the resulting transcendental equations for masses numerically and discuss in detail the resulting spectra as functions of R^{-1} and the (scaled) brane-localized parameters, r'_G and r'_Q. Unlike in mUED where the mass spectrum is essentially dictated only by R^{-1}, r'_G and r'_Q play major roles (in conjunction with R^{-1}) in determining the same in the nmUED scenario. This opens up the possibility that much larger (smaller) values of R^{-1} (which, still could result in lighter (heavier) KK spectra) can remain relevant at the LHC when compared to mUED. Nontrivial deviations from the mUED are noted in the strong and electroweak interaction vertices involving the level-1 quarks. The deviations are found to be functions of r'_G and r'_Q only. Arguably, the most nontrivial implication of the presence of non-vanishing brane-localized terms is that both masses and couplings of the KK excitations are simultaneously controlled by these free parameters and thus, these become correlated. We demonstrate the same and discuss its possible implications at the LHC and contemplated on the role it may play in extracting the fundamental parameters of such a scenario.

We then study the basic cross sections for production of level-1 KK gluon and KK quarks as functions of the free parameters of the scenario at two different center-of-mass

energies namely, 8 TeV and 14 TeV. It is noted that, when compared to the same in mUED, for a given R^{-1}, wildly varying yields are possible. This is because the final state KK gluon and quarks can now have masses freely varying over wide ranges.

It is pointed out that even if the level-1 KK gluon and the quarks happen to have masses compatible with mUED, they could actually result from an nmUED-type scenario with a value of R^{-1} different from that in the mUED case. Although the presence of a coupling ($g'_{G_1Q_1Q_0}$) with modified strength can signal an nmUED-like scenario, such departures are expected to be miniscule. This is since for a given R^{-1}, an mUED-like spectrum is obtained only with $r'_G \simeq r'_Q$ for which deviations in the said coupling remain negligible.

Further, an nmUED-type scenario where the masses of the KK excitations are much less constrained, can fake SUSY more completely than a conventional mUED scenario. Theoretically, one well-known approach to discriminate between these scenarios, is to compare the cross sections; the expectation being the same to be larger for UED for a given set of masses in the final state (noting that both scenarios have the respective couplings of equal strengths). However, it is unlikely that a SUSY-like spectrum (unless it is degenerate) could emerge from an nmUED scenario of the present type without making the deviation in coupling large from the corresponding SUSY values (which are identical to the corresponding SM or the mUED values). Thus, if $g'_{G_1Q_1Q_0} < 1$, this may bring down an otherwise large nmUED cross section close to the SUSY value.

To get an idea of the actual rates for different final states (comprised of jets, leptons and missing energy) we computed the branching fraction of different excitations that appear in the cascades. For this we bring in an EW sector (with gauge bosons and leptons and neutrinos) which resembles mUED. Some contrasting features with respect to mUED and SUSY are noted in the form of inverted branching probabilities to jets and leptons. This would result in an enhanced (depleted) lepton-rich (jet-rich) events at the LHC in an nmUED-type scenario. The feature can be exploited for partial amelioration of the infamous SUSY-UED confusion. It was also demonstrated that the latest LHC data can rule out (conservatively) R^{-1} up to around 1 TeV under some reasonable set of assumptions. Collider simulation and detector effects are certainly lacking in this analysis. A complete study would require the inclusion of boundary terms for the electroweak sector as well. In this context of comparison between SUSY and UED frameworks, it is noteworthy that the presence of higher KK levels in the latter can serve as a rather distinctive feature. In particular, level-2 KK excitations can be resonantly produced at LHC energies. This leads to a pair of SM states in the form of dijets or dileptons [64, 97] which can be reconstructed

as peaks in the corresponding invariant mass distributions. Recently reference [73] has constrained UED models with the help of dilepton data from the LHC. We shall discuss such level-2 resonances, but in a different context in chapter 5.

It should be kept in mind that the nmUED scenario considered in this chapter is of a rather prototype variety with some generic features governed by three to four basic parameters. This is a modest number for a new physics scenario. Hence, such a scenario is much more tractable than many of its SUSY counterparts. Nonetheless, this already offers a host of rich, new effects that can be studied at the LHC. Note that the brane-localized parameters we consider are all blind to flavours, the $SU(2)$ gauge quantum numbers and independent of the locations of the orbifold fixed-points they appear at. Moreover, wherever appropriate, we assumed some of them ($r_Q = r_Y$ or $r'_Q = r'_Y$, for that matter) are equal. Deviations from any of these assumptions would have important consequences. On the other hand, in the nmUED scenario, radiative corrections to the KK-spectrum can be expected to be somewhat significant just as they are in the case of conventional mUED. However, unlike in mUED where these corrections are the sole source of mass-splittings among an otherwise degenerate set of KK excitations, the nmUED spectrum may already come with a considerable splitting at a given KK-level even at the tree level, thus diluting the role of radiative corrections.

Chapter 4

The top quark sector of the nmUED scenario

4.1 Introduction

The top quark is altogether a different kind of a fermion in the realm of the Standard Model (SM) sheerly because of its large mass or equivalently, its large (Yukawa) coupling to the Higgs boson. Many new physics scenarios beyond the SM (BSM), which have extended top quark sectors offering top quark partners, derive theoretically nontrivial and phenomenologically rich attributes from this aspect. At colliders, they warrant dedicated searches which generically result in weaker bounds on them when compared to their peers from the first two generations. Moreover, the importance of top quark has become apparent after the discovery of the Higgs boson because of its large coupling with the Higgs. Many BSM scenarios (specially SUSY) provide interesting phenomenology at the colliders involving the top quark and its partners. Scenarios with universal extra dimensions (UED) are no exceptions in this regard. There has been a reasonable amount of activity involving comparatively light KK top quarks of the UED scenarios in the past [39,98–102] and also from recent times post Higgs-discovery [66,69,103,104]. The latter set of works have constrained the respective scenarios discussed to varying degrees by analyzing the Higgs results. In this chapter, we study the structure of the top quark sector of the non-minimal universal extra dimensions (nmUED), the nontrivial features it is endowed with and their implications for the LHC [105].

We will work on the setup introduced in section section 2.6. We have already discussed the crucial features of the nmUED scenario: the boundary-localized terms (BLTs) modify the masses of the KK modes and alter their wavefunctions thus affecting their physical couplings in four dimensions [82]. The BLTs are taken to be the same at both the

boundaries, hence the scenario we consider conserves KK parity [1].

The KK top quarks of the mUED scenario has earlier been studied at the LHC in ref. [108]. These are 'vector-like' states and can be lighter than the KK quarks from the first two generations from the same KK level. This is exactly the reason behind the current surge in studies on 'top-partners' at the LHC [109–116]. The characteristic feature of the top quark sector in the nmUED scenario is the mixing of top quarks from same KK levels of similar parities (even or odd). Such *level-mixings* are triggered by BLTs [77, 79] due to non-vanishing overlap integrals and arise from the Yukawa sector. Hence, such effects depend on the corresponding brane-local parameter. Such a level-mixing does exist for other light quarks also. However, this is dominant only for the third generation quarks (particularly for top quark) because of their large Yukawa couplings. In the context of the LHC, the only relevant mixings are going to be those involving the SM (level-0) and the level-2 KK top quarks.

In the nmUED scenario, the general setup for the quark sector involves BLTs of both kinetic and Yukawa type. This has already been discussed in the previous chapter 3. In this chapter, we extend the scheme to include the level-2 excitations as well with particular emphasis on the top quark. It is demonstrated how presence of level mixing may potentially open up interesting phenomenological possibilities at the LHC in the form of new modes of their production and decay some of which would necessarily involve KK excitations of the gauge and the Higgs bosons in crucial ways. This would no doubt have significant phenomenological implications at the LHC and could provide us with an understanding of how the same can be contrasted against other scenarios having similar signatures and/or can be deciphered from experimental data.

The chapter is organized as follows. In section 4.2 we briefly introduce some necessary details of the third generation quark sector in the nmUED scenario. The resulting mass spectra and the form of the relevant couplings are discussed in section 4.3. In section 4.4 we discuss in some details the experimental constraints that potentially restrict the parameter space of the scenario under consideration. A few benchmark points, which satisfy all these constraints, are also chosen for further studies. Section 4.5 is devoted to the basic phenomenology of the KK top quarks at the LHC by outlining their production and decay patterns. Finally, we conclude in section 4.6.

[1] Phenomenology of KK parity violating BLTs are discussed in [106, 107].

4.2 The top quark sector

The action involving the top quark is the same as discussed in chapter 2. We introduce brane local kinetic and Yukawa terms for the top quark (see equations 2.23 and 2.54). The Higgs sector comes into the picture inevitably for the discussion on top quark since it shares largest Yukawa coupling with the Higgs boson. Due to the presence of BLKT for the electroweak sector (see equation 2.41), the $5D$ vev of Φ is given by

$$\langle \Phi \rangle = \begin{pmatrix} 0 \\ \frac{\hat{v}}{\sqrt{2}} \end{pmatrix} = \begin{pmatrix} 0 \\ \frac{v}{\sqrt{2}} \frac{1}{\sqrt{\pi R + 2r_{\text{EW}}}} \end{pmatrix} \tag{4.1}$$

where $v = 246$ GeV is the usual $4D$ Higgs vev associated with the breaking of electroweak symmetry. r_{EW} is the brane local parameter for the electroweak sector. The $5D$ Yukawa couplings $\hat{Y}^u_{ij}, \hat{Y}^d_{ij}$ are related to their $4D$ counterparts Y^u_{ij}, Y^d_{ij} as

$$Y^{u/d}_{ij} = \frac{\hat{Y}^{u/d}_{ij}}{\sqrt{\pi R + 2r_{\text{EW}}}}. \tag{4.2}$$

Using that we can KK-expand the mass terms in S_{Yukawa} as follows:

$$-\int d^4x \sum_{i,j=1}^{3} \frac{v}{\sqrt{2}} \left\{ Y^u_{ij} F^{u,(0,0)}_{ij} \overline{u'^{(0)}_{iL}} u'^{(0)}_{jR} + Y^d_{ij} F^{d,(0,0)}_{ij} \overline{d'^{(0)}_{iL}} d'^{(0)}_{jR} + \text{h.c.} \right\}, \tag{4.3}$$

where, for simplicity, we only present the zero-mode part with fields redefined (to make them appear more conventional) as $u'^{(0)}_{iL} \equiv U'^{(0)}_{iL}$, $d'^{(0)}_{iL} \equiv D'^{(0)}_{iL}$. The fermionic mode functions for KK decomposition are described in an appropriate context in section 4.3. The concrete forms of the factors $F^{u/d,(0,0)}_{ij}$ (which arise from the mode functions of the L, R type fields participating in equation 4.3) are

$$F^{u,(0,0)}_{ij} = \frac{2r_Y + \pi R}{\sqrt{2r_{U_i} + \pi R}\sqrt{2r_{u_i} + \pi R}}, \quad F^{d,(0,0)}_{ij} = \frac{2r_Y + \pi R}{\sqrt{2r_{D_i} + \pi R}\sqrt{2r_{d_i} + \pi R}}. \tag{4.4}$$

The 3×3 matrices $Y^u_{ij} F^{u,(0,0)}_{ij}$ and $Y^d_{ij} F^{d,(0,0)}_{ij}$ are diagonalized by the following bi-unitary transformations

$$q'^{(0)}_{iR} = (U_{qR})_{ij} q^{(0)}_{jR}, \quad q'^{(0)}_{iL} = (U_{qL})_{ij} q^{(0)}_{jL} \qquad (\text{for } q = u, d), \tag{4.5}$$

as follows:

$$-\int d^4x \sum_{i=1}^{3} \frac{v}{\sqrt{2}} \left\{ \mathcal{Y}^u_{ii} \overline{u^{(0)}_{iL}} u^{(0)}_{iR} + \mathcal{Y}^d_{ii} \overline{d^{(0)}_{iL}} d^{(0)}_{iR} + \text{h.c. (+ KK excitations)} \right\}, \tag{4.6}$$

where $\mathcal{Y}^u_{ii}$ and $\mathcal{Y}^d_{ii}$ are the diagonalized Yukawa couplings for up and down quarks, respectively. We discuss later in this paper that the diagonalized values do not directly correspond to those in the SM due to level mixing effects. Also, from now on, we would consider universal values of the BLKT parameters r_Q for the quarks from the first two generations and r_T for those from the third generation. We will see later, this provides us with a separate handle (modulo some constraints from experiments) on the top quark sector of the nmUED scenario under consideration. Further, this simplifies the expressions in equation 4.4.

4.3 Mixings, masses and effective couplings in the top quark sector

Mixings in the fermion sector, quite generically, could have interesting implications as these affect both couplings and the spectra of the concerned excitations. Fermions with a certain flavour from a given KK level and belonging to $SU(2)$ doublet and singlet representations always mix once the electroweak symmetry is broken. Presence of BLTs affects such a mixing at every KK level. On top of this, the dynamics driven by the BLTs allows for mixing of fermions from different KK levels that have the same KK-parity. Both kinds of mixings are proportional to the Yukawa mass of the fermion in reference and thus, are pronounced for the top quark sector.

As pointed out in the introduction, since *level-mixing* among the even KK-parity top quarks involves the SM top quark (from level-0), this naturally evokes a reasonable curiosity about its consequences and it is indeed found to give rise to interesting phenomenological possibilities. However, the phenomenon draws significant constraints from experiments which we will discuss in some detail. We restrict ourselves to the mixing of level-0-level-2 KK top quarks ignoring all higher even KK states the effects of which would be suppressed by their increasing masses. Also, we do not consider the effects of level-mixings among KK states from levels with $n > 0$, including say, those among the excitations from levels with odd KK-parity. Generally, these could be appreciable. However, in contrast to the case where SM excitations mix with higher KK levels, these would only entail details within a sector yet to be discovered.

4.3.1 Mixing in level-1 top quark sector

We first briefly recount the mixing of the top quarks at KK level-1. This is similar to the mixing in the quarks of first two generations as described in ref. [82]. In presence of BLTs, the Yukawa part of the action embodying the mass-matrix is of the form

$$-\int d^4x\Bigg\{\begin{bmatrix}\overline{T}^{(1)}, & \overline{t}^{(1)}\end{bmatrix}_L\begin{bmatrix}M_{T_{(1)}} & r'_{T11}m_t^{\text{in}}\\ -R'_{T11}m_t^{\text{in}} & M_{T_{(1)}}\end{bmatrix}\begin{bmatrix}T^{(1)}\\ t^{(1)}\end{bmatrix}_R+\text{h.c.}\Bigg\}, \tag{4.7}$$

with "input" top mass m_t^{in} (which is an additional free parameter in our scenario) and

$$\begin{aligned} r'_{T11} &= \frac{1}{R_{T00}}\int_{-L}^{L}dy\Big(1+r_Y\left(\delta(y-L)+\delta(y+L)\right)\Big)f^2_{T^{(1)}}\\ &= \frac{2r_T+\pi R}{2r_Y+\pi R}\times\frac{2r_Y+\frac{1}{S^2_{T^{(1)}}}\left[\frac{\pi R}{2}-\frac{1}{2M_{T^{(1)}}}\sin(M_{T^{(1)}}\pi R)\right]}{2r_T+\frac{1}{S^2_{T^{(1)}}}\left[\frac{\pi R}{2}-\frac{1}{2M_{T^{(1)}}}\sin(M_{T^{(1)}}\pi R)\right]}, \end{aligned} \tag{4.8}$$

$$\begin{aligned} R'_{T11} &= \frac{1}{R_{T00}}\int_{-L}^{L}dy\Big(1+r_Y\left(\delta(y-L)+\delta(y+L)\right)\Big)g^2_{T^{(1)}}\\ &= \frac{2r_T+\pi R}{2r_Y+\pi R}\times\frac{2r_Y(C_{T^{(1)}}/S_{T^{(1)}})^2+\frac{1}{S^2_{T^{(1)}}}\left[\frac{\pi R}{2}+\frac{1}{2M_{T^{(1)}}}\sin(M_{T^{(1)}}\pi R)\right]}{\frac{1}{S^2_{T^{(1)}}}\left[\frac{\pi R}{2}+\frac{1}{2M_{T^{(1)}}}\sin(M_{T^{(1)}}\pi R)\right]} \end{aligned} \tag{4.9}$$

where R_{T00} is given by

$$R_{T00}=\int_{-L}^{L}dy\Big(1+r_Y\left(\delta(y-L)+\delta(y+L)\right)\Big)f^2_{T^{(0)}}=\frac{2r_Y+\pi R}{2r_T+\pi R}. \tag{4.10}$$

$f_{T^{(n)}}$ and $g_{T^{(n)}}$ represent the mode functions for n-th KK level and are given by [82]:

$$f_{T^{(n)}}\equiv f_{T_L^{(n)}}=f_{t_R^{(n)}}=N_{T^{(n)}}\times\begin{cases}\dfrac{\cos(M_{T^{(n)}}y)}{C_{T^{(n)}}} & \text{for } n \text{ even},\\ \dfrac{-\sin(M_{T_{(n)}}y)}{S_{T^{(n)}}} & \text{for } n \text{ odd},\end{cases} \tag{4.11}$$

$$g_{T^{(n)}}\equiv f_{T_R^{(n)}}=-f_{t_L^{(n)}}=N_{T^{(n)}}\times\begin{cases}\dfrac{\sin(M_{T^{(n)}}y)}{C_{T^{(n)}}} & \text{for } n \text{ even},\\ \dfrac{\cos(M_{T^{(n)}}y)}{S_{T^{(n)}}} & \text{for } n \text{ odd}\end{cases} \tag{4.12}$$

with

$$C_{T^{(n)}}=\cos\left(\frac{M_{T^{(n)}}\pi R}{2}\right),\quad S_{T^{(n)}}=\sin\left(\frac{M_{T^{(n)}}\pi R}{2}\right) \tag{4.13}$$

and the normalization factors $N_{T^{(n)}}$ for the mode functions are given by

$$N_{T^{(n)}}^{-2} = \begin{cases} 2r_T + \dfrac{1}{C_{T^{(n)}}^2}\left[\dfrac{\pi R}{2} + \dfrac{1}{2M_{T^{(n)}}}\sin(M_{T^{(n)}}\pi R)\right] & \text{for } n \text{ even}, \\ 2r_T + \dfrac{1}{S_{T^{(n)}}^2}\left[\dfrac{\pi R}{2} - \dfrac{1}{2M_{T^{(n)}}}\sin(M_{T^{(n)}}\pi R)\right] & \text{for } n \text{ odd}. \end{cases} \tag{4.14}$$

The KK mass $M_{T^{(n)}}$ for the n-th level top quark excitation follows from equation 2.51 where chiral zero modes occur [2]. Note that the off-diagonal terms are asymmetric and pick up nontrivial multiplicative factors. This is because two different mode functions, $f_{T^{(n)}}$ and $g_{T^{(n)}}$ (associated with the specific states with particular chiralities and gauge quantum numbers), contribute to them. On the other hand, the diagonal KK mass terms are now solutions of the appropriate transcendental equations. When expanded, the diagonal entries of the mixing matrix involve the L and R components of the same gauge multiplet (T from $SU(2)$ doublet or t from $SU(2)$ singlet). In contrast, the off-diagonal entries are of Yukawa-origin (signaled by the presence of m_t^{in}) and involve both r_T and r_Y. These terms represent the conventional Dirac mass-terms as they connect the L and the R components belonging to two different multiplets. It may be noted that even when either r_T or r_Y vanishes, the mixing remains nontrivial. Only the case with $r_T = r_Y = 0$ trivially reduces to the (tree-level) mUED.

The mass matrix of equation 2.63 can be diagonalized by bi-unitary transformation with the matrices $V_{tL}^{(1)}$ and $V_{tR}^{(1)}$ where

$$\begin{bmatrix} T^{(1)} \\ t^{(1)} \end{bmatrix}_L = V_{tL}^{(1)} \begin{bmatrix} t_l^{(1)} \\ t_h^{(1)} \end{bmatrix}_L, \quad \begin{bmatrix} T^{(1)} \\ t^{(1)} \end{bmatrix}_R = V_{tR}^{(1)} \begin{bmatrix} t_l^{(1)} \\ t_h^{(1)} \end{bmatrix}_R. \tag{4.15}$$

Then, equation 2.63 takes the diagonal form

$$-\int d^4x \begin{bmatrix} \bar{t}_l^{(1)}, & \bar{t}_h^{(1)} \end{bmatrix} \begin{bmatrix} m_{t_l^{(1)}} & \\ & m_{t_h^{(1)}} \end{bmatrix} \begin{bmatrix} t_l^{(1)} \\ t_h^{(1)} \end{bmatrix} \tag{4.16}$$

where $t_l^{(1)}$, $t_h^{(1)}$ are the level-1 top quark mass eigenstates and $(m_{t_l^{(1)}})^2$ and $(m_{t_l^{(1)}})^2$ are the mass-eigenvalues of the squared mass-matrix with $m_{t_h^{(1)}} > m_{t_l^{(1)}}$. Note that, for clarity and convenience, we have modified the notations and the ordering of the states in the presentations above from what appear in ref. [82].

[2] Here, we consider a situation where the fields $T_{L,R}^{(1)}$ and $t_{L,R}^{(1)}$ are rotated by the same matrices U_{qR} and U_{qL} (of equation 4.5) from the basis used in equations 2.23 and 2.54. We ignore the diagonal and non-diagonal modifications in the boundary conditions. In our scenario, these modifications are Cabibbo-suppressed (see equation C.4 in the appendix) and hence such a treatment is justified.

4.3.2 Mixing among level-0 and level-2 top quark states

The formulation described above can be extended in a straight-forward manner for the level-2 KK top quarks when this sector is augmented by the level-0 (SM) top quark. Thus, the mass-matrix for the even KK parity top quark sector (keeping only level-0 and level-2 KK excitations) takes the following form:

$$-\int d^4x \Bigg\{ \Big[\overline{t^{(0)}},\ \overline{T}^{(2)},\ \overline{t}^{(2)}\Big]_L \begin{bmatrix} m_t^{\rm in} & 0 & m_t^{\rm in} R'_{T02} \\ m_t^{\rm in} R'_{T02} & M_{T^{(2)}} & m_t^{\rm in} r'_{T22} \\ 0 & -m_t^{\rm in} R'_{T22} & M_{T^{(2)}} \end{bmatrix} \begin{bmatrix} t^{(0)} \\ T^{(2)} \\ t^{(2)} \end{bmatrix}_R + \text{h.c.} \Bigg\} \tag{4.17}$$

where r'_{T22}, R'_{T22}, R'_{T02} are defined as follows, in a way similar to the case for level-1 top quarks:

$$\begin{aligned} r'_{T22} &= \frac{1}{R_{T00}} \int_{-L}^{L} dy \Big(1 + r_Y \left(\delta(y-L) + \delta(y+L)\right)\Big) f^2_{T^{(2)}} \\ &= \frac{2r_T + \pi R}{2r_Y + \pi R} \times \frac{2r_Y + \frac{1}{C^2_{T^{(2)}}} \left[\frac{\pi R}{2} + \frac{1}{2M_{T^{(2)}}} \sin(M_{T^{(2)}} \pi R)\right]}{2r_T + \frac{1}{C^2_{T^{(2)}}} \left[\frac{\pi R}{2} + \frac{1}{2M_{T^{(2)}}} \sin(M_{T^{(2)}} \pi R)\right]}, \end{aligned} \tag{4.18}$$

$$\begin{aligned} R'_{T22} &= \frac{1}{R_{T00}} \int_{-L}^{L} dy \Big(1 + r_Y \left(\delta(y-L) + \delta(y+L)\right)\Big) g^2_{T^{(2)}} \\ &= \frac{2r_T + \pi R}{2r_Y + \pi R} \times \frac{2r_Y (S_{T^{(2)}}/C_{T^{(2)}})^2 + \frac{1}{C^2_{T^{(2)}}} \left[\frac{\pi R}{2} - \frac{1}{2M_{T^{(2)}}} \sin(M_{T^{(2)}} \pi R)\right]}{\frac{1}{C^2_{T^{(2)}}} \left[\frac{\pi R}{2} - \frac{1}{2M_{T^{(2)}}} \sin(M_{T^{(2)}} \pi R)\right]}, \end{aligned} \tag{4.19}$$

$$\begin{aligned} R'_{T02} &= \frac{1}{R_{T00}} \int_{-L}^{L} dy \Big(1 + r_Y \left(\delta(y-L) + \delta(y+L)\right)\Big) f_{T^{(0)}} f_{T^{(2)}} \\ &= \frac{2r_T + \pi R}{2r_Y + \pi R} \times \frac{2r_Y + 2(S_{T^{(2)}}/M_{T_{(2)}} C_{T^{(2)}})}{\sqrt{2r_T + \pi R} \sqrt{2r_T + \frac{1}{C^2_{T^{(2)}}} \left[\frac{\pi R}{2} + \frac{1}{2M_{T^{(2)}}} \sin(M_{T^{(2)}} \pi R)\right]}}, \end{aligned} \tag{4.20}$$

with R_{T00} given by equation 4.10. The lower 2×2 block of the mass-matrix in equation 4.17 is reminiscent of the level-1 top quark mass-matrix of equation 2.63. Beyond this, the mass-matrix contains as the first diagonal element the 'input' top quark mass, $m_t^{\rm in}$ and two other non-vanishing off-diagonal elements as the 13 and 21 elements. Obviously, the latter two play direct roles in the mixings of the level-0 and level-2 top quarks. Note that all the off-diagonal terms of the mass-matrix are proportional to $m_t^{\rm in}$ which is clearly indicative of their origins in the Yukawa sector. The zeros in turn reflect $SU(2)$ invariance.

Diagonalization of this 3×3 mass-matrix yields the physical states (3 of them) along with their mass-eigenvalues. Thus, the level-0 top quark (*i.e.*, the SM top quark) ceases

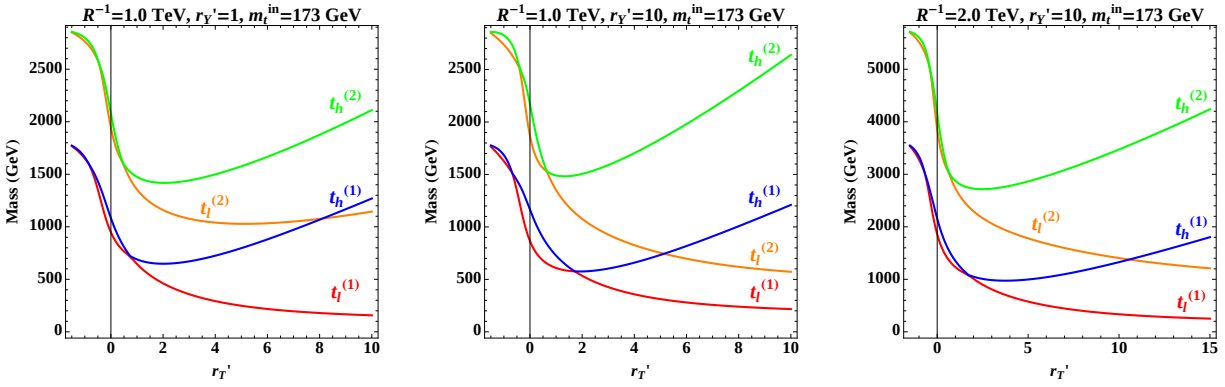

Figure 4.1: Masses of level-1 and level-2 KK top quarks as functions of r'_T for given r'_Y and R^{-1} with $m_t^{\text{in}} = 173\,\text{GeV}$.

to be a physical state and mixes with the level-2 top states. Given the rather involved structure of the mass-matrix, neither is it possible to express the eigenvalues analytically in a compact way nor they would be much illuminating theoretically. We, thus, diagonalize the mass-matrix numerically. Similar to the case of the level-1 states, we adopt the following conventions:

$$\begin{bmatrix} t^{(0)} \\ T^{(2)} \\ t^{(2)} \end{bmatrix}_L = V_{tL}^{(2)} \begin{bmatrix} t \\ t_l^{(2)} \\ t_h^{(2)} \end{bmatrix}_L , \qquad \begin{bmatrix} t^{(0)} \\ T^{(2)} \\ t^{(2)} \end{bmatrix}_R = V_{tR}^{(2)} \begin{bmatrix} t \\ t_l^{(2)} \\ t_h^{(2)} \end{bmatrix}_R \tag{4.21}$$

with the physical masses m_t^{phys}, $m_{t_l^{(2)}}$ and $m_{t_h^{(2)}}$ and with the ordering $m_t^{\text{phys}} < m_{t_l^{(2)}} < m_{t_h^{(2)}}$.

4.3.3 Quantitative estimates

As can be seen from the equations above, the free parameters of the top-quark sector in the nmUED scenario under consideration are R, r_T and r_Y. For the latter two, we use the dimensionless quantities r'_T and r'_Y where $r'_T = r_T R^{-1}$ and $r'_Y = r_Y R^{-1}$. In addition, m_t^{in} serves as an extra free parameter from the SM sector.

Top quark masses

In figure 4.1 we illustrate the variations of the masses, as functions of r'_T, of the two KK top quark eigenstates from level-1 and the two heavier mass eigenstates that result from the mixing of level-0 and level-2. The plot in the middle, when compared to the one in the left, demonstrates how the spectrum changes as r'_Y varies with R^{-1} held fixed. We set the input top mass m_t^{in} to 173 GeV in all the plots of figure 4.1. In turn, the effect of

changing R^{-1} can be seen as one goes from the plot in the middle ($R^{-1} = 1$ TeV) to the one on the right ($R^{-1} = 2$ TeV). An interesting feature common to all these plots is that there is a cross-over of the curves for $m_{t_h^{(1)}}$ and $m_{t_l^{(2)}}$, *i.e.*, as a function of r'_T, at some point, the lighter of the mixed level-2 state top quark eigenstates becomes less massive compared to the heavier of the level-1 KK top quark eigenstate. The cross-overs take place at smaller values of r'_T when r'_Y is increased for a given R^{-1} and at larger values of r'_T when R^{-1} is increased with r'_Y held fixed. Accordingly, the mass-values at those flipping points also go down or up, respectively. Here, the dominant role is being played by the 'chiral mixing' while *level-mixing* is unlikely to have much bearing. These plots also reveal that achieving a 'flipped-spectrum' (in the above sense) is difficult if one requires the light level-1 KK top quark to be heavier than about 400 GeV. Nonetheless, the overall trend could provide easier reach for a KK top quark from level-2 at the LHC. Thus, it may be possible for up to three excited top quark states ($m_{t_l^{(1)}}$, $m_{t_h^{(1)}}$, $m_{t_l^{(2)}}$) to pop up at the LHC.

Top quark mixings

Now, we take a quantitative look at the mixings in the top quark sector from the first KK level discussed earlier in section 4.3.1. The mixing is known to be near-maximal in the case of quarks (fermions) from the lighter generations [82]. Deviations from such maximal mixings occur in the top quark sector due to its nontrivial structure[3]. Such mixings are expected to follow similar trends at level-2 (and higher) KK levels and hence we do not present them separately. However, some deviations are expected in the presence of *level-mixings* which can at best be modest for the case of $t^{(0)} - t^{(2)}$ system that we discuss briefly in this chapter.

The elements of the V-matrices in equation 4.15 give the admixtures of different participating states in the KK top quark eigenstates. To be precise, $V^{(1)}_{tL_{(1,1)}}$ and $V^{(1)}_{tL_{(2,2)}}$ represent the admixture of $T_L^{(1)}$ in $t_{lL}^{(1)}$ and $t_L^{(1)}$ in $t_{hL}^{(1)}$ respectively while $V^{(1)}_{tL_{(1,2)}}$ and $V^{(1)}_{tL_{(2,1)}}$ indicate the same for $t_L^{(1)}$ in $t_{lL}^{(1)}$ and $T_L^{(1)}$ in $t_{hL}^{(1)}$ in that order. Similar descriptions hold for the $V_R^{(1)}$ matrix. In figures 4.2 and 4.3 we illustrate the deviations from maximal mixing in the level-1 top quark sector in terms of these components of the V matrices as functions of r'_T. Each figure contains multiples curves which present situations for different combinations of R^{-1} and r'_Y (see the captions for details). Note that the abrupt changes in sign of the mixings that happen between $-1 < r'_T < 2$ can be understood in terms of the trends of

[3]This is in direct contrast with competing SUSY scenarios where mixings in the light sfermion sector are always negligible while for top squark sector it could attain the maximal value.

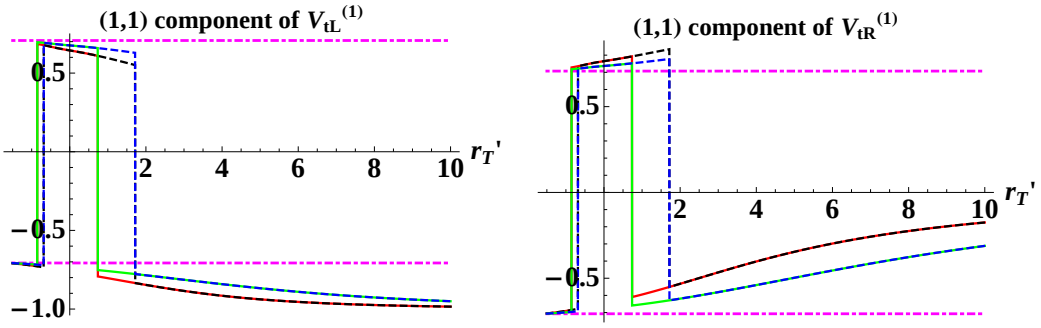

Figure 4.2: Variations of the (1,1) elements of the matrices $V_{tL}^{(1)}$ (left) and $V_{tL}^{(1)}$ (right) as functions of r_T' for fixed set of values of R^{-1} and r_Y'. Conventions used for different sets of R^{-1} and r_Y' values are: bold red for $R^{-1} = 1$ TeV and $r_Y' = 1$, dashed black for $R^{-1} = 1$ TeV and $r_Y' = 10$, bold green for $R^{-1} = 2$ TeV and $r_Y' = 1$ and dashed blue for $R^{-1} = 2$ TeV and $r_Y' = 10$.

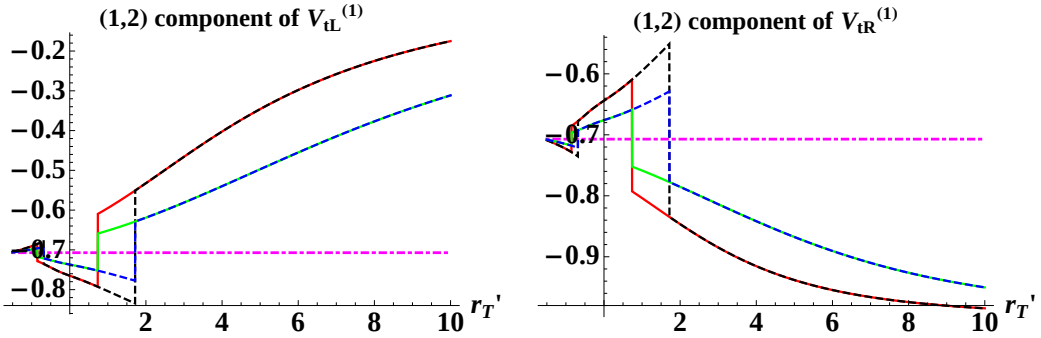

Figure 4.3: Same as in figure 4.2 but for the variations of the (1,2) elements of the matrices $V_{tL}^{(1)}$ (left) and $V_{tL}^{(1)}$ (right). The respective (2,1) elements can be obtained from the orthogonality of these matrices.

the red and blue curves in figure 4.1 (the blue curves smoothly evolve to the red ones and vice-versa).

The flat, broken magenta lines indicate maximal mixing ($|V_{tL_{(1,1)}}^{(1)}| = |V_{tL_{(1,2)}}^{(1)}| = 1/\sqrt{2}$). It is clear from these figures that there can be appreciable deviations from maximal mixing in all these cases. As can be seen, the effects are bigger for larger values of r_T' and smaller R^{-1}. Some dependence on r_Y' is observed for smaller values of r_T'. However, it is to be kept in mind that the effective deviations arise from the interplay of these elements which is again neither easy to present nor much illuminating.

4.3.4 Effective couplings

As mentioned earlier, not only masses undergo modifications in the presence of BLTs but also the wavefunctions get distorted. The latter affects the couplings through the overlap integrals. These are integrals over the extra dimension of a product of mode functions of

the states that appear at a given interaction vertex. In this section we briefly discuss the generic properties of some of these overlap integrals which play roles in the present study. Assuming the wavefunctions to be real, the general form of the multiplicative factor that scales the corresponding SM coupling strengths is given by

$$g_{f_i^{(l)} f_j^{(m)} f_k^{(n)}} = \mathcal{N}_{ijk} \int_{-L}^{L} dy \Big[1 + r_{ijk}^{(l,m,n)} \left(\delta(y-L) + \delta(y+L)\right)\Big] f_i^{(l)}(y) f_j^{(m)}(y) f_k^{(n)}(y) \qquad (4.22)$$

where i, j, k represent different interacting fields and $f_i^{(l)}, f_j^{(m)}, f_k^{(n)}$ are the corresponding mode functions with the KK indices l, m, n, respectively, as defined in sections 2.6.2, 4.3.1 and 4.3.2. The factor $r_{ijk}^{(l,m,n)}$ stands for relevant BLT parameter(s) while the normalization factor $\mathcal{N}_{ijk}$ is suitably chosen to recover the SM vertices when l=m=n=0 (except for the Yukawa sector of the nmUED scenario under consideration).

The key to understand the general structure is the flatness of the zero-mode ($n = 0$) profiles in our minimal configuration. For these, the factor takes the following form:

$$g_{f_i^{(l)} f_j^{(m)} f_k^{(0)}} = \mathcal{N}_{ijk} f_k^{(0)} \int_{-L}^{L} dy \Big[1 + r_{ijk}^{(l,m,0)} \left(\delta(y-L) + \delta(y+L)\right)\Big] f_i^{(l)}(y) f_j^{(m)}(y), \qquad (4.23)$$

where we see the zero-mode field has been taken out of the integral in equation 4.22. For $i = j$, the overlap integral reduces to Kronecker's delta function, $\delta_{l,m}$ and the overall strength turns out to be identically equal to 1. Orthonormality of the involved states constrains the possibilities. In table 4.1 we collect some of these interactions and group them in terms of their effective strengths (given by equation 4.23). This list, in particular, the set of couplings in the third column, is not exhaustive and presented for demonstrative purposes only.

In addition to these, mixings in the top quark sector in the form of both chiral mixing and *level-mixing* play roles in determining the effective couplings. In this subsection we briefly discuss such effects on some of the important interaction-vertices involving the top quarks, the gauge and the Higgs bosons from different KK levels. As in section 4.3.3, we further introduce the dimensionless parameters $r'_{\rm EW}\,(= R^{-1} r_{\rm EW})$, $r'_Q\,(= R^{-1} r_Q)$ and $r'_G\,(= R^{-1} r_G)$ replacing $r_{\rm EW}\,(= r_H)$, r_Q and r_G, the BLKT parameters for the electroweak gauge boson and Higgs sectors, the first two generation quark sector and the gluon sector, respectively. In addition, we also introduce a corresponding universal parameter r_L for the lepton sector which we will use in section 4.4.3. Later, in section 4.5, we will refer back to this discussion in the context of phenomenological analyses of the scenario.

$Q^{(2)}_{R/L} - V^{(0)} - Q^{(0)}_{R/L}$ $q^{(2)}_{R/L} - V^{(0)} - q^{(0)}_{R/L}$ $V^{(2)} - V^{(0)} - V^{(0)}$	$V^{(2)} - V^{(2)} - V^{(0)}$ $V^{(1)} - V^{(1)} - V^{(0)}$ $Q^{(1)}_{R/L} - V^{(0)} - Q^{(1)}_{R/L}$ $q^{(1)}_{R/L} - V^{(0)} - q^{(1)}_{R/L}$ $Q^{(2)}_{R/L} - V^{(0)} - Q^{(2)}_{R/L}$ $q^{(2)}_{R/L} - V^{(0)} - q^{(2)}_{R/L}$	$Q^{(1)}_{R/L} - V^{(1)} - Q^{(0)}_{R/L}$ $q^{(1)}_{R/L} - V^{(1)} - q^{(0)}_{R/L}$ $Q^{(0)}_{R/L} - V^{(2)} - Q^{(0)}_{R/L}$ $Q^{(1)}_{L} - H^{(0)} - q^{(1)}_{R}$ $Q^{(2)}_{L} - H^{(0)} - q^{(0)}_{R}$ $Q^{(0)}_{L} - H^{(2)} - q^{(0)}_{R}$ $Q^{(0)}_{L} - H^{(0)} - q^{(2)}_{R}$
0	1	non-zero

Table 4.1: Classes of different effective (tree level) couplings (given by equation 4.23) involving the gauge boson (V), Higgs (H) and the left- and right-handed, $SU(2)$ doublet (Q) and singlet (q) quark excitations and their relative strengths (shown in the last row) compared to the corresponding SM cases.

Effective couplings involving the gauge bosons

The set of couplings that we briefly discuss here are those that would appear in the production of the KK top quarks at the LHC and their decays. In figure 4.4 we illustrate the coupling-deviation (a multiplicative factor of the corresponding SM value at the tree level) $g^{(2)}$-$q^{(0)}$-$q^{(0)}$ (left) and $g^{(2)}$-$q^{(2)}$-$q^{(0)}$ (right) in the generic $r'_V - r'_{Q/T/L}$ plane. In both of these plots, the mUED case is realized along the diagonals over which $r'_G = r'_Q$. In the first case, the mUED value is known to be vanishing at the tree level since KK number is violated. Hence, the diagonal appears with the contour-value of zero. For vertices involving the top quarks, r'_T replaces r'_Q. For a process like $pp \to \bar{t}^{(2)}_l t$ + h.c., the former kind of coupling appears at the parton-fusion (initial state) vertex while the latter shows up at the production vertex. The combined strength of these two couplings controls the production rate for the mentioned process. Further, the situation is not much different for the level-2 electroweak gauge bosons except for some modifications due to mixings present in the electroweak sector. In general, it can be seen from the first plot of figure 4.4 that the coupling $g^{(2)}$-$q^{(0)}$-$q^{(0)}$ picks up a negative sign for $r'_G > r'_Q$. This could have nontrivial phenomenological implications for processes in which interfering Feynman diagrams are present. On the other hand, $g^{(2)}$-$q^{(2)}$-$q^{(0)}$ remains always positive as is clear from the second plot of figure 4.4. Note that the three-point vertex $V^{(0)}$-$V^{(0)}$-$V^{(2)}$ and the generic ones of the form $V^{(0)}$-$f^{(0)}$-$f^{(2)}$ are absent because the corresponding overlap integrals vanish

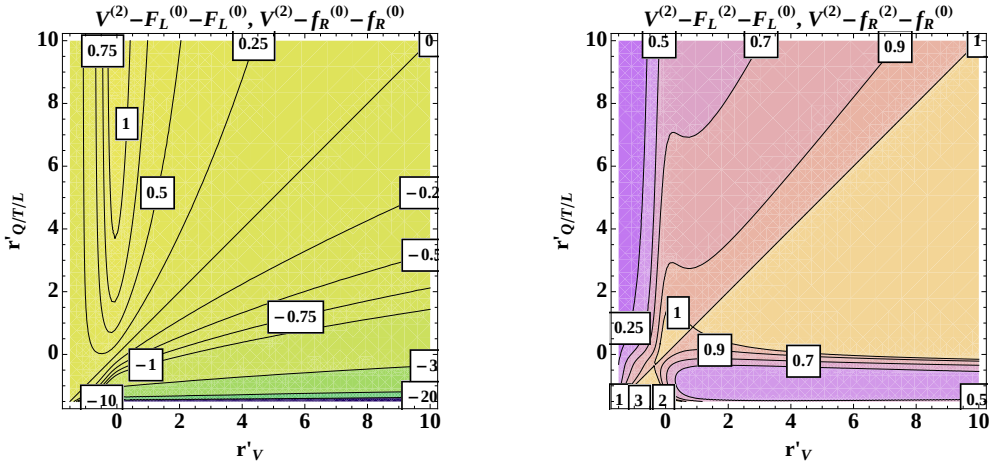

Figure 4.4: Contours of deviation for the generic couplings $V^{(2)}$-$F^{(0)}$-$F^{(0)}$ (or $V^{(2)}$-$f^{(0)}$-$f^{(0)}$) (left) and $V^{(2)}$-$F^{(2)}$-$F^{(0)}$ (or $V^{(2)}$-$f^{(2)}$-$f^{(0)}$) (right) from the corresponding SM values in the $r'_V - r'_{Q/T/L}$ plane. V, F and f stand for generic gauge boson, $SU(2)$ doublet and singlet fermion fields (with corresponding chiralities), respectively. Note that when V is the (KK) W boson, types of the two fermions involved at a given vertex are different.

due to orthogonality of the involved mode functions.

In figure 4.5 we present the corresponding contours of similar deviations in the couplings involving the level-2 KK gauge bosons and the level-1 KK quarks. The plot on left shows the situation for the left- (right-) chiral component of the $SU(2)$ doublet (singlet) quarks while the plot on right illustrates the case for left- (right-) chiral component of the $SU(2)$ singlet (doublet) quarks. These are in conformity with the mode functions for these individual components of the level-1 KK quarks. However, it should be noted that the KK quarks being vector-like states, each of the $SU(2)$ doublet and singlet partners have both left- and right-chiral components. Thus, the effective couplings are obtained only by suitably combining (with appropriate weights) the strengths as given by the two plots. In the case of KK top quarks, the situation would be further complicated because of significant mixing between the two gauge eigenstates. For brevity, a list of relevant couplings is presented in table 4.1 with mentions of the kind of modifications they undergo in the nmUED scenario. It is clear from these figures that these (component) couplings involving level-2 KK states are in general suppressed compared to the relevant SM couplings except over a small region with $r'_{Q/T/L} < 0$.

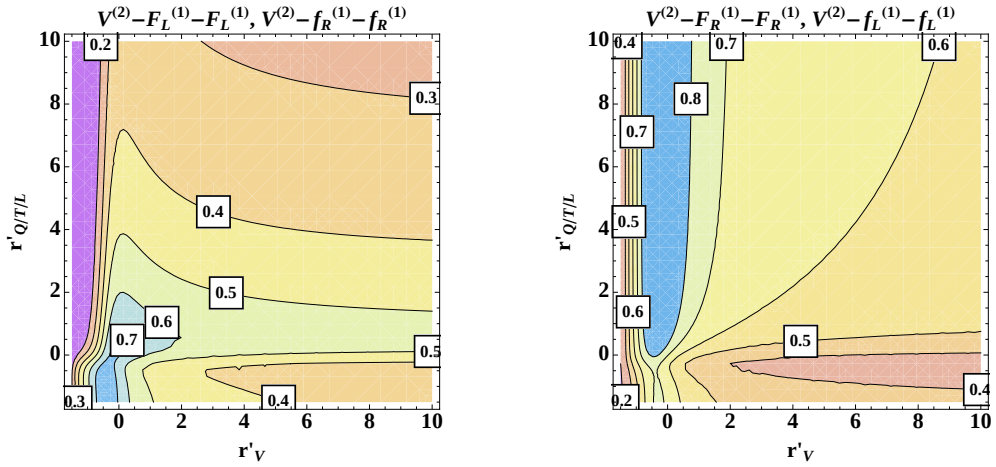

Figure 4.5: Same as in figure 4.4 but for the generic couplings $V^{(2)}$-$F_L^{(1)}$-$F_L^{(1)}$ or $V^{(2)}$-$f_R^{(1)}$-$f_R^{(1)}$ (left) and $V^{(2)}$-$f_L^{(1)}$-$f_L^{(1)}$ or $V^{(2)}$-$F_R^{(1)}$-$F_R^{(1)}$ (right).

Effective couplings involving the Higgs bosons

The association of the Higgs sector with the third SM family is rather intricate and has deep implications which unfold themselves in many scenarios beyond the SM. SUSY scenarios provide very good examples of this, some analyses have been done in the mUED [117] and the nmUED scenario is also no exception. The couplings among the Higgs bosons and the KK top quarks of the nmUED scenario can deviate significantly from the corresponding SM Yukawa coupling. However, the zero-mode (SM) Higgs Yukawa couplings do not depend upon $r'_H\,(=\,r'_{\rm EW})$. In the left panel of figure 4.6 we illustrate the possible deviation in the SM Yukawa coupling itself in the $r'_T - r'_Y$ plane. Along the diagonal of this figure (with $r'_T = r'_Y$) the SM value of the Yukawa coupling is preserved. Note that the latest LHC data still allows for significant deviations in the H-t-t coupling [118–121].

In the right panel we show deviations of the generic H-$t^{(2)}$-t which appears at the tree level in nmUED. Unlike in the case of the interaction vertex $V^{(0)}$-$f^{(2)}$-$f^{(0)}$ (where $V^{(0)}$ is a massive SM gauge boson) where the involved coupling vanishes in the absence of *level-mixing* between $f^{(2)}$ and $f^{(0)}$, the analogous Higgs vertex remains non-vanishing even in the absence of *level-mixing* between the fermions. However, in this case, for $r'_T = r'_Y$ the coupling vanishes. This implies that the more the Yukawa coupling involving the level-0 fields appears to agree with the SM expectation (from future experimental analyses), the weaker the coupling H-$t^{(2)}$-t in such a scenario would get to be. In both cases, however, we find that the coupling strengths get enhanced for smaller values of r'_T with $r'_T < r'_Y$.

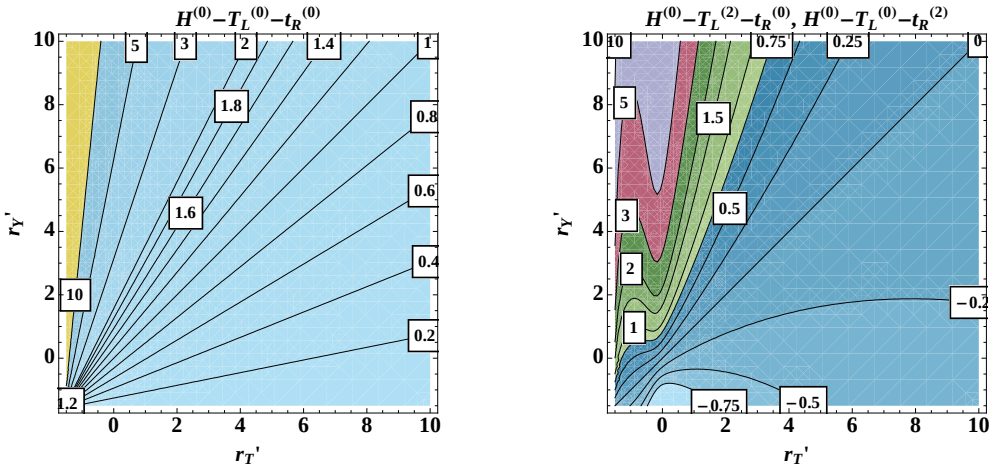

Figure 4.6: Contours of deviation in the $r'_T - r'_Y$ plane for the generic couplings $H^{(0)}$-$T_L^{(0)}$-$t_R^{(0)}$ (left) and $H^{(0)}$-$T_L^{(2)}$-$t_R^{(0)}$ or $H^{(0)}$-$T_L^{(0)}$-$t_R^{(2)}$ compared to the corresponding SM cases.

All these indicate that production of the SM Higgs boson via gluon-fusion and its decay to di-photon final state can receive non-trivial contributions from such couplings and thus might get constrained from the LHC data.

4.4 Experimental constraints and benchmark scenarios

Several different experimental observations put constraints of varying degrees on the parameters (like R^{-1}, r'_T, r'_Q, r'_Y and the input top quark mass (m_t^{in})) that control the KK top quark sector. First and foremost, R^{-1} is expected to be constrained from the searches for level-1 KK quarks and KK gluon at the LHC. In the absence of any such dedicated search, a rough estimate of $R^{-1} > 1$ TeV has been derived in ref. [82] by appropriate recast of the LHC constraints obtained for the squarks and the gluino in SUSY scenarios.

As discussed in the previous subsection, observed mass of the top quark restricts the parameter space in a nontrivial way. Also, important constraints come from the experimental bounds on flavour changing neutral currents (FCNC), electroweak precision bounds in terms of the Peskin–Takeuchi parameters (S, T and U) and bounds on effective four-fermion interactions. In this section we discuss these constraints briefly and choose a few benchmark scenarios that satisfy them and are phenomenologically interesting.

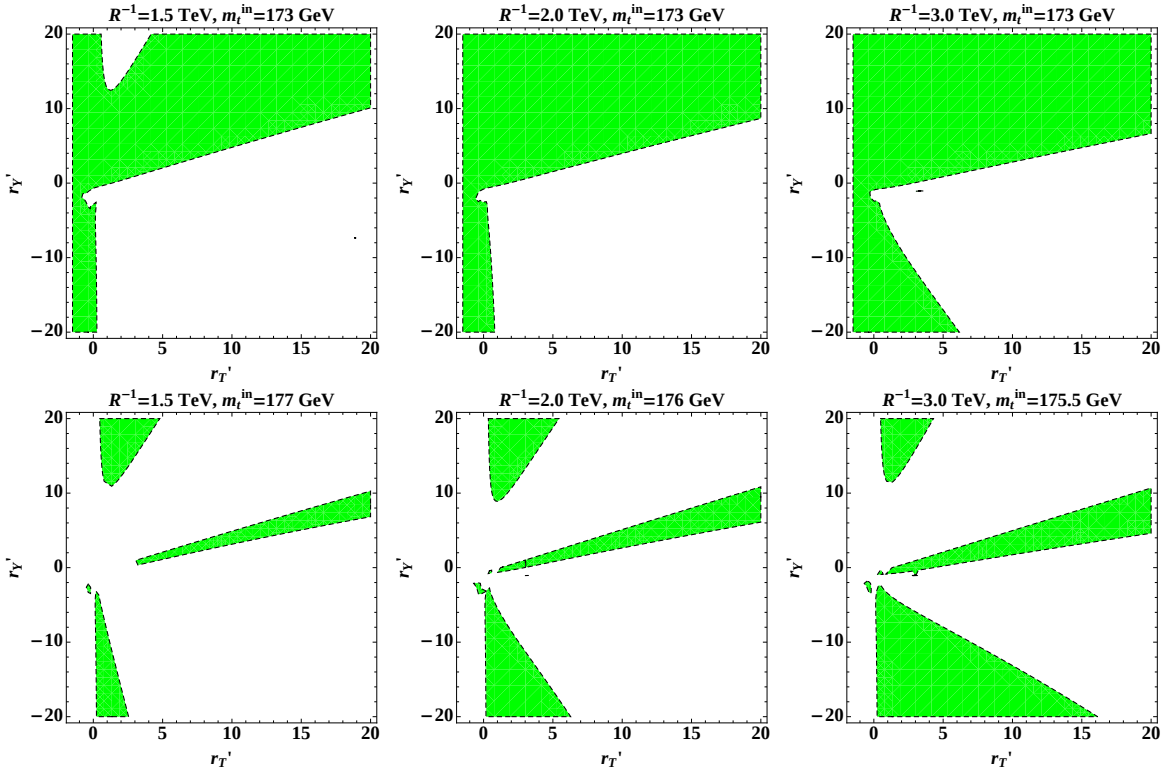

Figure 4.7: Regions (in green) in the $r'_T - r'_Y$ plane for three R^{-1} values of (1.5, 2 and 3 TeV, varying along the rows) and for different suitable values of $m_t^{\rm in}$ (indicated on top of each plot) that are consistent with physical (SM-like) top quark mass ($m_t^{\rm phys}$) being within the range $m_t^{\rm phys} = 173 \pm 2$ GeV.

4.4.1 Constraints from the observed mass of the SM-like top quark

In figure 4.7 we show the allowed regions in the $r'_T - r'_Y$ plane that result in top quark pole mass within the range 171-175 GeV [122] (which is argued to be a more appropriate range than what the experiments actually quote [123]) for given values of R^{-1} and input top quark masses.

Some general observations are that the physical top quark mass ($m_t^{\rm phys}$) rarely becomes larger than the input top quark mass ($m_t^{\rm in}$). This means, to have $m_t^{\rm phys}$ at least of 171 GeV, $m_t^{\rm in}$ has to be larger than 171 GeV. Further, increasing $m_t^{\rm in}$ beyond around 175 GeV, as we go over to the second row of figure 4.7, opens up disjoint sets of allowed islands in the $r'_T - r'_Y$ plane with increasing region allowed for negative r'_Y (and extending to larger r'_T values) at the expense of the same with positive r'_Y. Increasing $m_t^{\rm in}$ further (beyond say, 180 GeV) results in allowed regions diminishing to an insignificant level. These features remain more or less unaltered as R^{-1} is increased, as we go from left to right along a horizontal panel. A palpable direct effect that can be attributed to increasing R^{-1} is in the

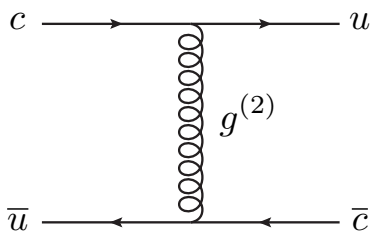

Figure 4.8: Feynman diagram showing the induced FCNC vertex.

moderate increase of the region in the $r'_T - r'_Y$ plane consistent with $m_t^{\rm phys}$, in particular, for negative r'_Y values and when $m_t^{\rm in}$ is not terminally large (*i.e.*, below 190 GeV, say) for the purpose. Although a moderate range of input top quark mass $171 < m_t^{\rm in} \lesssim 190$ is consistent with $171 < m_t^{\rm phys} < 175$ GeV in the space of $R^{-1} - r'_T - r'_Y$, the allowed region there is rather sensitive to the variation in $m_t^{\rm in}$. Thus, the allowed range of the $m_t^{\rm phys}$ restricts the nmUED parameter space in a significant way which, in turn, influences the masses and the couplings of the KK top quarks. An important point is to be noted here. The level-1 top quark sector, though does not talk to either level-0 or level-2 sector directly (because of conserved KK-parity), is influenced by these constraints since r'_T, r'_Y and R^{-1} also govern the same.

4.4.2 Flavour constraints

The BLKTs (r'_Q) and the BLYTs (r'_Y) are matrices in the flavour space. Hence, their generic choices may induce large FCNCs at the tree level. It is possible to choose a basis in which the BLKT matrix is diagonal. This ensures no mixing among fermions of different flavours or from different KK levels arising from the gauge kinetic terms. However, with the Yukawa sector included, off-diagonal terms (mixings) appear in the gauge sector on rotating the gauge kinetic terms into a basis where the quark mass matrices are diagonal. These terms could induce unacceptable FCNCs at the tree levels and thus, would be constrained by experiments. In figure 4.8 we present the tree level diagram that could give rise to unwanted FCNC effects. A rather high compactification scale ($R^{-1} \sim \mathcal{O}(10^5)$ GeV; the so-called decoupling mechanism) or a near-perfect mass-degeneracy among the KK quarks at a given level ($\frac{\Delta m}{m^{(1)}} \lesssim 10^{-6}$; across all three generations) could suppress the FCNCs to the desired level [124]. While the first option immediately renders all the KK particles rather too massive, the second one makes the KK top quarks as heavy as the KK quarks from the first two generations thus making them quite difficult to be accessed at the LHC. A third option in the form of "alignment" (of the rotation matrices) [124] can

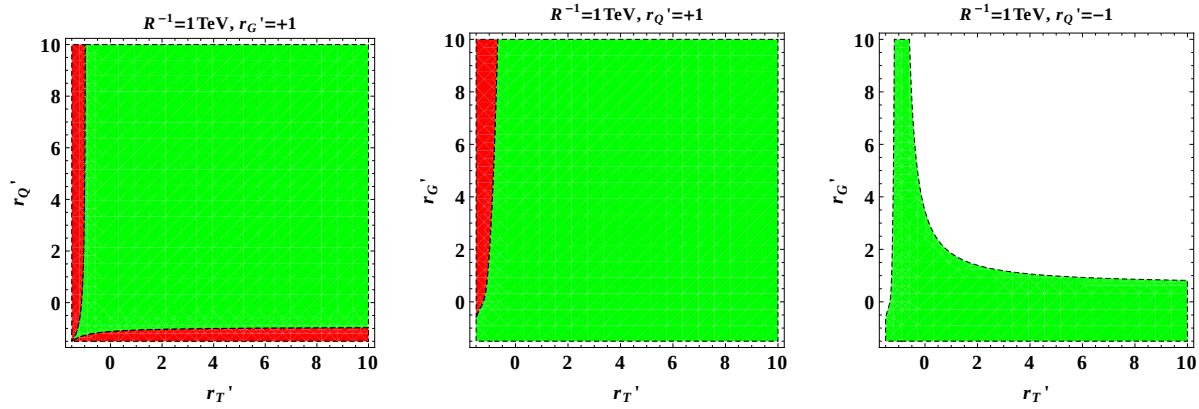

Figure 4.9: Regions in the $r'_T - r'_Q$ (for fixed r'_G; the left-most plot) and $r'_T - r'_G$ (for fixed r'_Q; the middle and the right-most plot) planes for $R^{-1} = 1$ TeV that are allowed (in green) by FCNC constraints. For the first two figures, thin strip(s) of the disallowed regions (in red) are highlighted for better visibility.

make way for significant lifting of degeneracy thus allowing for light enough quarks from the third generation that are within the reach of the LHC. In such a setup, FCNC occurs in the up-type doublet sector. Hence, the strongest of the bounds in terms of the relevant Wilson coefficient (C_D^1) comes from the recent observation of $D^0 - \overline{D^0}$ mixing [125] (and not from the K or the B meson systems) and the requirement is $|C_D^1| < 7.2 \times 10^{-7}$ TeV^{-2} [126], attributed solely to the gluonic current which is by far the dominant contribution. The essential contents of the setup are summarized in appendix C.1.

In the left-most panel of figure 4.9 we demonstrate the allowed/disallowed region in the $r'_T - r'_Q$ plane for $r'_G = 1$ with $R = 1$ TeV. The panel in the middle demonstrates the corresponding regions in the $r'_T - r'_G$ plane for $r'_Q = +1$. It is seen that some region with $r'_T < 0$ is disallowed when r'_G is large, *i.e.*, when the level-2 KK gluon is relatively light. The right-most panel illustrates the region allowed in the same plane but for $r'_Q = -1$. The bearing of the FCNC constraint is most pronounced in this case.

It can be noted that the smaller the value of r'_G is, the heavier is the mass of the level-2 gluon and hence, the stronger is the suppression of the dangerous FCNC contribution. Such a suppression could then allow r'_T to be significantly different from r'_Q but still satisfying the FCNC bounds. This feature is apparent from the rightmost panel of figure 4.9. Note that a rather minimal value for R^{-1} (=1 TeV) is chosen for this demonstration. A larger R^{-1} results in a more efficient suppression of FCNC effects and hence, leads to a larger allowed region. In summary, it appears that FCNC constraints do not seriously restrict the third generation sector as yet.

4.4.3 Precision constraints

It is well known that the Peskin–Takeuchi parameters S, T and U that parametrize the so-called oblique corrections to the electroweak gauge boson propagators [127, 128] put rather strong constraints on the mUED scenario. These observables are affected by the modification in the Fermi constant G_F (determined experimentally by studying muon decay) due to induced effective 4-fermion vertices originating from exchange of electroweak gauge bosons from even KK levels. These were first calculated in refs. [66, 129–132] assuming mUED tree-level spectrum while ref. [133] expressed them in terms of the actual (corrected) masses of the KK modes.

As discussed in refs. [30, 58, 134–136], the correction to G_F can be incorporated in the electroweak fit via the modifications it induces in the Peskin–Takeuchi parameters and contrasting them with the experimentally determined values of the latter. Note that in the nmUED scenario we consider, level-2 electroweak gauge bosons have tree-level couplings to the SM fermions and these modify the effective 4-fermion couplings. These effects are over and above what mUED induces[4] where such KK number violating couplings appear only at higher orders. It is thus natural to expect that usual oblique corrections to S, T and U induced at one-loop level would be sub-dominant when compared to the above nmUED tree-level contributions. Thus, in our present analysis, we neglect the one-loop contributions but otherwise follow the approach originally adopted in ref. [136] and which was later used in ref. [133].The nmUED effects are thus parametrized as:

$$S_{\text{nmUED}} = 0, \qquad T_{\text{nmUED}} = -\frac{1}{\alpha}\frac{\delta G_F}{G_F}, \qquad U_{\text{nmUED}} = \frac{4\sin^2\theta_W}{\alpha}\frac{\delta G_F}{G_F} \tag{4.24}$$

where α is the electromagnetic coupling strength, θ_W is the $\overline{MS}$ Weinberg angle, both given at the scale M_Z and G_F is given by

$$G_F = G_F^0 + \delta G_F \tag{4.25}$$

with G_F^0 (δG_F) originating from the s-channel SM (even KK) $W^\pm$ boson exchange. The concrete forms of these effects are calculated in our model following ref. [136]. Using our notations, these are given by:

[4]To be precise, in general, the mUED type higher-order contributions (usual one-loop-induced oblique corrections) would not be exactly the same as that from the actual mUED scenario. However, as pointed out in ref. [136], in the "minimal" case of $r_W = r_B = r_H$ along with the requirements on the relations involving μ-s and λ-s as given in equations 2.42 and 2.50, exact mUED limits for the couplings are restored while departures in the KK masses (from the corresponding mUED values) still remain.

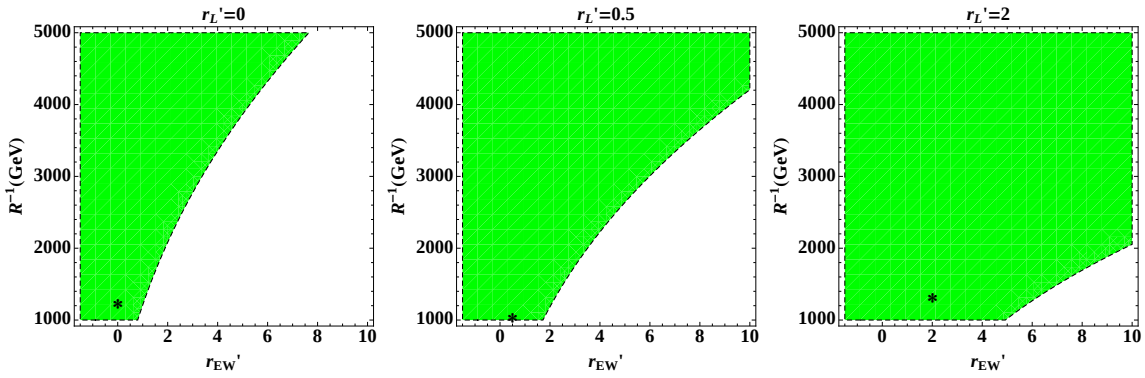

Figure 4.10: Regions (in green) in the $r'_{\rm EW} - R^{-1}$ plane allowed by electroweak precision data at 95% C.L. The black asterisks represent the global minimum in each one of them: $\chi^2_{\rm min} = 8.8 \times 10^{-9}$ at $(r'_{\rm EW}, R^{-1})$ = $(6.11 \times 10^{-3}, 1229\,{\rm GeV})$ when $r'_L = 0$, $\chi^2_{\rm min} = 3.9 \times 10^{-9}$ at $(r'_{\rm EW}, R^{-1})$ = $(0.505, 1029\,{\rm GeV})$ when $r'_L = 0.5$, $\chi^2_{\rm min} = 1.5 \times 10^{-8}$ at $(r'_{\rm EW}, R^{-1})$ = $(2.02, 1306\,{\rm GeV})$ when $r'_L = 2$.

$$G_F = G_F^0 + \delta G_F \tag{4.26}$$

with G_F^0 (δG_F) originating from the s-channel SM (even KK) $W^\pm$ boson exchange. The concrete forms of these effects are calculated in our model following ref. [136]. Using our notations, these are given by:

$$G_F^0 = \frac{g_2^2}{4\sqrt{2}}\frac{1}{M_W^2}, \quad \delta G_F = \sum_{n\geq 2:\text{even}} \frac{g_2^2}{4\sqrt{2}}\frac{1}{m_{W_{(n)}}^2}\left(g_{L_{(0)}W_{(n)}L_{(0)}}\right)^2, \tag{4.27}$$

$$\begin{aligned} g_{L_{(0)}W_{(n)}L_{(0)}}\Big|_{n:\text{even}} &\equiv \frac{1}{f_{W^{(0)}}}\int_{-L}^{L} dy\,(1 + r_{\rm EW}\,[\delta(y-L) + \delta(y+L)])\, f_{L_{(0)}} f_{W_{(n)}} f_{L_{(0)}} \\ &= \frac{2\sqrt{4r_{\rm EW} + 2\pi R}\left(M_{W_{(n)}} r_L + \tan\left(\frac{M_{W_{(n)}}\pi R}{2}\right)\right)}{M_{W_{(n)}}\,(2r_L + \pi R)\sqrt{4r_{\rm EW} + \pi R\sec^2\left(\frac{M_{W_{(n)}}\pi R}{2}\right) + 2\tan\left(\frac{M_{W_{(n)}}\pi R}{2}\right)}/M_{W_{(n)}}} \end{aligned} \tag{4.28}$$

where $M_{W^{(n)}}$ is determined by equation 2.51. Even though the KK leptons do not appear in the process, the BLKT parameter r_L in the lepton sector (to be precise, the one for the 5D muon doublet) inevitably influences the coupling-strength given in equation 4.28. We, however, assume a flavour-universal BLKT parameter r_L (just like what we do in the quark sector when we take $r_Q = r_T$) which help trivially circumvent tree-level contributions to lepton-flavour-violating processes.

We perform a χ^2 fit of the parameters $S_{\rm nmUED}$, $T_{\rm nmUED}$ and $U_{\rm nmUED}$ (with δG_F evaluated for $n = 2$ only) for three fixed values of r'_L ($r'_L = r_L R^{-1} = 0$, 0.5 and 2) to the experi-

mentally fitted values of the allowed new physics (NP) components in these respective observables as reported by the GFitter group [137] which are given by

$$S_{\rm NP} = 0.03 \pm 0.10, \qquad T_{\rm NP} = 0.05 \pm 0.12, \qquad U_{\rm NP} = 0.03 \pm 0.10,$$

the correlation coefficients being

$$\rho_{ST} = +0.89, \qquad \rho_{SU} = -0.54, \qquad \rho_{TU} = -0.83,$$

and the reference input masses of the SM top quark and the Higgs boson being $m_t = 173$ GeV and $m_H = 126$ GeV, respectively.

In figure 4.10 we show the 95% C.L. allowed region in the $r'_{\rm EW} - R^{-1}$ plane as a result of the fit performed. As can be expected, the bound refers to $r'_{\rm EW}$ as the only brane-local parameter which, unlike in ref. [133], can be different from the corresponding parameters governing other sectors of the theory. Such a constraint is going to restrict the mass-spectrum and the couplings in the electroweak sector which is relevant for our present study. It is not unexpected that for larger values of $r_{\rm EW}$ which result in decreasing masses for the electroweak gauge bosons, only larger values of R^{-1} (which compensates for the former effect) remain allowed thus rendering these excitations (appearing in the propagators) massive enough to evade the precision bounds. Interestingly, it is possible to relax the bounds by introducing a positive r'_L as shown in figure 4.10, a feature that can be taken advantage of as we explore the nmUED parameter space further. This is since the coupling involved $g_{L_{(0)}W_{(n)}L_{(0)}}$ gets reduced in the process (see the left plot in figure 4.4).

4.4.4 Benchmark scenarios

For our present analysis, we now choose some benchmark scenarios which satisfy the constraints discussed in the previous subsection. The parameter space of these scenarios mainly spans over r'_T, r'_Y, R^{-1} and, as a minimal choice, $r'_{\rm EW} = r'_H$[5]. We also include r'_G, r'_Q and r'_L which are the BLKT parameters for the KK gluon, the KK quark and the KK lepton sectors, respectively. r'_G has some non-trivial implications for the couplings of the KK top quarks to the gluonic excitations as discussed in section 4.3.4. The parameter r'_Q, though enters our discussion primarily through FCNC considerations (see section 4.4.2 and appendix C.1), governs the couplings $V^{(2)}$-$q^{(0)}$-$q^{(0)}$ (as shown in figure 4.4) that control

[5]Departure from this assumption makes the gauge boson zero modes non-flat and hence correct values (within experimental errors) of the SM parameters like $\alpha_{em}, G_f, m_W, m_Z$ can only be reproduced in a constrained region of $r'_{\rm EW} - r'_H$ parameter space [83].

KK top quark production processes. Both r'_G and r'_Q serve as key handles on the masses of the KK gluon and the KK quarks from the first two generations, respectively. Similar is the status of r'_L which enters through the oblique parameters and controls the masses and couplings in the lepton sector.

In search for suitable benchmark scenarios, we require the following conditions to be satisfied. We require the approximate lower bound on R^{-1} to hover around 1 TeV which is obtained by recasting the LHC bounds on squarks (from the first two generations) and the gluino in terms of level-1 KK quarks and KK gluons in the nmUED scenario [82]. Further, the lighter of the level-1 KK top quark ($t_l^{(1)}$) is required to be at least about 500 GeV. This safely evades current LHC-bounds on similar excitations while lower values may still be allowed given that these bounds result from model-dependent assumptions.

The above requirements together calls for a non-minimal sector for the electroweak gauge bosons ($r'_{\rm EW} \neq 0$) such that the lightest KK gauge boson, the KK photon ($\gamma^{(1)}$) is the lightest KK particle (LKP, a possible dark matter candidate)[6]. Incorporation of a non-minimal gauge sector affects the couplings of the gauge bosons which, as we will see, could be phenomenologically non-trivial. The choice $r'_{\rm EW} = r'_H$ renders the KK excitations of the gauge and the Higgs boson very close in mass thus allowing them to take part in the phenomenology of the KK top quarks. In the present scenario, other BLT parameters in the Higgs sector, μ_b and λ_b, are constrained by equations 2.42 and 2.50 in addition to the measured Higgs mass as an input. Therefore, these are not independent degrees of freedom.

In table 4.2 we present the spectra for three such benchmark scenarios: two of them with $R^{-1} = 1$ TeV and the other with $R^{-1} = 1.5$ TeV. The BLKT parameters r'_G and r'_Q are so chosen such that the masses of the level-1 KK gluon are in the range 1.6-1.7 TeV (*i.e.*, somewhat above the current LHC lower bounds on similar (SUSY) excitations) while the KK quarks from the first two generations are heavier[7]. Note that in both cases we are having negative r'_G and r'_Q. In the top quark sector, the BLKT parameter r'_T are fixed at values for which both light and heavy level-1 KK top quarks have sub-TeV masses and hence expected to be within the LHC reach. Also, r'_Y, the BLT parameter for the Yukawa sector, has been tuned in the process to end up with such spectra. Note that the choices of values for r'_T and r'_Y are consistent with the constraints from the physical top quark

[6]This is a possible choice for the dark matter candidate in the nmUED scenario. Ref. [83] explores other possible candidates in such a scenario.

[7]Such a hierarchy of masses opens up the possibility of level-1 KK top quarks being produced in the cascade decays of the KK gluon and the KK quarks.

mass as discussed in section 4.4.1 and the flavour constraints discussed in section 4.4.2. Larger values of R^{-1} would tend to make the level-2 KK top quark a little too heavy ($\lesssim 1.5$ TeV) to be explored at the LHC while if one requires the lighter level-1 KK top quark not too light ($\lesssim 300$ GeV) which can be quickly ruled out by the LHC experiments even in an nmUED scenario which we consider. Nonetheless, the lighter of the level-2 top quark may anyway be heavy and only the level-1 top quarks remain to be relevant at the LHC. In that case, larger values of R^{-1} also remain relevant.

Values of $r'_{\rm EW}$ are so chosen as to have $\gamma^{(1)}$ as the LKP with masses around half a TeV. This renders the level-2 electroweak gauge bosons to have masses around 1.5 TeV thus making them possibly sensitive to searches for gauge boson resonances at the LHC [138, 139][8].

In table 4.2 we also indicate the masses of the level-2 KK excitations. It is to be noted that the lighter of the level-2 KK top quark may not be that heavy ($\lesssim 1.5$ TeV). Level-2 gluon, for our choices of parameters, is pushed to around 3 TeV and hence, unless their couplings to quarks (SM ones or from level-1) are enhanced, LHC may be barely sensitive to their presence. This is a rather involved issue which again warrants dedicated studies and is beyond the scope of the present work.

For the first benchmark point (BM1) with $R^{-1} = 1$ TeV, the mass-splitting between the two level-1 top quark states is much smaller (~ 100 GeV) with a somewhat heavier $t_l^{(1)}$ when compared to the second case (BM2) for which $R^{-1} = 1.5$ TeV. We will see in section 4.5 that such mass-splittings and the absolute masses themselves for the KK top quarks have interesting bearing on their phenomenology at the LHC. Further, the relevant couplings do change (see figures 4.4, 4.5 and 4.6) in going from one point to the other. The third benchmark point BM3 is just BM1 but with different r'_Y and $m_t^{\rm in}$. BM3 demonstrates a situation with enhanced Higgs-sector couplings and its ramifications at the LHC. It is found that for all the three benchmark points, the coupling $V^{(2)}$-$f^{(0)}$-$f^{(0)}$ get enhanced when level-2 W or Z boson is involved.

Note that the KK bottom quark masses are also governed by r'_T and r'_Y for a given R^{-1}. However, since the splitting between the two physical states at a given KK level is proportional to the SM bottom quark mass, the KK bottom quarks at each given level are almost degenerate (just as it is for the KK quark flavours from the first two generations) in

[8]The caveats are that these level-2 gauge bosons could have very large decay widths (exceptionally fat) due to enhanced $V^{(2)}$-$f^{(0)}$-$f^{(0)}$ couplings as opposed to narrow-width approximation for the resonances assumed in the experimental analysis [139] and hence need dedicated studies for them at the LHC [140]. Further, the involved assumption of a 100% branching fraction for the resonance decaying to quarks may also not hold. These two issues would invariably relax the mentioned bounds on level-2 gauge bosons.

mass unlike their top quark counterparts. Thus, some of the KK bottom quarks can have masses comparable to those of the corresponding KK top quark states and hence would eventually enter a collider study otherwise dedicated for the latter.

BM1	$R^{-1} = 1$ TeV, $r'_G = -1$, $r'_Q = -1.2$, $r'_T = 1$, $r'_Y = 0.5$, $r'_{\rm EW} = 1.5$, $r'_L = 0.4$, $m_t^{\rm in} = 173$ GeV
Gauge bosons & Higgs	$m_{\gamma^{(1)}} = 556.9$, $m_{Z^{(1)}} = m_{A^{(1)^0}} = 564.4$, $m_{W^{(1)^\pm}} = m_{H^{(1)^\pm}} = 562.7$, $m_{g^{(1)}} = 1653.8$ $m_{\gamma^{(2)}} = 1301.4$, $m_{Z^{(2)}} = m_{A^{(2)^0}} = 1304.6$, $m_{W^{(2)^\pm}} = m_{H^{(2)^\pm}} = 1303.9$, $m_{g^{(2)}} = 2780.2$ $m_{H^{(1)^0}} = 570.8$, $m_{H^{(2)^0}} = 1307.4$
Quarks & Leptons	$m_{q^{(1)}} = 1711.5$, $m_{q^{(2)}} = 2816.9$ $m_t^{\rm phys} = 172.6$, $m_{t_l^{(1)}} = 620.4$, $m_{t_h^{(1)}} = 714.5$ $m_{t_l^{(2)}} = 1359.6$, $m_{t_h^{(2)}} = 1471.7$ $m_{b^{(1)}} = 638.3$, $m_{b^{(2)}} = 1395.8$ $m_{l^{(1)}} = 802.3$, $m_{l^{(2)}} = 1631.8$
BM2	$R^{-1} = 1.5$ TeV, $r'_G = -0.1$, $r'_Q = -1.1$, $r'_T = 4$, $r'_Y = 8$, $r'_{\rm EW} = 5.5$, $r'_L = 2$, $m_t^{\rm in} = 173$ GeV
Gauge bosons & Higgs	$m_{\gamma^{(1)}} = 487.3$, $m_{Z^{(1)}} = m_{A^{(1)^0}} = 495.7$, $m_{W^{(1)^\pm}} = m_{H^{(1)^\pm}} = 493.9$, $m_{g^{(1)}} = 1601.6$ $m_{\gamma^{(2)}} = 1655.9$, $m_{Z^{(2)}} = m_{A^{(2)^0}} = 1658.4$, $m_{W^{(2)^\pm}} = m_{H^{(2)^\pm}} = 1657.8$, $m_{g^{(2)}} = 3200.8$ $m_{H^{(1)^0}} = 503.0$, $m_{H^{(2)^0}} = 1660.6$
Quarks & Leptons	$m_{q^{(1)}} = 2527.5$, $m_{q^{(2)}} = 4200.2$ $m_t^{\rm phys} = 172.4$, $m_{t_l^{(1)}} = 504.2$, $m_{t_h^{(1)}} = 813.3$ $m_{t_l^{(2)}} = 1366.3$, $m_{t_h^{(2)}} = 2220.2$ $m_{b^{(1)}} = 561.9$, $m_{b^{(2)}} = 1706.6$ $m_{l^{(1)}} = 750.0$, $m_{l^{(2)}} = 1865.1$
BM3	Input values same as in BM1 except for $r'_Y = 5$ and $m_t^{\rm in} = 176$ GeV
Gauge bosons & Higgs	Masses same as in BM1
Quarks & Leptons	Masses same as in BM1 except for $m_t^{\rm phys} = 173.4$ and $m_{t_l^{(1)}} = 626.3$, $m_{t_h^{(1)}} = 710.5$ $m_{t_l^{(2)}} = 1350.7$, $m_{t_h^{(2)}} = 1488.6$

Table 4.2: Masses (in GeV) of different KK excitations in three benchmark scenarios. With $r'_H = r'_{\rm EW}$, the level-1 Higgs boson masses are very much similar to the masses of the level-1 electroweak gauge bosons. Choices of the input parameters satisfy the experimental bounds discussed earlier.

4.5 Phenomenology at the LHC

Given the nontrivial structure of the top quark sector of the nmUED it is expected that the same would have a rich phenomenology at the LHC. A good understanding of the same requires a thorough study of the decay patterns of the KK top quarks and their production rates. In this section we discuss these issues at the lowest order in perturbation theory.

Towards this we implement the scenario in `MadGraph` 5 [88] using `Feynrules` version 1 [89] via its `UFO` (Univeral Feynrules Output) [90, 91] interface. This now contains the KK gluons, quarks (including the top and the bottom quarks), leptons[9] and the electroweak gauge bosons up to KK level-2. Level-1 and level-2 KK Higgs bosons are also incorporated. The mixings in the quark sector, including 'level-mixing' between KK level-2 and level-0, have now been incorporated in a generic way. In this section we discuss these with the help of the benchmark scenarios discussed in section 4.4.4. We then consolidate the information to summarize the important issues in the search for such excitations at the LHC.

4.5.1 Decays of the KK top quarks

Decays of the KK top quarks are mainly governed by the two input parameters, r'_T and $r'_{\rm EW}$, for a given value of R^{-1} [10]. The dependence is rather involved since these two parameters not only determine the spectra of the KK top quarks and the KK electroweak gauge bosons but also the involved couplings. The latter, in turn, are complicated functions of the input parameters as given by equation 4.23 and as illustrated in figures 4.4, 4.5 and 4.6. In the following, we briefly discuss the possible decay modes of the KK top quarks and the significance of some of them at the LHC. In table 4.3 we list the branching fractions for the three benchmark points presented earlier in table 4.2. For our choices of input parameters, two decay modes are possible for $t_l^{(1)}$: $t_l^{(1)} \to bW^{(1)^+}$ and $t_l^{(1)} \to bH^{(1)^+}$. Decays to $tZ^{(1)}/t\gamma^{(1)}/tH^{(1)^0}/tA^{(1)^0}$ are also possible when the mass-splitting between $t_l^{(1)}$ and $Z^{(1)}/\gamma^{(1)}/H^{(1)^0}/A^{(1)^0}$ is larger than the mass of the SM-like top quark. In our scenario, its decays to $b_l^{(1)}$ and $b_h^{(1)}$ are prohibited on kinematic grounds. Unlike in some competing scenarios (like the MSSM) where channels like, say, $\tilde{t}_1 \to b\chi_1^+$ and $\tilde{t}_1 \to t\chi_1^0$) could attain a 100% branching fraction, the spectra of the involved KK excitations in our scenario would not allow $t_l^{(1)}$ decaying exclusively to either $bW^{(1)^\pm}$ or $t\gamma^{(1)}$. The reason

[9] The KK leptons would eventually get into the cascades of the KK gauge bosons.

[10] In the present analysis, the level-1 KK gluon is taken to be heavier than all three KK top quark states that are relevant for our present work, *i.e.*, the two level-1 and the lighter level-2 KK top quarks.

behind this is that $W^{(1)^\pm}$ and $\gamma^{(1)}$ are rather close in mass and hence if decays to $t\gamma^{(1)}$ is allowed, the same to $bW^{(1)^+}$ is also kinematically possible. Further, even the latter mode has to compete with $t_l^{(1)} \to bH^{(1)^+}$ as $m_{W^{(1)^\pm}} \approx m_{H^{(1)^\pm}}$. Translating constraints on such KK top quarks from those obtained in the LHC-studies of, say, the top squarks is not at all straight-forward since the latter explicitly assume either $\tilde{t}_1 \to b\chi_1^+ = 100\%$ [141, 142] or $\tilde{t}_1 \to t\chi_1^0 = 100\%$ [142]. Further, $W^{(1)^\pm}$ (and also $Z^{(1)}$), being among the lighter most ones of all the level-1 KK excitations, would only undergo three-body decays to LKP ($\gamma^{(1)}$) accompanied by leptons or jets that would be rather soft because of the near-degeneracy of the masses of the level-1 KK gauge bosons. This would lead to loss of experimental sensitivity for final states with more number of hard leptons and jets [141].

The situation with $t_h^{(1)}$ is not qualitatively much different as long as decay modes similar to $t_l^{(1)}$ are the dominant ones. This is the case with BM1. Under such circumstances, they could turn out to be reasonable backgrounds to each other (if their production rates are comparable) and dedicated studies would be required to disentangle them. In any case (even in the absence of good discriminators), simultaneous productions of both $t_l^{(1)}$ and $t_h^{(1)}$ would enhance the new-physics signal. On the other hand, in a situation like BM2, more decay modes may be available to $t_h^{(1)}$ although decays to level-1 bottom and top quarks along with SM $W^\pm$ and Z are the dominant ones. The ensuing cascades of these states would inevitably make the analysis challenging. However, under favorable circumstances, reconstructions of the $W^\pm$ and/or Z bosons along with b- and/or *top-tagging* could help disentangle the signals. Thus, it appears that search for level-1 KK top quarks involves complicated issues (some of which are common to top squark searches in SUSY scenarios) and a multi-channel analysis could turn out to be very effective.

We now turn to the case of level-2 top KK top quarks. The lighter of the two states, $t_l^{(2)}$ can have substantial rates at the LHC which is discussed in some detail in section 4.5.2. This motivates us to study the decay patterns of $t_l^{(2)}$. In the last column of table 4.3 we present the decay branching fractions of $t_l^{(2)}$. As can be seen, the decay modes that are usually enhanced involve a pair of level-1 KK excitations which would cascade to the LKP. We, however, strive to understand to what extent $t_l^{(2)}$, being an even KK-parity state, could decay directly to a pair of comparatively light (level-0) particles (and hence, boosted) comprising of an SM fermion and an SM gauge/Higgs boson[11]. Thus, in the one hand, these decay products are unlikely to be missed in an experiment while on the other hand, new techniques to reconstruct (like the study of jet substructure [143, 144]

[11]These may be contrasted with the popular SUSY scenarios (sparticles carrying odd R-parity) where such possibilities are absent.

BM1	$t_l^{(1)} \to bW^{(1)^+} = 0.597$ $bH^{(1)^+} = 0.403$	$t_h^{(1)} \to bW^{(1)^+} = 0.615$ $bH^{(1)^+} = 0.370$ $t_l^{(1)}Z = 0.016$	$t_l^{(2)} \to b_h^{(1)}W^{(1)^+} = 0.351$ $t_h^{(1)}A^{(1)^0} = 0.177$ $\boldsymbol{bW^+ = 0.062}$ $\boldsymbol{tH = 0.062}$ $b_h^{(1)}H^{(1)^+} = 0.057$ $b_l^{(1)}H^{(1)^+} = 0.055$ $\boldsymbol{tZ = 0.031}$
BM2	$t_l^{(1)} \to bH^{(1)^+} = 0.842$ $bW^{(1)^+} = 0.158$	$t_h^{(1)} \to b_h^{(1)}W^+ = 0.305$ $t_l^{(1)}Z = 0.180$ $b_l^{(1)}W^+ = 0.141$ $tA^{(1)^0} = 0.130$ $t_l^{(1)}H = 0.126$ $bH^{(1)^+} = 0.069$ $bW^{(1)^+} = 0.020$ $tH^{(1)^0} = 0.015$	$t_l^{(2)} \to t_h^{(1)}A^{(1)^0} = 0.377$ $b_h^{(1)}H^{(1)^+} = 0.208$ $b_l^{(1)}H^{(1)^+} = 0.200$ $t_l^{(1)}H^{(1)^0} = 0.109$ $t_l^{(1)}A^{(1)^0} = 0.055$ $\boldsymbol{tH = 0.014}$ $\boldsymbol{bW^+ = 0.0022}$ $\boldsymbol{tZ = 0.00058}$
BM3	$t_l^{(1)} \to bH^{(1)^+} = 0.946$ $bW^{(1)^+} = 0.054$	$t_h^{(1)} \to bH^{(1)^+} = 0.941$ $bW^{(1)^+} = 0.060$	$\boldsymbol{t_l^{(2)} \to tH = 0.448}$ $t_l^{(1)}A^{(1)^0} = 0.102$ $t_h^{(1)}A^{(1)^0} = 0.092$ $t_l^{(1)}H^{(1)^0} = 0.082$ $t_h^{(1)}H^{(1)^0} = 0.063$ $\boldsymbol{bW^+ = 0.046}$ $\boldsymbol{tZ = 0.022}$

Table 4.3: Decay branching fractions of different KK top quarks for the three benchmark points presented in table 4.2. Modes having branching fractions less than about a percent are not presented except for the ones with a pair of SM particles in the final state. Tree level decays of $t_l^{(2)}$ to SM states are shown in bold in the right-most column.

etc.) some of them have to be employed.

In scenario BM1, the total decay branching fraction to SM states (shown in bold) is just about 15% while in scenario BM2 such decays are practically absent. Given the large phase space available, such small (or non-existent) decay rates to SM particles can only be justified in terms of rather feeble (effective) couplings among the involved states. The couplings of $t_l^{(2)}$ to the SM gauge bosons and an SM fermion would have vanished (due to the orthogonality of the mode functions involved) had $t_l^{(2)}$ been a pure level-2 state. The smallness of these couplings thus readily follows from the tiny admixture of the SM

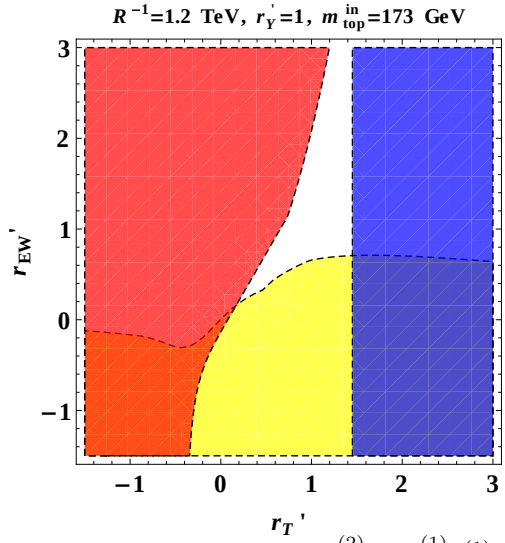

Figure 4.11: Region in $r'_T - r'_{\rm EW}$ plane where the decays $t_l^{(2)} \to t_l^{(1)}\gamma^{(1)}$, $t_l^{(1)}Z^{(1)}$, $b_l^{(1)}W^{(1)^+}$ are kinematically prohibited (in yellow), $\gamma^{(1)}$ is the LKP with $m_{\gamma^{(1)}} > 400$ GeV (in red) and $m_{t_l^{(2)}} < 1.5$ TeV (in blue). The entire region shown is compatible with the acceptable range of the mass of the top quark and other precision constraints.

top quark in the physical $t_l^{(2)}$ state and thus, results in its small branching fractions to SM gauge bosons. The same argument does not hold for the corresponding coupling $t_l^{(2)}$-t-H that controls the other SM decay mode of $t_l^{(2)}$, *i.e.*, $t_l^{(2)} \to tH$. However, it is clear from figure 4.6 that this coupling is going to be small for both the benchmark points BM1 and BM2.

Since direct decays of $t_l^{(2)}$ to SM states could provide the 'smoking guns' at the LHC in the form of rather boosted objects (top and bottom quarks, Z, $W^\pm$ and Higgs boson) that could eventually be reconstructed to their parent, this motivates us to study if such decays can ever become appreciable. We find that the coupling $t_l^{(2)}$-t-H gets significantly enhanced with a slight modification in the parameters of BM1 (called BM3 in table 4.2) by setting $r'_Y = 5$ (see figure 4.6) and $m_t^{\rm in} = 176$ GeV while keeping other parameters untouched and still satisfying all the experimental constraints that we discussed. As we can see, the branching fraction to tH final state could attain a level of 50% which should be healthy for the purpose. Efficient tagging of boosted top quarks [145–148] and boosted Higgs bosons [149] would hold the key in such a situation. Some such techniques have already been proposed in recent literature [112], in particular, in the context of vector-like top quarks or more generally, in the study of 'top-partners'.

On the other hand, since the $t_l^{(2)}$-t-Z and $t_l^{(2)}$-b-$W^\pm$ are dynamically constrained, these could only get enhanced if the competing modes (decays to a pair of level-1 KK states)

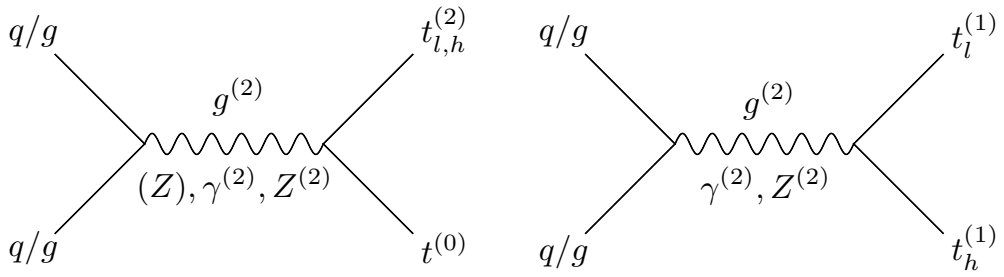

Figure 4.12: Feynman diagrams for the associated $t^{(2)}_l - t^{(0)}$ (left) and $t^{(1)}_l - t^{(1)}_h$ productions at the LHC. The gluon-initiated processes are only mediated by $g^{(2)}$ while the quark-initiated processes are mediated by both $g^{(2)}$ and other electroweak gauge bosons from level-0 (Z) and level-2 ($\gamma^{(2)}$, $Z^{(2)}$).

face closure. As the couplings involved in the latter cases are generically of SM strength, these could only be effectively suppressed by having them kinematically forbidden. From figure 4.11 we find that, by itself, this is not very difficult to achieve (in yellow shade) over the nmUED parameter space. However, rather conspicuously, the simultaneous demands for the KK photon to be the LKP with $m_{\gamma^{(1)}} > 400$ GeV (the red-shaded region) and that of $m_{t^{(2)}_l} < 1.5$ TeV (in blue shade) leave no overlapping region in the nmUED parameter space. It may appear that one simple way to find some overlap is by moving down in r'_T. However, this implies $t^{(2)}_l$ becomes more massive thus loosing in its production cross section in the first place. Although the interplay of events that leads to this kind of a situation is not an easy thing to follow, the issue that is broadly conspiring is the similarity in the basic evolution-pattern of the masses of the KK excitations as functions of the BLKT parameters (see figure 4.1 and ref. [82]).

4.5.2 Production processes

In this section we discuss different production modes of the KK top quarks at the 14 TeV (the design energy) LHC with reference to the nmUED parameter space. These are of following four broad types (in line with top squark phenomenology in SUSY scenarios):

- the generic mode with two top quark excitations in the final state that receives contributions from processes involving both strong and electroweak interactions,
- exclusively electroweak processes leading to a single top quark excitation
- the associated production of a pair of KK top quarks and the (SM) Higgs boson and
- production from the cascades of KK gluons and KK quarks.

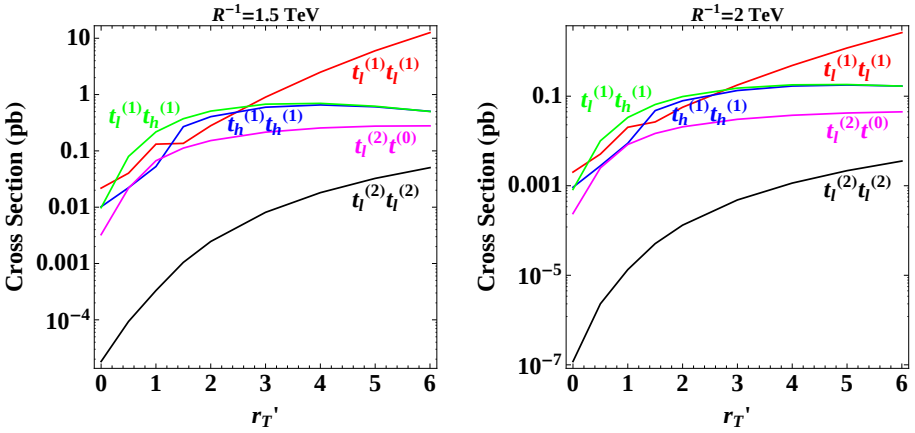

Figure 4.13: Cross sections (in picobarns, at tree level) for different production processes involving the KK top quarks as functions of r'_T at the 14 TeV LHC for $R^{-1} = 1.5$ TeV (left) and $R^{-1} = 2$ TeV (right), $r'_Y = 3$, $r'_G = 0.5$ and the other parameters are chosen as in the BM2. CTEQ6L1 parton distributions [150] are used and the factorization/renormalization scale is set at the sum of the masses in the final state.

Final states with a pair of top quark excitations

These are the processes where two similar or different kind of top quark excitations are produced in the final state. The interesting modes in this category are pair-production of $t_l^{(1)}$ and $t_h^{(1)}$ along with the associated productions of $t_l^{(1)}t_h^{(1)}$ and $t_l^{(2)}t$. The latter two processes are possible in an nmUED scenario and the corresponding Feynman diagrams are presented in figure 4.12. Note that the requirement of current conservation does not allow the massless SM gauge bosons (gluon and photon) to mediate these processes while the pair-productions receive contributions from all possible mediations. Also, these two associated production modes have no counter-parts in a competing SUSY scenario like the MSSM. In figure 4.13 we illustrate the variations of the rates for these processes with r'_T for R^{-1}=1 TeV (left) and 2 TeV (right). As can be seen, pair production of $t_l^{(1)}$, has by far the largest cross section for $r'_T \gtrsim 3$ reaching up to 10 (1) pb for R^{-1} = 1.5 (2) TeV. This is not unexpected since $t_l^{(1)}$ is the lightest of the KK top quarks. In this regime, the yields for $t_h^{(1)}$-pair and $t_l^{(1)}t_h^{(1)}$ associated productions are very similar touching 1 (0.1) pb for R^{-1} = 1.5 (2) TeV. The corresponding rates for $t_l^{(2)}t$ associated production do not lag much notching 0.5 (0.05) pb, respectively. Further, the $t_l^{(2)}$-pair has a trend similar to that of the $t_l^{(1)}$-pair in this respect but, rate-wise, falls out of the competition.

Note that with increasing r'_T masses of all the KK states decrease. Interestingly enough, this effect is reflected in a straight-forward manner only in the case of $t_l^{(1)}$-pair for which the rates increase with growing r'_T. For other competing processes mentioned above, the curves flatten out. This behavior signals non-trivial interplays of the intricate couplings

Benchmark	$t_l^{(1)}\bar{t}_l^{(1)}$ (pb)	$t_l^{(1)}\bar{t}_h^{(1)}$ (pb)	$t_h^{(1)}\bar{t}_h^{(1)}$ (pb)	$t\bar{t}_l^{(2)}$ (pb)
BM1	0.63	0.10	0.35	0.07
BM2	2.24	0.35	0.76	0.21
BM3	0.76	0.11	0.30	0.07

Table 4.4: Production cross sections (in picobarns, at tree level) for different pairs of KK top quarks for the benchmark points. Contributions from the Hermitian conjugate processes are taken into account wherever applicable. The choices for the parton distribution and the scheme for determining the factorization/renormalization scale are the same as in figure 4.13.

involved. These have much to do with when all these rates become comparable for $r'_T \lesssim 3$ [12]. In the process, the rate for usual $t\bar{t}$ pair production also gets affected to some extent. However, our estimates are all being at the tree level, these do not pose any immediate concern while facing the measured $t\bar{t}$ cross section which is much larger and agrees with its estimation at higher orders in perturbation theory. Also, in table 4.4 we present the cross sections for the three benchmark points. The bottom-line is that the production rates of three different KK top quark excitations remain moderately healthy over favorable region of the nmUED parameter space at a future LHC run. With the knowledge of their decay patterns (see table 4.3) and the associated features discussed in section 4.5.1 it is required to chalk out a strategy to reach out to these excitations.

Single production processes

We consider two broad categories of single production of KK top quarks which are closely analogous to single top production in the SM once the issue of KK-parity conservation is taken into account. In the first case, a level-1 KK top quark is produced in association with level $W^{(1)^\pm}$ or $b^{(1)}$ quark. The second one involves the lighter of the level-2 KK top quarks along with an SM $W^\pm$ boson or an SM bottom quark. The generic, tree-level Feynman diagrams that contribute to the processes are presented in figure 4.14.

Single production of level-1 top quarks: Single production of level-1 top quarks along with a level-1 $W^\pm$ boson proceeds via gb fusion in s-channel and gb scattering in t-channel.

[12] It may be noted in this context that an effective $SU(3)$ coupling involving a set of KK excitations is not necessarily stronger than the effective electroweak coupling among them and these might even have relative signs between them (see figures 4.4, 4.5 and 4.6). Thus, contributions from different mediating processes heavily depend on the nmUED parameters.

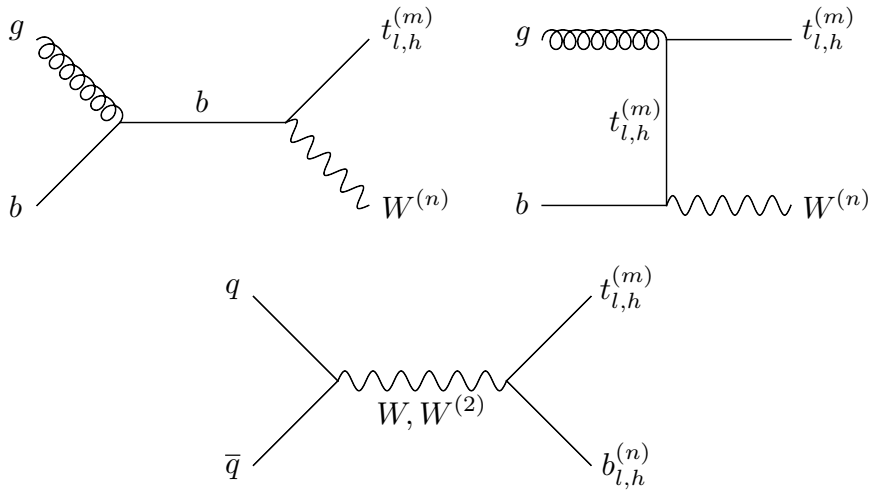

Figure 4.14: Generic Feynman diagrams for the single production of a KK top quark along with KK excitations of $W^{\pm}$ boson (upper panel) and KK bottom quark (lower panel) at the LHC. Superscripts m and n standing for the KK levels can be different (like '0' and '2') but should ensure KK-parity conservation.

Benchmark	$t_l^{(1)}W^{(1)-}$ (pb)	$t_l^{(1)}\bar{b}_l^{(1)}$ (pb)	$t_l^{(2)}b$ (pb)	$t_l^{(1)}\bar{t}_l^{(1)}H$ (pb)	$t_l^{(1)}\bar{t}_h^{(1)}H$ (pb)	$t_h^{(1)}\bar{t}_h^{(1)}H$ (pb)	$t\bar{t}_l^{(2)}H$ (pb)	$t\bar{t}H$ (pb)
BM1	0.01	0.11	0.11	$\sim 10^{-5}$	$\sim 10^{-4}$	$\sim 10^{-3}$	0.03	0.24
BM2	0.04	0.21	0.13	0.73	5.39	0.17	0.11	1.25
BM3	$\sim 10^{-3}$	0.23	0.11	$\sim 10^{-4}$	$\sim 10^{-3}$	0.01	0.04	2.21

Table 4.5: Cross sections (in picobarns, at tree level) for single and (SM) Higgs-associated KK top quark productions for the benchmark points. The mass of the SM Higgs boson is taken to be 125 GeV. Contributions from the Hermitian conjugate processes are taken into account wherever applicable. The choices for the parton distribution and the scheme for determining the factorization/renormalization scale are the same as in figure 4.13.

The rates are at best a few tens of femtobarns as can be seen from table 4.5. On the other hand, the mode in which a level-1 bottom quark is produced in association proceeds through s-channel fusion of light quarks and propagated by $W^{\pm}$ and $W^{(2)\pm}$ bosons. The cross sections are found to be rather healthy ranging from 110 fb to 230 fb. The observed rates for $t_l^{(1)}W^{(1)\pm}$ production appear to be consistently lower than that for $t_l^{(1)}b_l^{(1)}$ production. This can be traced back to the presence of enhanced q-q'-$W^{(2)\pm}$ coupling. Moreover, cross sections for other combinations involving heavier states of $t^{(1)}$ and $b^{(1)}$ in the final state could have comparable strengths because of such enhanced couplings.

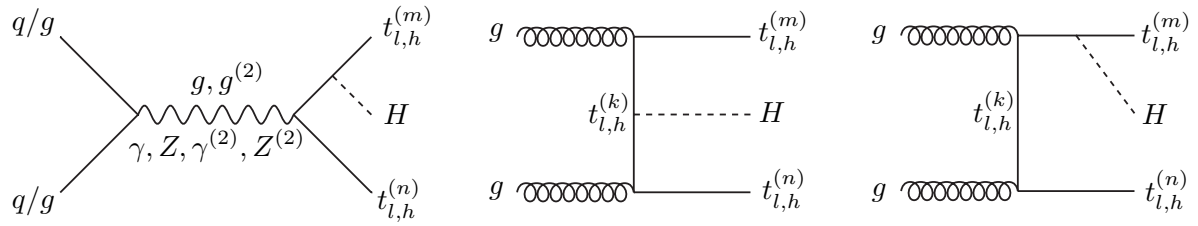

Figure 4.15: Generic Feynman diagrams for the associated (SM) Higgs production along with a pair of KK excitations of the top quark. Superscripts k, m and n can be different (like 0 and 2) but should ensure KK-parity conservation.

Single production of level-2 top quark: The associated $t_l^{(2)}W^-$ production involves the vertex $t_l^{(2)}$-$W^\pm$-b which, as we discussed earlier (see sections 4.3.4 and 4.5.1), vanishes but for a small admixture of level-0 top in the physical state $t^{(2)}$. Hence, the rates in this mode turn out to be insignificant. Further, the $W^\pm$-mediated diagram in the associated $t_l^{(2)}b$ production also has the same vertex and thus contributes negligibly. The only contribution here comes from the diagram mediated by $W^{(2)^\pm}$ which is somewhat massive. Thus, the prospect of having healthy rates for the single production of $t^{(2)}$ depends entirely on the coupling strength $t_l^{(2)}$-$W^{(2)^\pm}$-b and $W^{(2)^\pm}$-q-q (see figure 4.4). Fortunately, this is the case here and the cross sections for all three benchmark points, as can be seen from table 4.5, are above and around 100 fb.

We also looked into the production of $t_l^{(2)}$ along with light quark jets which is analogous to, by far the most dominant, 't-channel' single top production process (the so-called W-gluon fusion process) in the SM. However, in our scenario, such a process with somewhat heavy $t_l^{(2)}$ yields a few tens of a femtobarn for all the three benchmark points.

For both the categories mentioned above, the new-physics contributions to the corresponding SM processes are systematically small. This is since these contain the couplings that involve level-mixing effect in the top-quark sector which is not large.

Associated production of KK top quarks with the SM Higgs boson

The associated Higgs production processes we consider involve both light and heavy level-1 top quarks in pairs and the level-2 lighter top quark along with the SM top quark. The generic tree level Feynman diagrams are presented in figure 4.15. Given that the study of the SM $t\bar{t}H$ production is by itself complicated enough, it is only natural to expect that the same with its KK counterparts would not be any simpler. Cross sections for such processes are listed in table 4.5 for the benchmark points we consider. To have a feel about the their phenomenological prospects, these can be compared with similar

processes in the SM and a SUSY scenario like the MSSM. In the MSSM, the lowest order cross section is around a few tens of a fb for the process $\tilde{t}_1\tilde{t}_1^* H$ with $m_{\tilde{t}_1} \approx 300$ GeV and for the most favorable values of the involved couplings [151, 152] while for the SM the corresponding rate is about 430 fb [153, 154]. It is encouraging to find that the yield for $tt_l^{(2)}H$ is either comparable (for BM1 and BM3) or larger (BM2) than what can at best be expected in MSSM. Note that the level-1 lighter KK top quark is somewhat heavier (with mass around or above 500 GeV) for our benchmark points when compared to the mass of the top squark as indicated above. For other processes, BM2 consistently leads to larger cross sections. The interplay of different Feynman diagrams (see figure 4.15) along with the modified strengths of the participating gauge and Yukawa interactions play roles in some such enhancements.

In the last column of table 4.5 we indicate the lowest order cross sections for the SM process $t\bar{t}H$ which now gets affected in an nmUED scenario. Note that for BM1 the cross section is smaller than the SM value of ≈ 430 fb while for BM2 and BM3 the same is about 3 and 5 times as large, respectively. Such deviations can be expected if we refer back to the left panel of figure 4.6 that illustrates how the t-$\bar{t}$-H coupling gets modified over the nmUED parameter space. Note that, non-observation of such a process at the LHC, till recently, could only restrict the rate up to around five times the SM rate [118–120]. Thus, benchmark point BM3, as such, can be considered as a borderline case. But given that $t\bar{t}H$ cross section depends on other nmUED parameters like r'_G, r'_Q etc., one could easily circumvent this restriction without requiring a compromise with the parameters like r'_T and r'_Y that define the essential feature of BM3, *i.e.*, the enhanced couplings among the top quark excitations and the SM Higgs boson. It is interesting to find that in favorable regions of parameter space, the cross section for Higgs production in association with a pair of rather heavy KK top quarks could compare with or even exceed the $t\bar{t}H$ cross section. Note that in the MSSM, such enhancement only happens for large mixing in the stop sector and when $m_{\tilde{t}_1} < m_t$ [152]. Further, once the level-1 KK Higgs bosons are taken up for studies, the associated production of a charged KK Higgs boson (from level-1) in the final state $bt_l^{(1)}H^{(1)^\pm}$ would become rather relevant and may turn out to be interesting as the total mass involved in this final state can be comparatively much lower. The prospect there depends crucially on the strength of the involved 3-point vertex though.

Production of KK top quarks under cascades

KK gluon(s) and quarks, once produced, can cascade to KK top quarks. This would result in multiple top quarks (upto four of them) in the final state at the LHC. In our benchmark scenarios where $m_{g^{(1)}} < m_{q^{(1)}}$, KK gluons would directly decay to KK top quarks while KK quarks from the first two generations would undergo a two-step decay via KK gluon to yield a KK top quark. The latter one has thus suppressed contribution. We find that the branching fraction for $g^{(1)} \to t^{(1)}t$ is around 50% for all three benchmark points (the rest 50% is to level-1 bottom quark states). With strong production rates for the $g^{(1)}$-pair, $g^{(1)}q^{(1)}$ and $q^{(1)}$-pair ranging between 0.01 pb to 2.6 pb (in increasing order), the yield of a single level-1 KK top final state could be anywhere between 10 fb to a few pb. These seem quite healthy. However, one has to cope with backgrounds which now have enhanced level of jet activity.

4.6 Conclusions and outlook

We discuss the structure and the phenomenology of the top quark sector in a scenario with one flat extra spatial dimension orbifolded on S^1/Z_2 and containing non-vanishing BLTs. The discussion inevitably draws reference to the gauge and the Higgs sectors. The scenario, by construct, preserves KK-parity.

The main purpose of the present work is to organize and work out the necessary details in the involved sectors and explore the salient features with their broad phenomenological implications in terms of a few benchmark scenarios. This lay down the basis for future, detailed studies of such a top quark sector at the LHC.

The masses and the couplings of the Kaluza-Klein excitations are estimated at the lowest order in perturbation theory as functions of R^{-1} and the BLT parameters. For the KK top quarks, the extended mixing scheme (originating in the Yukawa sector) is thoroughly worked out by incorporating *level-mixing* among the level-0 and the level-2 KK top quark states, a phenomenon that is not present in the popular mUED scenario. In addition, unlike in the mUED, tree-level couplings that violate KK-number (but conserve KK-parity) are possible. We demonstrate how all these new effects, together, attract constraints from different precision experiments and shape the phenomenology of such a scenario.

The nmUED scenario we consider has eight free parameters: R^{-1} and the scaled (by R^{-1}) BLT coefficients r'_Q, r'_L, r'_T, r'_Y, r'_G, $r'_{\rm EW}$ $(= r'_W = r'_B = r'_H)$ and $m_t^{\rm in}$. However, in the present study, the most direct roles are played by r'_T, r'_Y and $r'_{\rm EW}$ (= r'_H) in conjunction

with R^{-1}. r'_Q and r'_G play roles in the production processes by determining some relevant gauge-fermion couplings beside controlling the KK quark and gluon masses, respectively. On the other hand, r'_L and m_t^{in} only play some indirect roles through their influence on the experimentally measured effects that determine the allowed region of the parameter space.

The scenario has been thoroughly implemented in `MadGraph` 5. Three benchmark scenarios that satisfy all the relevant experimental constraints are chosen for our study. These give conservatively light KK spectra with sub-TeV masses for both level-1 electroweak KK gauge bosons (with $\gamma^{(1)}$ as the LKP) and the KK top quarks while having the lighter level-2 top quark below 1.5 TeV thus making them all relevant at the LHC. Level-1 KK quarks from the first two generations and the KK gluon are taken to be heavier than 1.6 TeV.

Near mass-degeneracy of the electroweak KK gauge bosons and the KK Higgs bosons (at a given KK level) is a feature. This influences the decays of the KK top quarks. The lighter of the level-1 KK top quark can never decay 100% of the time to a top quark and the LKP photon. This is in sharp contrast to a similar possibility in a SUSY scenario like the MSSM when a top squark can decay 100% of the time to a top quark and the LSP neutralino, an assumption that is frequently made by the LHC collaborations. Instead, such a KK top quark has significant branching fractions to both charged KK Higgs boson and to KK W bosons at the same time. Further, split between the KK top quark and the KK electroweak gauge bosons that is attainable in the nmUED scenario would generically lead to hard primary jets in the decays of the former. This is again in clear contrast to the mUED scenario. However, near mass-degeneracy prevailing in the gauge and the Higgs sector would still result in rather soft leptons/secondary jets. Limited mass-splitting among the KK gauge and Higgs bosons is a possibility that has non-trivial ramifications and hence needs closer scrutiny.

The level-2 KK top quark we consider can decay directly to much lighter SM particles like the W, the Z, the Higgs boson and the top quark. These would then be boosted and hence may serve as 'smoking guns'. Recent studies of the vector-like top partners [155–157] are in context. However, these studies mainly bank on their pair-production and decays that comprise only of pairs of SM particles like $bW^{\pm}$ and/or tZ and/or tH. In the nmUED model that we consider, these are *always* accompanied by other modes that may be dominant as well. The level-2 top quark decaying to a pair of level-1 KK states is one such example.

Thus, phenomenology of the KK top quarks could turn out to be rather rich (and com-

plex) at the LHC. Clearly, strategies tailor-made for searches of similar excitations under different scenarios could at best be of very limited use. Even recasting the analyses for some of them to the nmUED scenario is not at all straight-forward. This calls for a dedicated strategy that incorporates optimal triggers and employs advanced techniques like analysis of jet-substructures *etc.* to tag the boosted objects in the final states.

In any case, viability of a dedicated hunt depends crucially on optimal production rates. We study these for the 14 TeV run of the LHC. For all the possible modes in which KK top quarks can be produced (like the pair-production, the single production and the associated production with the SM Higgs boson), the rates are found to be rather encouraging and may even exceed the corresponding MSSM processes, a yard-stick that can perhaps be used safely (with a broad brush, though) for the purpose.

The LHC experiments are either already sensitive or will be achieving the same soon in the next run for all the generic processes discussed in this work. Given that the nmUED provides several top quark KK excitations with different characteristic decays and production rates, the sensitivity to them can only be increased if multi-channel searches are carried out. It is thus possible that the LHC, running at its design energy of 14 TeV (or even a little less), finds some of these states. However, concrete studies with rigorous detector-level simulations are prerequisites to chalking out a robust strategy.

Last but not the least, the intimate connection between the top quark and the Higgs sectors raises genuine curiosity in the phenomenology for the KK Higgs bosons as well. The nmUED Higgs sector holds good promise for a rather rich phenomenology at the LHC which has become further relevant after the discovery of the 'SM-like' Higgs boson and hence can turn out to be a fertile area to embark upon.

Chapter 5

Broad resonances at the LHC and the nmUED

5.1 Introduction

Appearance of new, heavy vector bosons is common in extensions of the SM [158, 159]. These can be associated with a new gauge group which is spontaneously broken as in the case of Grand Unified theories or extensions of the SM at the weak scale with, say, an additional $U(1)$ gauge group. New vector bosons also appear in theories with extra dimensions like the Randall-Sundrum (RS) or the UED scenarios and models based on Little Higgs mechanism where these are the partners of the SM Z and $W^{\pm}$ bosons and the photon. From both phenomenological and experimental point of view, these exotic particles are exciting enough as they can be produced as resonances which decay to a pair of SM leptons or quarks. Accordingly, they are expected to show up through the bumps in the spectra of dilepton and/or dijet invariant mass similar to the cases of the Z or $W^{\pm}$ boson of the SM. Out of these, the Drell-Yan type dilepton final state is exceptionally clean even at the hadron colliders. Thus, search for such new heavy vector bosons has remained to be an integral part of the 'new physics' programme at the colliders. The LHC is not an exception and constraints on such sectors have already started arriving from it.

One major area of research involves new resonances that are weakly interacting. Studies of Z' boson associated with an extra $U(1)$ gauge group is a concrete example. Naturally, such an excitation has a small decay width (i.e., a narrow resonance). As is well known, this simplifies the situation from both theoretical and experimental point of view. On the one hand, the so-called "Narrow Width Approximation" (NWA) can be applied in the theoretical analysis of its production and subsequent decays thus simplifying the calculation and the computation/simulation. On the other hand, in experiments one expects

a narrow but a sharp peak to be searched for. Such a setup has become so standard that deviation from this has not attracted due attention until very recently. Attempts are now being made to understand possible ramifications of broad resonances for phenomenological analyses and experimental programmes.

"Narrow-" or "broad-"ness of a resonance is understood in terms of the ratio of its total (decay) width to mass (Γ/M). As can be appreciated, the basis of such an attribute is not sharp. For example, various popular Z' scenarios discussed in the literature and frequently been taken up by the experimental collaborations to put bounds on have Γ/M ratios ranging between 0.5% to 3% [160]. The latter number corresponds to the Z' boson of the so-called sequential standard model (SSM) for which the involved Z' couplings are identical to that of the SM Z boson. Clearly, the SSM Z' has the largest Γ/M ratio (the Γ/M ratio for the SM Z boson is in the same ballpark, as can be expected) and considered to be reasonably narrow. Thus, for a long time there had been hardly any popular scenario which genuinely represents the "broad" width case. This is the situation on the ground although couplings ranging from extremely weak to strong are theoretically possible for such Z'-like states [160].

Over the last few years, it is realized how "broad" resonances could naturally emerge in scenarios like the RS [140] and very recently, in the so-called non-minimal UED (nmUED) scenario [82]. These immediately highlighted the practical limitations of the NWA on both theoretical and experimental grounds and shed light on possible new issues and phenomena which need to be addressed for the case of such "broad" resonances. Our ongoing study involving "broad" resonances draws motivation from the nmUED scenario which offers multiple such resonances at KK level-2. However, to present the related issues we choose the SSM Z' as a starting point and turn it to a suitably "fat" state by altering its coupling to SM fermions. This approach is convenient on two counts: first, one can have a neat control over the width as the coupling is varied and then, it is possible to use a popular event generator like Pythia with some minimal modification in its existing implementation of the scenario.

The rest of this chapter is organized as follows. In section 5.2 we briefly outline our setup based on an analysis of a Z'-like state whose couplings can be tuned to modify its decay width thus eventually obtaining a broad enough Z' state suitable for our study. Such a broad excitation immediately calls for improvement of the scheme of analytical calculation which we discuss briefly. In section 5.3 we present the focus of our study given current experimental bounds. We then present some preliminary results. In section 5.4 we collect some important observations and present the outlook of this continuing

study in reference to the level '2' gauge bosons of the nmUED scenario. We like to point out at this stage that the current chapter presents an ongoing work and the results are *preliminary* in nature.

5.2 The setup

We demonstrate the basic issues pertaining to a broad Z' resonance in the following minimal setup:

- Z' couples to the SM fermions only; no coupling with the gauge bosons or the Higgs boson is included.
- The Lorentz structure of the coupling to SM fermions is exactly that is present in the SM, i.e., $ie\gamma_\mu(v_i - a_i\gamma_5)$
- Deviations from the SM is obtained by simple scaling: $v_i \to \alpha_i v_i$ and $a_i \to \beta_i a_i$, for the 'i'-th generation.

The total decay width of a resonance like Z' ($\Gamma_{Z'}$) controls its phenomenology in several ways through the Breit-Wigner (BW) type propagator. The resonant ($2 \to 1$) cross section at a hadron collider is given by

$$\sigma = \int\int \frac{d\tau}{\tau} dy\, x_1 f_1(x_1, Q^2)\, x_2 f_2(x_2, Q^2)\, \hat{\sigma}(\hat{s})$$

where $\hat{\sigma}(\hat{s})$ is the parton-level cross section convoluted with the parton densities $f_1(x_1, Q^2)$ and $f_2(x_2, Q^2)$ to yield the total cross section $\sigma(s)$, x_1 and x_2 being the momenta-fraction carried by the colliding partons, $\tau = \frac{\hat{s}}{s} = x_1 x_2$, $y = \frac{1}{2}\ln\frac{x_1}{x_2}$ and $Q^2 = \hat{s}$. $\hat{s}$ is the partonic center-of-mass energy. In the zero-width approximation, $\hat{\sigma}(\hat{s}) \propto \delta(\hat{s} - m_R^2)$, where m_R is the mass of the resonance. Using a scaled mass $\tau_R = m_R^2/s$ the modified δ-function becomes $\delta(\tau - \tau_R)$. Usually, this δ-function is replaced by the appropriate Breit-Wigner shape and for a constant resonance width Γ_R, this is obtained by

$$\delta(\tau - \tau_R) \to \frac{s}{\pi} \frac{m_R \Gamma_R}{\left(s\tau - m_R^2\right)^2 + m_R^2 \Gamma_R^2}.$$

However, as we know, the total width (Γ_R) is not a Lorentz invariant quantity and thus would vary with $\hat{s}$. Implementing an $\hat{s}$-dependent width would provide an improved description of the resonance shape. In an event generator like Pythia, such an $\hat{s}$-dependence

of Γ_R is introduced via a quantity $H_R(\hat{s})$ and the the modified Breit-Wigner is written as [161]

$$\delta(\tau - \tau_R) \to \frac{s}{\pi} \frac{H_R(s\tau)}{\left(s\tau - m_R^2\right)^2 + H_R^2(s\tau)}$$

where H_R is obtained by summing over all possible final-state channels.

For large widths ($\Gamma/M > 10 - 15\%$) that are envisaged, a more precise estimate should involve renormalization of the two-point vertex function at one loop. This has been carried out by including wave-function renormalization in the on-shell scheme and assuming only SM fermions running in the loops. The improved propagator has the following form:

$$\frac{1}{\left(1 - Re\left[\Pi_T'(m_R^2)\right]\right)\left(\hat{s} - m_R^2\right) + \Pi_T(\hat{s}) - Re\left[\Pi_T(m_R^2)\right]}$$

where $\Pi_T(\hat{s})$ relates to the running decay width of the resonance and corresponds to the last term in the denominator of the earlier equation above. Terms indicated as the real parts of some self-energies are the direct outcomes of wave-function renormalization (in the on-shell scheme). We consider only the transverse part as the longitudinal part is negligible with lighter fermions in the initial state. We have incorporated this form of the propagator in Pythia 6. Later in this chapter, we would demonstrate how the treatments of the propagator in going from the simple on-shell Breit-Wigner scheme to Pythia's in-built energy-dependent one and then finally to the fully renormalized two-point function affect the quantitative estimates when the resonance is broad.

5.3 The focus of the study

The ongoing study focusses on the phenomenology of s-channel gauge boson resonances from the electroweak sector that have comparatively large total widths and for which NWA fails. Large widths could affect the phenomenology in various ways. It would result in broadened mass peaks thus affecting the sensitivity of kinematic selection criteria originally tailored for narrow resonances. The overall rates are also altered. Further, as has been recently stressed in ref. [162], contribution to new physics is, in general, dependent on known physics, i.e., there may be significant interference between the two, even when the respective widths of the resonances are small. Interfering Z' and SM Z mediated diagrams for a dilepton/dijet final state is a concrete example. The nature and the amount of interference can indeed be governed by the size of the total width. We will illustrate this issue in the next section. Moreover, the amount of interference depend on the proximity of the resonances. In our toy example, the interference effect demonstrated is

between an SM Z-mediated diagram and a diagram with a possibly fat and much heavier Z' (thus far away from the Z-pole). However, there are possible scenarios like the nmUED where there could be two neighbouring resonances, with moderate to large decay widths, that take part in the interference. This clearly presents a rather complicated situation on every possible count: starting from the involved dynamics to the resultant kinematic profile that these intricate issues could lead to.

In the present study, we focus on the Drell-Yan process of the type $pp \to Z, Z' \to \mu^+\mu^-$. The electron final state is left out as it derives very strong constraints from LEP (by referring to contact interactions) when the couplings of a Z'-like state to electrons get enhanced. In essence, our study is on the same footing as ref. [140] in this respect and implicitly assumes family non-universal couplings in the leptonic sector. We take careful note of the current bounds on such resonances from the LHC experiments [29, 163] run at 7 and 8 TeV. Note that these bounds are obtained by categorically assuming narrow resonances and departure from that, under certain circumstances, could make the interpretation for moderate to large-width resonances not so straight forward. Reasons for this include the possibility of loss of sensitivity due to broadened peak(s), presence of nontrivial interference effects that lower the rates and any combination of such issues. In the next section, we present some *preliminary* results on the expectations at the 13 TeV run of the LHC.

5.4 Simulation for the 13 TeV LHC

In the first part of the simulation study we take up the toy example of Z' boson to have a general understanding of how a large width for it affects issues at the LHC. We then follow it up by a preliminary study on the level-2 gauge bosons of the nmUED scenario.

5.4.1 The simulation setup

We use Pythia 6.4 [161] for simulation purpose. The default Pythia modules for studying Z' physics are suitably modified to incorporate varying Z' couplings to SM fermions as discussed in section 5.2. This in turn directly affects the width of the Z' boson. We also incorporated Breit-Wigner propagators with fixed Γ_R and the one resulted from fully renormalized (at one loop order) propagator that includes wave-function renormalization in the on-shell scheme as described in section 5.2. We retain the original Pythia Breit-Wigner form which incorporates energy-dependent width. These help us draw a

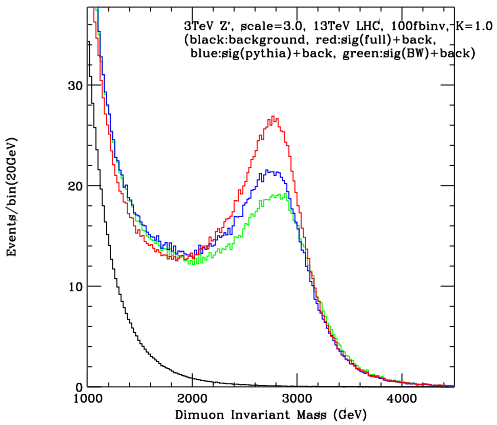

Figure 5.1: Dimuon invariant mass distribution for a Z' scenario of mass 3.0 TeV with coupling factor 3.0 times the SM Z coupling to fermions. Enhancement of cross section can be seen using our improved propagator over the BW or Pythia propagators. The SM background is shown in black curve and can be easily neglected. This is normalized to 100 fb^{-1} luminosity.

quantitative comparison among various propagator-forms for resonances with moderate to large widths.

We use CTEQ6L parton distribution function. The factorization/renormalization scale is set at M'_Z. The following kinematic cuts are imposed:

- $p_T^\mu > 30$ GeV
- $|\eta| < 2.5$
- $M_{\mu^+\mu^-} > 2$ TeV: although for a broad resonance, setting such a flat cut on the invariant mass on the muon-pair may not be optimal.
- To estimate the reach, we adopt a rather strict set of criteria: we demand a minimum of 5 events with a significance equal to or larger than 5σ. We use the following Poisson significance estimator formula

$$S = \sqrt{2\left((s+b)\log\left(1+\frac{s}{b}\right)-s\right)}$$

where 'b' stands for the number of expected background events while 's' denotes number of background-subtracted signal events.

5.4.2 General findings using a toy Z'

With our toy Z' implementation in Pythia we are able to vary the couplings of the Z' boson to SM fermions freely. We thus have a direct control on its total width Γ'_Z whose

enhanced value plays a central role in the phenomenology of such resonances. We observed that up to a coupling scale factor of 2, the Breit-Wigner (BW) form implemented in Pythia gives reliable results. However, for couplings larger than that, the effect of the improved propagator implemented by us becomes noticeable. Use of this may lead to a 10-20% enhancement in the production cross sections. Also, it is important to note that the resonance peaks shift further to the side of the small invariant mass. The overall resonance shape gets tilted with an enhanced low-mass tail at the cost of the same in the high-mass region. This is illustrated in figure 5.1 where three different implementations of the propagator are compared.

As has been recently highlighted by authors of ref. [162] we also take up a closer study of how such modifications of the propagator could influence possible interference when compared to the standard situation. It is observed that a destructive interference effect up to 10% is possible at the tail of the invariant mass distribution. It is also noted that the usual approach of focusing on an invariant mass window around the resonant peak proves in general more efficient and promises a better discovery reach rather than adopting an one-sided (a lower cut on $M_{\mu^+\mu^-}$) cut.

Pattern (constructive or destructive) of the interference effects can also be influenced by the relative sign appearing in the couplings at the two vertices of a scattering diagram. For example, in a process like $pp \to Z' \to \mu^+\mu^-$, one vertex involves Z' coupling to a pair of quarks while the other one involves a pair of muons. In general, in a new physics scenario, these vertices can have any relative sign between them. Furthermore, in a scenario like nmUED the relative sign between these couplings can well be dependent on the input parameters. Thus, we exploit the toy scenario with Z' implemented in Pythia to study this possibility as well.

As an illustrative example, in the left panel of figure 5.2 we present the target luminosity at the 13 TeV LHC for accessing a 3 TeV Z' as a function of the coupling scaling factor (with respect to the SM coupling; thus, the scale factor of 1 represents the SM situation). The right panel of this figure presents the variation of the ratio of the target luminosities obtained with Pythia's (blue) and BW (green) original implementation of the Z' propagator and the improved one by us, as a function of the scaled coupling. As can be seen, BW propagator works really good upto scale factor 2.0. For large coupling it starts to deviate and Pythia's propagator treatment gives better and sensible result. For this figure, we choose an universal scale factor not only for the vector and the axial-vector couplings but also across the quark and the lepton sectors.

In figure 5.3 we present a more general situation where we differentiate between Z'

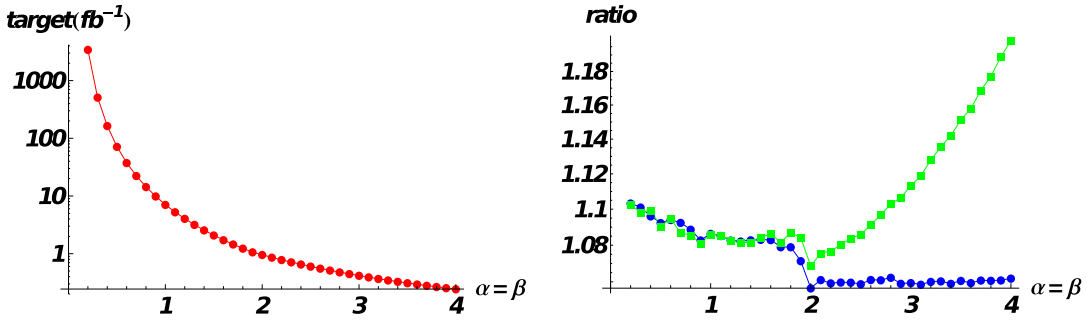

Figure 5.2: Left: Discovery reach for a $Z^{'}$ of mass 3 TeV at 13 TeV LHC run for $\mu^+\mu^-$ final state with the scaled coupling factor. Right: Ratio of luminosities with Pythia propagator and full 1-loop implemented propagator (blue dots). The green dots correspond to same ratio with BW propagator and the full 1-loop propagator. In both the above cases, we use $M_{\mu\mu} > 2$ TeV for the signal, to reduce the background.

couplings to the quarks and the leptons and hence they are varied independently. The target luminosities for the discovery of a 3 TeV Z' at the 13 TeV LHC run are presented as contours in the plane of scaling factors for the quarks and the leptons. The left plot is with the same sign for the quark and lepton couplings while the panel on the right is with a relative sign between them. The effect of destructive interference can be obvious when we compare the contours in the two panels at given values of α_{quark}.

5.4.3 Case with two neighbouring resonances

We now move on to the case of a scenario where there are two neighbouring resonances. This is a possibility in some well-motivated realistic scenarios that include nmUED, the phenomenology of which is the subject matter of the present thesis. As discussed earlier in this chapter, presence of such multiple close-by resonances could genuinely affect the phenomenology of each of them. Beyond a critical point, there may even be a situation when it could be a rather challenging task to decipher their individual presence and collectively they may start behaving more like a single, even-broader, resonance. Clearly, possibility of such a situation would affect the credibility of an interpretation in terms of one or the other scenario.

In figure 5.4 we illustrate the situation with a toy scenario that contains a pair of Z'-like excitations (say, Z' and Z'') that are suitably close in mass (differs by 150 GeV with the lighter state having a mass of 4 TeV) that may be representative of a scenario like the nmUED. To demonstrate some interesting effects it is required that these states have moderately large values of total decay widths which is again possible in the nmUED scenario. Here we plot the ratio of the target luminosities, without and with the interference effects,

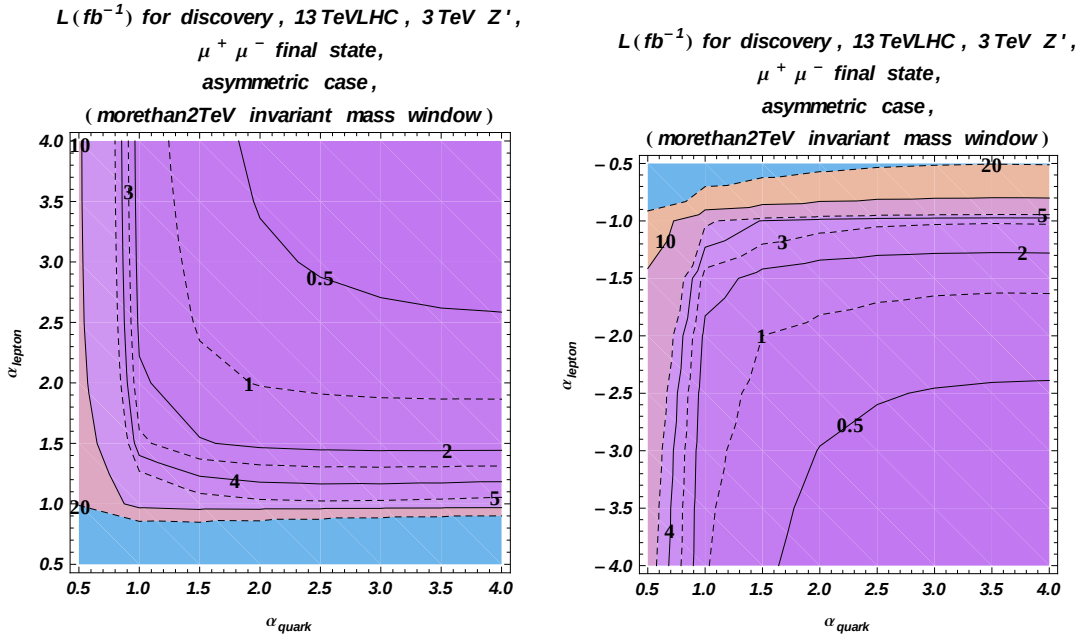

Figure 5.3: Reach plots for the non-universal scaled coupling in the quark and the lepton sector for a $Z^{'}$ of mass 3 TeV at 13 TeV LHC. The left plot is with same-sign of scale factor for both quarks and leptons. The right plot contains negative scaling factor for leptons as compared to quarks. This results in destructive interference with the SM background.

that would yield a combined excess (from two such nearby states) necessary (following the criteria as laid down earlier) to confirm their presence as a function of the scaled coupling. The downward turn of the curve for a value of the scale factor between 2 and 3 indicates a reversal of the nature of the interference between the closely lying states. Clearly, such a reversal takes place at a moderately large value of the coupling which is not quite unexpected. This is because, with increasing couplings, the widths of the excitations increase and hence the two states become more and more in the active influence of each other thus enhancing the interference effects. Furthermore, since the shape of the individual invariant-mass distributions for the two excitations undergo substantial alteration as the couplings change, the nature of interference could pick up nontrivial effects from that. Together, these may reverse the effect of interference in the kinematic region of our interest. For this figure, we used our improved propagator and an one-sided cut of $M_{\mu^+\mu^-} > 2$ TeV.

In figure 5.5 we demonstrate how the total cross section (left panel) and the target luminosity for a 5σ (collective) excess vary in the plane of scaled vector (α) and axial-vector (β) couplings. Contribution of nontrivial interference effects as demonstrated in the last figure is also included

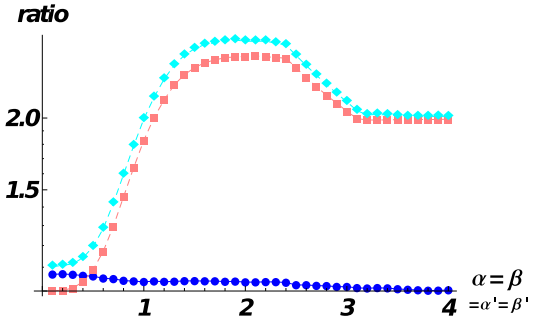

Figure 5.4: Z' of mass 4 TeV and Z'' of mass 4.15 TeV are considered in standard SSM scenario with coupling scaled as before. The figure shows the ratio of required reach estimation for the 13 TeV LHC with various circumstances. The blue dots are the ratios of luminosity for discovery calculated with Pythia propagator and full 1-loop propagator. The pink dots are the same with full 1-loop propagator without interference and with interference. The cyan dots are the similar ratios with Pythia propagator without interference and full 1-loop propagator with interference. The figure (pink curve) shows the implication of non-trivial constructive interference pattern. α, β, α' and β' are the scale factors for Z' and Z'' respectively.

For the nmUED part, we consider closely-spaced resonances as the brane local parameter for the electroweak sector is common for the $SU(2)$ and $U(1)$ gauge fields. Therefore, we expect them to be degenerate. However, radiative corrections can lift such degeneracy. We consider mUED-like mass splitting between $Z^{(2)}$ (level-2 Z boson) and $B^{(2)}$ (level-2 photon). Note that the effective Weinberg angle of such level-2 gauge bosons is assumed to be zero to a very good approximation [60]. Hence, $Z^{(2)}$ is a purely $SU(2)$ and similarly, $B^{(2)}$ is purely a $U(1)$ gauge bosons. As we have already mentioned, level-2 gauge bosons have tree level couplings with the SM particles. Hence, the couplings are different than the usual $Z^{'}$ scenario considered above. We calculate the cross sections for various brane local parameters (which is equivalent to different scale factors). We assume same brane local parameters for the quarks ($r_Q^{'}$) and leptons $r_L^{'}$ with $r_Q^{'} = r_L^{'}$. Table 5.1 shows the discovery reach for dimuon process for both standard Breit-Wigner form of the propagator and full propagator. Interference effects are also taken into account. In fact, one can easily notice that how the required luminosity for discovery decreases as one take interference of the two resonances. This is clearly the case of constructive interference. For nmUED such interference is much more complicated. According to the choice of quark and lepton boundary localized parameters, there may appear relative sign in the quark-gauge boson coupling and lepton-gauge boson coupling.

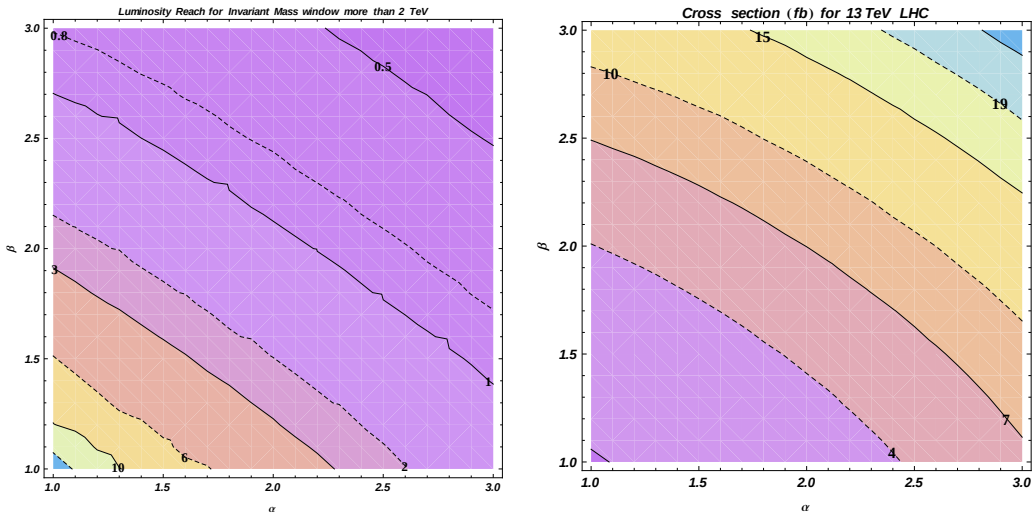

Figure 5.5: Discovery luminosity (left panel) and cross section (right panel) plots for a dibump scenario as mentioned above. Scaled couplings are made to vary for both the gauge bosons. Interference has been taken into account.

$r_Q^{'}$, $r_L^{'}$ (scale factor)	full, w int	BW, w int	full, wo int	BW wo int	Width (GeV)
-1.0 (-3.5)	0.352	0.411	0.368	0.43	826 1805
-0.5 (-1.46)	5.32	5.46	6.22	6.38	154 397
0.0 (-0.72)	108	109.5	109.7	115.7	47 173
0.5 (-0.34)	8516	8601	8611	8785	20 116

Table 5.1: Luminosity required for the discovery of level-2 electroweak gauge bosons estimated for both the BW propagator and full 1-loop implemented propagator form. 'w int' stands for "with interference" and 'wo int' means "without interference". Luminosity numbers are in the unit of fb^{-1}.

5.5 Conclusion

This work is in preparation. The results presented here are thus preliminary in nature. The main focus of this study is the resonances with large widths. In such cases, simple narrow-width-approximation fails. One of our main goals is to study how to improve upon the Breit-Wigner type of propagator in order to capture the effects of large width. In addition, we also try to work on how to implement such improvements in a well-known event generators, like Pythia.

We set the stage by studying massive Z' associated with an extra $U(1)$ gauge group. We start with sequential SM (SSM) where the extra Z' has exactly the same coupling as the SM Z boson. We then obtain large coupling by simple scaling of the SSM-like coupling and achieve really large widths. We restrict ourselves to resonance production of a Z' decaying into leptons *i.e.,*a Drell-Yan type process, $pp \to Z' \to \mu^+\mu^-$. Scaled coupling enhances the production cross section. We provide estimate on required luminosity for 13 TeV LHC for discovering such a excitation. Interference effect (with the SM Z boson) turns out to be non-trivial.

Next we discuss the "dibump" scenario where we consider two such closely-spaced masses. nmUED may provide a natural example for such a scenario. We discuss the phenomenology of such close-by resonances with large couplings and large widths. A relative sign in gauge boson quark coupling and gauge boson lepton coupling may appear for some values of brane local parameters ($r_Q^{'}$ and $r_L^{'}$). This is very characteristic since the pattern of interference may change thus altering the phenomenology. Another interesting aspect is that close-by resonances with large width(s) may get merged and look like a single bump. Invariant mass distribution may not be sufficient to handle such a situation. One can check various asymmetry variables to extract information about underlying physics of invariant mass peaks. We must mention that our observations are based on parton-level analysis and no detail detector simulations have been performed. Inclusion of those details may reduce some of the effects, but overall results will still remain valid.

Chapter 6

Conclusion

In this thesis, we discuss the role of non-vanishing boundary localized (kinetic and Yukawa) terms for the strongly interacting sector in minimal universal extra dimension framework and their impact on the current and future runs at the LHC. We know that the introduction of boundary terms changes the mass spectrum of the conventional mUED scenario. The KK masses are no longer the partial derivative of the extra dimensional coordinate acting on the KK mode functions. Rather, we solve for the transcendental equations numerically to determine the KK masses. We discuss the resulting spectra of the QCD sector as functions R^{-1} and the scaled brane local parameters for gluon ($r_G^{'}$) and quarks ($r_Q^{'}$). Smaller R^{-1} (which would, otherwise (in mUED), have been ruled out by recent experiments) are still relevant at the LHC. Thus, a much wider range of spectrum is available for studies at the LHC.

One interesting feature of the nmUED scenario is the change in the coupling strength as found in mUED due to the overlap integrals of the involved fields. The deviations from the corresponding mUED coupling are found to be functions of the brane local parameters. Thus, the introduction the brane local terms affect both the masses and couplings of the KK excitations simultaneously. We shed light on such correlated variations and their possible ramifications for the LHC.

Another interesting aspect of the nmUED scenario is the chiral mixing among KK quark states of a particular level. The origin of such mixing is the Yuwaka interaction. The amount of mixing is proportional to the quark mass. Hence, the mixing is negligible for 1st two generations of quarks. However, for the top quark, the mixing is somewhat significant, although not large enough to see such effects in the experiments. After diagonalization of the mass matrix, the mixing factors appear in the interactions involving gauge eigenstates. In addition there arise a new kind of mixing in the nmUED scenario,

called *level mixing*. This also originates from the Yukawa sector and hence, predominant for the top quark only. Theoretically, the flavour eigenbases of all the KK levels with similar parity should mix to give the mass eigenstates. However, only the lighter KK levels are relevant for the LHC phenomenology. We thoroughly work out the *level mixing* among the level-0 (SM) and the level-2 KK top quarks.

We would like to stress that the entire scenario has been implemented for the event generator Madgraph with the help of FeynRules. This tedious attempt involves writing down the model in an appropriate way that works in the FeynRules environment which in turn, provides the output in a suitable format usable in Madgraph. We then study the cross sections for the production of level-1 KK gluon and KK quarks of the 1st two generations for LHC energies of 8 and 14 TeV. It is noted that wildly varying yields are possible compared to mUED scenario. This is simply because the KK gluon and quarks have masses varying over wide ranges. It is pointed out that an nmUED scenario can fake a SUSY signal raising confusion over the underlying nature of the new physics scenario. One way to distinguish between them is to compare the cross sections. mUED cross sections are known to be larger (for a similar mass spectrum) than the corresponding SUSY numbers. However, the nmUED scenario can imitate SUSY cross sections with smaller couplings. For example, with $g_{G^1Q^1Q^0} < 1$, one can have reduced cross section values for the production of $G^{(1)}G^{(1)}$, $G^{(1)}Q^{(1)}$ and $Q^{(1)}\bar{Q}^{(1)}$ at the LHC for comparable masses in the two competing scenarios. Thus, it may, in general, become difficult to pin down the new physics scenario at work from a small number of observables. More detailed studies are thus required in this aspect.

Given the unique stature of the top quark, we consider separate brane local parameter $r_T^{'}$ for this sector which is different from $r_Q^{'}$ that is used for the 1st two generations. We incorporate the brane local parameters ($r_{EW}^{'}$) for the electroweak sector as well. Therefore, the scenario we consider here has eight free parameters: R^{-1}, $r_T^{'}$, $r_Q^{'}$, $r_G^{'}$, $r_L^{'}$, $r_Y^{'}$, $r_{EW}^{'}$ and m_t^{in} over the mUED parameters. However, for the phenomenology of the top quark sector, only $r_T^{'}$, $r_Y^{'}$ and $r_{EW}^{'}$ play crucial role. We consider three benchmark points which satisfy all the relevant experimental constraints. These give considerably light spectra for the level-1 KK top quark. We choose the mass of level-2 KK top quark to be around 1.5 TeV so that this also can be accessed at the LHC. The level-2 KK top quark can directly decay to much lighter SM particles. These would then be heavily boosted and hence may serve as the "smoking gun" signal. We also point out the associated production rate of level-2 KK top quark along with a SM top/bottom quarks. This kind of a process has a highly suppressed rate in mUED.

Another striking observation in nmUED scenario is that some KK states may become "fat" with a large width to mass ratio (Γ/M) $\gg$ 10%. In such case, the usually adopted scheme of narrow-width approximation (NWA) becomes inadequate for studying resonances. We work out discovery reach for sequential Z' scenario with large width at the LHC. The situation becomes much more complicated in nmUED due to its closely lying masses of level-2 electroweak gauge bosons. We derive fully resummed 1-particle irreducible diagrams and implement the energy dependent form of the propagator. We provide simple reach estimation for 13 TeV LHC run for such a scenario.

In the mUED scenario, the conservation of KK parity makes the lightest KK particle (LKP) stable. Moreover, if the LKP is electromagnetically neutral and weakly interacting, it may serve as a WIMP dark matter. Level-1 KK photon ($\gamma^{(1)}$) is always the LKP in such a scenario. Interestingly, in the non-minimal extension of UED model with brane local terms, $\gamma^{(1)}$ is not always the LKP. Rather, $W_\mu^{3(1)}$ (level-1 KK Z boson) or $H^{(1)}$ (level-1 KK Higgs boson) or $\nu^{(1)}$ (level-1 KK neutrino) [83, 164] are also eligible dark matter candidates depending on the choice of brane local parameters. Thus, the scenario resembles supersymmetric models where a variety of particles (neutralino, gravitino, sneutrino) can be WIMP dark matter. However, in this thesis, we mainly focus on LHC phenomenology of the strongly interacting sector of the nmUED scenario. Hence a detail discussion on dark matter and the related phenomenology is beyond the scope of the present thesis. Interested readers may refer to references [68, 165] where DM issues have been discussed.

Varieties of non-minimal UED scenarios although known for some time, have not been studied particularly in reference to the LHC. This thesis focusses on such a scenario keeping the LHC in mind. Clearly, strongly interacting sector is the most promising one for the discovery at the LHC because of the large production rates. Just like the squark and gluino searches in supersymmetric scenario, KK quarks and KK gluons can be either discovered or ruled out up to certain masses at the LHC. In this context, it is worth mentioning that one of the attractive features of mUED from exclusion point of view is that its mass scale (or, equivalently R^{-1}) is bounded from below by the LHC data and, at the same time, it is bounded from above by the relic density constraint. Interestingly, this is not the case with nmUED which can survive future runs of LHC and also DM constraints which could rule out many other similar models. At a time when the LHC is widening its search strategies to look for new physics signals, physicists are trying to exhaust various phenomenological possibilities which have not yet been studied in detail. This thesis is a step in that direction. Prospects of this scenario have been discussed many a times in earlier chapters. We would also like to point out that many other possibilities are

not explored in this thesis including studies with detector simulation. Phenomenology of the electroweak sector including KK Higgs bosons is a fertile area to work on. Studies on dark matter and the explanation various related experimental results in terms of nmUED model are still largely missing in the literature. The scenario extended with suitable mechanism of generating neutrino mass might be of interest as well. Although the studies included in this thesis refer to the experimental situations existing at that time, the stage is already set to take them forward taking into account new results as they become available.

As the LHC is gearing up for the next phase of run with full strength, we must get ready with the knowledge of diverse theoretical possibilities. The new energy regime may open the door for new physics. Therefore, new areas must be explored and old ideas need to be refined before we can fully utilize the discovery potential of both the ongoing and future experiments. This thesis is an attempt to contribute to some aspects of this challenge.

Appendix A

A.1 Universal Extra Dimension with boundary localized terms for a generic scalar field

In this appendix we show the formulation of the nmUED with brane local (kinetic) terms. We provide the calculations of bulk and boundary equation of motions (EoM) and the orthonormal conditions emerging from it.

We consider a massive real scalar field Φ in five dimensional framework compactified on S^1/Z_2. The bulk action is given by,

$$S_{\text{bulk}} = \frac{1}{2}\int d^4x \int dy \left(\partial^M \Phi(x,y)\partial_M \Phi(x,y) - m^2\Phi^2(x,y)\right) \tag{A.1}$$

where m is the mass of the scalar field. The Lorentz index $M = 0,1,2,3,y$. Now, in addition to this, we have the following brane localized kinetic term (BLKT) for the scalar field at the two orbifold fixed points,

$$S_{\text{BLKT}} = \frac{1}{2}\int d^4x \int dy\, r_\Phi\, \partial^\mu \Phi(x,y)\partial_\mu \Phi(x,y)\left[\delta(y-L)+\delta(y+L)\right] \tag{A.2}$$

where r_Φ is the brane local parameter at both the boundaries ($\pm L$). Using the variational principle $\delta S = \delta S_{\text{bulk}} + \delta S_{\text{BLKT}} = 0$ we obtain the bulk equation of motion,

$$\left(\Box - \partial_y^2 + m^2\right)\Phi(x,y) = 0. \tag{A.3}$$

The non-zero boundary term appearing from integration by parts provides the modified boundary conditions in the following form,

$$-\int d^4x \Big(\partial_y \Phi(x,y) + r_\Phi\, \Box\Phi(x,y)\Big)\, \delta\Phi(x,y)\Big|_{y=L} = 0, \tag{A.4}$$

$$\int d^4x \Big(\partial_y \Phi(x,y) - r_\Phi\, \Box\Phi(x,y)\Big)\, \delta\Phi(x,y)\Big|_{y=-L} = 0 \tag{A.5}$$

Therefore, for arbitrary $\delta\Phi(x,y)$ the boundary conditions modified by the introduction of the BLKT are,

$$\Big(\partial_y\Phi(x,y) + r_\Phi\ \Box\Phi(x,y)\Big)\Big|_{y=L} = 0, \tag{A.6}$$

$$\Big(\partial_y\Phi(x,y) - r_\Phi\ \Box\Phi(x,y)\Big)\Big|_{y=-L} = 0 \tag{A.7}$$

Using the separation of variables we decompose Φ into infinite numbers of Fourier modes

$$\Phi(x,y) = \sum_n \Phi^{(n)}(x) f_n(y) \tag{A.8}$$

Plugging the above expansion into the five dimensional EoM in A.3 we obtain,

$$\Box\Phi^{(n)}(x) = -m_n^2\Phi^{(n)}(x), \tag{A.9}$$

$$\partial_y^2 f_n(y) = -\left(m_n^2 - m^2\right) f_n(y) \equiv M_n^2 f_n(y) \tag{A.10}$$

Note that the mass m we wrote the action is known as the bulk mass. M_n and m_n are the KK mass and the actual physical mass at level-n respectively. Hence, the physical mass at level-n can be written as, $m_n^2 = M_n^2 + m^2$. It is easy to see that $f_n(y)$ are harmonic functions. The solutions are either odd or even under the Z_2 symmetry. Setting the boundary at $L = \pi R/2$ (following our convention) we obtain the so-called mode functions,

$$f_n(y) = N_n \times \begin{cases} \dfrac{\cos(M_n y)}{\cos(M_n \pi R/2)} & \text{for } n \text{ even} \\ \\ -\dfrac{\sin(M_n y)}{\sin(M_n \pi R/2)} & \text{for } n \text{ odd} \end{cases} \tag{A.11}$$

Now, we replace the KK mode functions as obtained in A.11 in the boundary EoM A.7 to get the KK mass determining conditions as,

$$r_\Phi\ m_n^2 = \begin{cases} -M_n \tan\left(\frac{M_n \pi R}{2}\right) & \text{for } n \text{ even} \\ \\ M_n \cot\left(\frac{M_n \pi R}{2}\right) & \text{for } n \text{ odd} \end{cases} \tag{A.12}$$

Solving these transcendental equations we determine the KK masses of the field Φ. The mode functions of A.11 obey pairwise orthonormal relation as,

$$\int_{-L}^{L} dy \Big[1 + r_\Phi\left(\delta(y-L) + \delta(y+L)\right)\Big] f_m(y) f_n(y) = \delta_{mn} \tag{A.13}$$

Carrying out this integral for $m = n$ and for even and odd mode functions separately, we determine the normalization constants N_n,

$$N_n^{-2} = \begin{cases} 2r_\Phi + \dfrac{1}{\cos^2\left(M_n \pi R/2\right)} \left[\dfrac{\pi R}{2} + \dfrac{1}{2M_n}\sin(M_n \pi R)\right] & \text{for } n \text{ even} \\ 2r_\Phi + \dfrac{1}{\cos^2\left(M_n \pi R/2\right)} \left[\dfrac{\pi R}{2} - \dfrac{1}{2M_n}\sin(M_n \pi R)\right] & \text{for } n \text{ odd} \end{cases} . \tag{A.14}$$

This is a general formulation shown for a scalar field. However, this can be carried out for any field (fermions or gauge bosons) and one can arrive at the similar mass determining conditions and orthonormal relations.

Appendix B

B.1 The gauge and the Higgs sector of the nmUED: some relevant details

In this appendix we briefly supplement our discussion in section 2.6.2 with some necessary details pertaining to the gauge fixing conditions, the inputs that go into the mass-determining conditions.

B.1.1 Gauge fixing conditions

We introduce the gauge-fixing terms in the bulk and at the boundaries in the following way to obtain the physical states:

$$
\begin{aligned}
S_{\text{gf}} = \int d^4x \int_{-L}^{L} dy \Bigg\{ & -\frac{1}{2\xi_A}\left[\partial_\mu A^\mu - \xi_A \partial_y A_y\right]^2 - \frac{1}{\xi_W}\left|\partial_\mu W^{+\mu} - \xi_W\left(\partial_y W_y^+ + i M_W \phi^+\right)\right|^2 \\
& - \frac{1}{2\xi_Z}\left[\partial_\mu Z^\mu - \xi_Z\left(\partial_y Z_y + M_Z \chi\right)\right]^2 - \frac{1}{2\xi_G}\left[\partial_\mu G^{a\mu} - \xi_G \partial_y G_y^a\right]^2 \\
& - \frac{1}{2\xi_{A,b}}\Big\{\left[\partial_\mu A^\mu + \xi_{A,b} A_y\right]^2 \delta(y-L) + \left[\partial_\mu A^\mu - \xi_{A,b} A_y\right]^2 \delta(y+L)\Big\} \\
& - \frac{1}{\xi_{W,b}}\Big\{\left|\partial_\mu W^{+\mu} + \xi_{W,b}\left(W_y^+ - i r_H M_W \phi^+\right)\right|^2 \delta(y-L) + \left|\partial_\mu W^{+\mu} - \xi_{W,b}\left(W_y^+ + i r_H M_W \phi^+\right)\right|^2 \delta(y+L) \\
& - \frac{1}{2\xi_{Z,b}}\Big\{\left[\partial_\mu Z^\mu + \xi_{Z,b}\left(Z_y - r_H M_Z \chi\right)\right]^2 \delta(y-L) + \left[\partial_\mu Z^\mu - \xi_{Z,b}\left(Z_y + r_H M_Z \chi\right)\right]^2 \delta(y+L)\Big\} \\
& - \frac{1}{2\xi_{G,b}}\Big\{\left[\partial_\mu G^{a\mu} + \xi_{G,b} G_y^a\right]^2 \delta(y-L) + \left[\partial_\mu G^{a\mu} - \xi_{G,b} G_y^a\right]^2 \delta(y+L)\Big\}\Bigg\}
\end{aligned}
\tag{B.1}
$$

Type	m_F^2	$m_{F,b}^2$	r_F
W_μ^+	M_W^2	$r_H M_W^2$	r_{EW}
Z_μ	M_Z^2	$r_H M_Z^2$	r_{EW}
H	$(\sqrt{2}\hat{\mu})^2$	$(\sqrt{2}\mu_b)^2$	r_H
ϕ^+, $\partial_y W_y^+$	M_W^2	$r_H M_W^2$	r_H
χ, $\partial_y Z_y$	M_Z^2	$r_H M_Z^2$	r_H

Table B.1: Input parameters that determine the masses of the KK gauge and the Higgs bosons. See section 2.6.2 for notations and conventions.

where the eight gauge-fixing parameters are ξ_A, ξ_W, ξ_Z, ξ_G (in the bulk), $\xi_{A,b}$, $\xi_{W,b}$, $\xi_{Z,b}$, $\xi_{G,b}$ (at the boundary) and M_W, M_Z are the masses of the W and Z bosons[1].

Imposing the unitary gauge in both the bulk and at the boundaries by setting

$$\xi_A,\ \xi_W,\ \xi_Z,\ \xi_G,\ \xi_{A,b},\ \xi_{W,b},\ \xi_{Z,b},\ \xi_{G,b} \to \infty \tag{B.2}$$

we obtain the following relations:

$$\begin{aligned} A_y = 0, \qquad & Z_y \mp r_H M_Z \chi = 0, \\ W_y^+ \mp i r_H M_W \phi^+ = 0, \qquad & G_y^a = 0, \qquad \text{at } y = \pm L, \end{aligned} \tag{B.3}$$

$$\begin{aligned} \partial_y A_y = 0, \qquad & \partial_y W_y^+ + i M_W \phi^+ = 0, \\ \partial_y Z_y + M_Z \chi = 0, \qquad & \partial_y G_y^a = 0, \qquad \text{in the bulk.} \end{aligned} \tag{B.4}$$

As we see, A_y and G_y^a are totally gauged away from the theory as would-be Nambu-Goldstone bosons. The two mixed boundary conditions in equation B.3 can be cast into a set containing the individual fields with the help of equation B.4 as

$$\begin{aligned} \chi \pm r_H \partial_y \chi = 0, \qquad & \phi^+ \pm r_H \partial_y \phi^+ = 0, \\ Z_y \pm r_H \partial_y Z_y = 0, \qquad & W_y^+ \pm r_H \partial_y W_y^+ = 0, \qquad \text{at } y = \pm L. \end{aligned} \tag{B.5}$$

[1]This part of the action is also symmetric under the reflection $y \to -y$.

Appendix C

C.1 Tree-level FCNCs and constraints from $D^0 - \overline{D^0}$ mixing

It has been demonstrated in ref. [124] that an appropriate short-distance description for a ΔF=2 FCNC process like $D^0 - \overline{D^0}$ can be found in processes involving only the even KK modes (starting at level-2) of the gauge bosons and the '0' mode fermions. In an effective Hamiltonian approach, such a process would reduce to a four-Fermi interaction whose strength is suppressed by the mass of the exchanged KK gauge boson. The effective FCNC Hamiltonian can be expressed in terms of suitable fermionic operators and their associated Wilson coefficients. The latter involve the overlap matrices in the gauge kinetic terms (by now, suitably rotated to the basis where the quark mass matrix is diagonal) which are functions of the BLKT parameter, r'_Q and r'_T. Thus, any constraint on the Wilson coefficients can be translated into constraints in the r'_Q-r'_T plane.

The gauge interactions in the diagonalized basis involving the level-0 quarks and the KK gluons $g^{(k)}$, with the KK index k being even and $k \geq 2$, are given by:

$$g_s \sum_{i,j,l=1}^{3} \left(\overline{q_{iL}^{(0)}} \gamma^\mu T^a \left[(U_{qL}^\dagger)_{il} F_{g,ll}^{Q,[k]} (U_{qL})_{lj} \right] q_{jL}^{(0)} + \overline{q_{iR}^{(0)}} \gamma^\mu T^a \left[(U_{qR}^\dagger)_{il} F_{g,ll}^{q,[k]} (U_{qR})_{lj} \right] q_{jR}^{(0)} \right) g_\mu^{(k)}, \quad \text{(C.1)}$$

where the 4D and the 5D (the 'hatted' one) gauge couplings are related by $g_s \equiv \hat{g}_s/\sqrt{2r_G + \pi R}$. T^a represents the $SU(3)$ generators, a being the color index. $U_{q(L,R)}$ are the matrices that diagonalize the $q_{L,R}$ fields in the Yukawa sector. $F_{g,ll}^{Q,[k]}$ and $F_{g,ll}^{q,[k]}$ are the diagonal overlap matrices (in the original bases)

$$F_{g,ll}^{Q,[k]} = \frac{1}{f_{g^{(0)}}} \int_{-L}^{L} dy \left(1 + r_{Q_l} \left[\delta(y-L) + \delta(y+L)\right]\right) f_{Q_l^{(0)}} f_{g^{(k)}} f_{Q_l^{(0)}}, \quad \text{(C.2)}$$

$$F_{g,ll}^{q,[k]} = \frac{1}{f_{g^{(0)}}} \int_{-L}^{L} dy \left(1 + r_{q_l} \left[\delta(y-L) + \delta(y+L)\right]\right) f_{q_l^{(0)}} f_{g^{(k)}} f_{q_l^{(0)}} \quad \text{(C.3)}$$

while the explicit form is shown in equation 4.28. Similar FCNC processes are also induced by the KK photons and the KK Z bosons. However, because of weaker couplings their contributions are only sub-leading and henceforth neglected in the present work.

The so-called "aligned" scenario in which the rotation matrices for the left- and the right-handed quark fields are tuned to avoid as many flavor constraints as possible can be summarized as

$$U_{uR} = U_{dR} = U_{dL} = \mathbf{1}_3, \qquad U_{uL} = V_{\rm CKM}^\dagger \tag{C.4}$$

along with universal BLKT parameters r'_Q and r'_T, for the first two and the third quark generations respectively, irrespective of their chiralities. In such a scenario, by construct, dominant tree-level FCNC is induced via KK gluon exchange and only through the doublet up-quark sector. Note that no FCNC appears at the up-quark singlet part and the down-quark sector. The latter helps evade severe bounds from the K and B meson sectors. The forms of the 4D Yukawa couplings, before diagonalization, are determined simultaneously as:

$$Y^u_{ij} = \sum_{l=1}^{3} \frac{\left(V_{\rm CKM}^\dagger\right)_{il} \mathcal{Y}^u_{lj}}{F^{d,(0,0)}_{ij}}, \qquad Y^d_{ij} = \begin{cases} \dfrac{\mathcal{Y}^d_{ii}}{F^{d,(0,0)}_{ii}} & \text{for } i = j, \\ 0 & \text{for } i \neq j. \end{cases} \tag{C.5}$$

In this configuration, the structure of the vertex $\overline{u^{(0)}_{iL}} - d^{(0)}_{jL} - W^{+(0)}_\mu$ is reduced to that of the SM. The overlap matrices in the gauge kinetic sector receive bi-unitary transformations when these terms are rotated to a basis where the quark mass matrices in the Yukawa sector are diagonal. These rotated overlap matrices are given by

$$\begin{aligned} \sum_{l=1}^{3} (U^\dagger_{uL})_{il} F^{U,[k]}_{g,ll} (U_{uL})_{lj} &= \left\{ F^{U,[k]}_{g,11} \mathbf{1}_3 + V_{\rm CKM} \begin{pmatrix} 0 & & \\ & 0 & \\ & & \underbrace{F^{U,[k]}_{g,33} - F^{U,[k]}_{g,11}}_{=:\Delta F^{U,[k]}_g} \end{pmatrix} V^\dagger_{\rm CKM} \right\}_{ij} \\ &\simeq \left\{ F^{U,[k]}_{g,11} \mathbf{1}_3 + \Delta F^{U,[k]}_g \begin{pmatrix} A^2\lambda^6 & -A^2\lambda^5 & A\lambda^3 \\ -A^2\lambda^5 & A^2\lambda^4 & -A\lambda^2 \\ A\lambda^3 & -A\lambda^2 & 1 \end{pmatrix} \right\}_{ij} \end{aligned} \tag{C.6}$$

where $A(= 0.814)$ and $\lambda(= 0.23)$ are the usual Wolfenstein parameters and we use the relation $F^{U,[k]}_{g,11} = F^{U,[k]}_{g,22}$. Clearly, the difference of the two overlap matrices in that diagonal term governs the FCNC contribution and thus, in turn, relative values of the corresponding BLKT parameters, r'_Q and r'_T that shape the overlap matrices, get constrained.

To exploit the model independent constraints provided by the UTfit collaboration [126], the effective Hamiltonian for the t-channel KK gluon exchange process (that describes the $D^0 - \overline{D^0}$ mixing effect) needs to be written down in terms of the following quark operators and the associated Wilson coefficient:

$$\Delta\mathcal{H}_{\text{eff}}^{\Delta C=2} = C_D^1(\overline{u}_L^a\gamma_\mu c_L^a)(\overline{u}_L^b\gamma^\mu c_L^b) \tag{C.7}$$

where a and b are the color indices and we use $SU(3)$ algebra and appropriate Fierz transformation to obtain

$$C_D^1 = \sum_{k\geq 2:\text{even}} \frac{g_s^2(\mu_D)}{6}\frac{1}{m_{g^{(2)}}^2}(-A^2\lambda^5\Delta F_g^{U,[k]})^2 \simeq \frac{2\pi\alpha_s(\mu_D)}{3m_{g^{(2)}}^2}A^4\lambda^{10}(\Delta F_g^{U,[k]})^2. \tag{C.8}$$

As it appears, the value of C_D^1 is highly Cabibbo-suppressed. Heavier KK gluons (except the one from level '2') effectively decouples. The QCD coupling at the D^0-meson scale ($\mu_D \simeq 2.8\,\text{GeV}$) is estimated by the relation,

$$\alpha_s^{-1}(\mu_D) = \alpha_s^{-1}(M_Z) - \frac{1}{6\pi}\left(23\ln\frac{M_Z}{m_b} + 25\ln\frac{m_b}{\mu_D}\right) \simeq 1/0.240 \tag{C.9}$$

with $\alpha_s(M_Z) = 0.1184$ **[?]**. One would now be able to put bounds on the parameter space by use of the result by the UTfit collaboration [126],

$$|C_D^1| < 7.2\times 10^{-7}\,\text{TeV}^{-2} \tag{C.10}$$

which, for a given set of values for R^{-1} and r'_G, actually exploits the dependence of $\Delta F_g^{U,[k]}$ (appearing in equation (B.6)) on the BLKT parameters r'_Q and r'_T.

Bibliography

[1] For a general introduction on Standard Model, see, F. Halzen and A.D. Martin, *Quarks and Leptons: An introductory course in modern particle physics*, (John Wiley, 1984); C. Burgess and G. Moore, *The Standard Model A Primer*, (Cambridge University Press).

[2] N. Cabibbo, Phys. Rev. Lett., **10** 531 (1963); M. Kobayashi, T. Maskawa, Prog. Theor. Phys., **49** 652 (1973)

[3] J. Beringer *et al.* (Particle Data Group), Phys. Rev. D **86**, 010001 (2012).

[4] For pedagogic discussions on spontaneous symmetry breaking, see, for example, M. Peskin and D. Schroeder, *An introduction to Quantum Field Theory*, (Frontiers in Physics); V. Rubakov, *Classical Theory of Gauge Fields*, (Princeton University Press).

[5] Y. Nambu and G. Jona-Lasinio, Phys. Rev. **122**, 345 (1961); Y Nambu and G. Jona-Lasinio, Phys. Rev. **124**, 246 (1961).

[6] J. Goldstone, Nuovo cimento **19**, 154 (1961).

[7] J. Goldstone, A. Salam, S. Weinberg, Phys. Rev. **127**, 965 (1962).

[8] P. W. Higgs, Phys. Lett., **12** 132 (1964); P. W. Higgs, Phys. Rev. Lett., **13** 508 (1964).

[9] F. Englert, R. Brout, Phys. Rev. Lett., **13**, 321 (1964).

[10] G. S. Guralnik, C. R. Hagen, T. W. B. Kibble, Phys. Rev. Lett., **13**, 585 (1964).

[11] G. 't Hooft, Nuc. Phys. B **35**, 167 (1971).

[12] S. L. Glashow, Nuc. Phys., **22**, 579 (1961).

[13] S. Weinberg, Phys. Rev. Lett. **19** 1264 (1967); A. Salam, Proceedings of the Nobel Symposium, Ed. N. Svartholm (1968).

[14] K. Jakobs, "Physics at the LHC – From Standard Model measurements to Searches for New Physics," arXiv:1206.7024 [hep-ex].

[15] F. Zwicky, 1933, Helv. Phys. Acta 6, 110.

[16] D. Clowe, A. Gonzalez and M. Markevitch, "Weak lensing mass reconstruction of the interacting cluster 1E0657-558: Direct evidence for the existence of dark matter," Astrophys. J. **604**, 596 (2004) [astro-ph/0312273].

[17] M. Markevitch, A. H. Gonzalez, D. Clowe, A. Vikhlinin, L. David, W. Forman, C. Jones and S. Murray *et al.*, "Direct constraints on the dark matter self-interaction cross-section from the merging galaxy cluster 1E0657-56," Astrophys. J. **606**, 819 (2004) [astro-ph/0309303].

[18] Theodor Kaluza, "On The Unification Problem In Physics", *Sitzungsberichte Pruss. Acad. Sci.* (1921) p. 966, reprinted in English translation in reference [17].

[19] Oskar Klein, "Quantum Theory And Five-Dimensional Theory Of Relativity," *Z.Phys.* 37 (1926) p. 895, reprinted in English translation in reference [3]; "The Atomicity Of Electricity As A Quantum Theory Law," *Nature* 118 (1926) p. 516, reprinted in [17].

[20] T. Appelquist, A. Chodos, and P. G. O. Freund, eds., "Modern Kaluza-Klein Theories" (Addison-Wesley, 1987).

[21] Raman Sundrum, "To the Fifth Dimension and Back", TASI Lecture, 2004;
Kaustubh Agashe, "Extra Dimensions", TASI Lecture, 2006;
Bogdan A. Dobrescu, "Particle physics in extra dimensions", TASI Lecture, 2008;
Hsin-Chia Cheng, "Introduction to Extra Dimensions" TASI Lecture, 2009;
Thomas G. Rizzo, "Introduction to Extra Dimensions", arXiv:1003.1698v1 [hep-ph].

[22] I. Antoniadis, "A Possible new dimension at a few TeV," Phys. Lett. B **246**, 377 (1990).

[23] N. Arkani-Hamed, S. Dimopoulos and G. R. Dvali, "The Hierarchy problem and new dimensions at a millimeter," Phys. Lett. B **429**, 263 (1998) [hep-ph/9803315].

[24] N. Arkani-Hamed, S. Dimopoulos and G. R. Dvali, "Phenomenology, astrophysics and cosmology of theories with submillimeter dimensions and TeV scale quantum gravity," Phys. Rev. D **59**, 086004 (1999) [hep-ph/9807344].

[25] I. Antoniadis, N. Arkani-Hamed, S. Dimopoulos and G. R. Dvali, "New dimensions at a millimeter to a Fermi and superstrings at a TeV," Phys. Lett. B **436**, 257 (1998) [hep-ph/9804398].

[26] G. Aad *et al.* [ATLAS Collaboration], "Search for dark matter candidates and large extra dimensions in events with a jet and missing transverse momentum with the ATLAS detector," JHEP **1304**, 075 (2013) [arXiv:1210.4491 [hep-ex]].

[27] L. Randall and R. Sundrum, "A Large mass hierarchy from a small extra dimension," Phys. Rev. Lett. **83**, 3370 (1999) [hep-ph/9905221].

[28] L. Randall and R. Sundrum, "An Alternative to compactification," Phys. Rev. Lett. **83**, 4690 (1999) [hep-th/9906064].

[29] G. Aad *et al.* [ATLAS Collaboration], "Search for high-mass dilepton resonances in pp collisions at sqrt(s) = 8 TeV with the ATLAS detector," arXiv:1405.4123 [hep-ex].

[30] H. Davoudiasl, J. L. Hewett and T. G. Rizzo, "Bulk gauge fields in the Randall-Sundrum model," Phys. Lett. B **473**, 43 (2000) [hep-ph/9911262].

[31] S. Chang, J. Hisano, H. Nakano, N. Okada and M. Yamaguchi, "Bulk standard model in the Randall-Sundrum background," Phys. Rev. D **62**, 084025 (2000) [hep-ph/9912498].

[32] T. Gherghetta and A. Pomarol, "Bulk fields and supersymmetry in a slice of AdS," Nucl. Phys. B **586**, 141 (2000) [hep-ph/0003129].

[33] T. Appelquist, H. -C. Cheng and B. A. Dobrescu, "Bounds on universal extra dimensions," Phys. Rev. D **64** (2001) 035002 [hep-ph/0012100].

[34] B. A. Dobrescu and E. Ponton, "Chiral compactification on a square," JHEP **0403**, 071 (2004) [hep-th/0401032].

[35] G. Burdman, B. A. Dobrescu and E. Ponton, "Resonances from two universal extra dimensions," Phys. Rev. D **74**, 075008 (2006) [hep-ph/0601186].

[36] B. A. Dobrescu, D. Hooper, K. Kong and R. Mahbubani, "Spinless photon dark matter from two universal extra dimensions," JCAP **0710**, 012 (2007) [arXiv:0706.3409 [hep-ph]].

[37] A. Freitas and K. Kong, "Two universal extra dimensions and spinless photons at the ILC," JHEP **0802**, 068 (2008) [arXiv:0711.4124 [hep-ph]].

[38] K. Ghosh and A. Datta, "Phenomenology of spinless adjoints in two Universal Extra Dimensions," Nucl. Phys. B **800**, 109 (2008) [arXiv:0801.0943 [hep-ph]].

[39] K. Nishiwaki, "Higgs production and decay processes via loop diagrams in various 6D Universal Extra Dimension Models at LHC," JHEP **1205**, 111 (2012) [arXiv:1101.0649 [hep-ph]].

[40] K. R. Dienes, E. Dudas and T. Gherghetta, "Extra space-time dimensions and unification," Phys. Lett. B **436**, 55 (1998) [hep-ph/9803466].

[41] H. -C. Cheng, B. A. Dobrescu and C. T. Hill, "Gauge coupling unification with extra dimensions and gravitational scale effects," Nucl. Phys. B **573**, 597 (2000) [hep-ph/9906327].

[42] R. N. Mohapatra and A. Perez-Lorenzana, "Neutrino mass, proton decay and dark matter in TeV scale universal extra dimension models," Phys. Rev. D **67**, 075015 (2003) [hep-ph/0212254].

[43] N. Arkani-Hamed and S. Dimopoulos, "New origin for approximate symmetries from distant breaking in extra dimensions," Phys. Rev. D **65**, 052003 (2002) [hep-ph/9811353].

[44] B. A. Dobrescu and E. Poppitz, "Number of fermion generations derived from anomaly cancellation," Phys. Rev. Lett. **87**, 031801 (2001) [hep-ph/0102010].

[45] H. -C. Cheng, B. A. Dobrescu and C. T. Hill, "Electroweak symmetry breaking and extra dimensions," Nucl. Phys. B **589**, 249 (2000) [hep-ph/9912343].

[46] N. Arkani-Hamed, H. -C. Cheng, B. A. Dobrescu and L. J. Hall, "Selfbreaking of the standard model gauge symmetry," Phys. Rev. D **62**, 096006 (2000) [hep-ph/0006238].

[47] G. Servant and T. M. P. Tait, "Is the lightest Kaluza-Klein particle a viable dark matter candidate?," Nucl. Phys. B **650**, 391 (2003) [hep-ph/0206071].

[48] H. -C. Cheng, J. L. Feng and K. T. Matchev, "Kaluza-Klein dark matter," Phys. Rev. Lett. **89**, 211301 (2002) [hep-ph/0207125].

[49] G. Servant and T. M. P. Tait, "Elastic scattering and direct detection of Kaluza-Klein dark matter," New J. Phys. **4**, 99 (2002) [hep-ph/0209262].

[50] D. Majumdar, "Detection rates for Kaluza-Klein dark matter," Phys. Rev. D **67**, 095010 (2003) [hep-ph/0209277].

[51] F. Burnell and G. D. Kribs, "The Abundance of Kaluza-Klein dark matter with coannihilation," Phys. Rev. D **73**, 015001 (2006) [hep-ph/0509118].

[52] K. Kong and K. T. Matchev, "Precise calculation of the relic density of Kaluza-Klein dark matter in universal extra dimensions," JHEP **0601**, 038 (2006) [hep-ph/0509119].

[53] M. Kakizaki, S. Matsumoto and M. Senami, "Relic abundance of dark matter in the minimal universal extra dimension model," Phys. Rev. D **74**, 023504 (2006) [hep-ph/0605280].

[54] P. A. R. Ade *et al.* [Planck Collaboration], "Planck 2013 results. XVI. Cosmological parameters," Astron. Astrophys. (2014) [arXiv:1303.5076 [astro-ph.CO]].

[55] G. Hinshaw *et al.* "Nine-Year Wilkinson Microwave Anisotropy Probe (WMAP) Observations: Cosmological Parameter Results" [http://arxiv.org/abs/1212.5226]

[56] W. J. Marciano, "Precision electroweak measurements and new physics," eConf C **9808031**, 13 (1998) [hep-ph/9902332].

[57] M. Masip and A. Pomarol, "Effects of SM Kaluza-Klein excitations on electroweak observables," Phys. Rev. D **60**, 096005 (1999) [hep-ph/9902467].

[58] T. G. Rizzo and J. D. Wells, "Electroweak precision measurements and collider probes of the standard model with large extra dimensions," Phys. Rev. D **61**, 016007 (2000) [hep-ph/9906234].

[59] R. Casalbuoni, S. De Curtis, D. Dominici and R. Gatto, "SM Kaluza-Klein excitations and electroweak precision tests," Phys. Lett. B **462**, 48 (1999) [hep-ph/9907355].

[60] H. -C. Cheng, K. T. Matchev and M. Schmaltz, "Radiative corrections to Kaluza-Klein masses," Phys. Rev. D **66**, 036005 (2002) [hep-ph/0204342].

[61] A. Datta, K. Kong and K. T. Matchev, "Minimal Universal Extra Dimensions in CalcHEP/CompHEP," New J. Phys. **12**, 075017 (2010) [arXiv:1002.4624 [hep-ph]].

[62] A. Belyaev, M. Brown, J. Moreno and C. Papineau, "Discovering Minimal Universal Extra Dimensions (MUED) at the LHC," JHEP **1306**, 080 (2013) [arXiv:1212.4858].

[63] M. Battaglia, A. K. Datta, A. De Roeck, K. Kong and K. T. Matchev, "Contrasting supersymmetry and universal extra dimensions at colliders," eConf C **050318**, 0302 (2005) [hep-ph/0507284].

[64] A. Datta, K. Kong and K. T. Matchev, "Discrimination of supersymmetry and universal extra dimensions at hadron colliders," Phys. Rev. D **72**, 096006 (2005) [Erratum-ibid. D **72**, 119901 (2005)] [hep-ph/0509246].

[65] A. Datta, G. L. Kane and M. Toharia, "Is it SUSY?," hep-ph/0510204.

[66] T. Kakuda, K. Nishiwaki, K. y. Oda and R. Watanabe, "Universal extra dimensions after Higgs discovery," Phys. Rev. D **88**, 035007 (2013) [arXiv:1305.1686 [hep-ph]].

[67] G. Servant, "Status Report on Universal Extra Dimensions After LHC8," arXiv:1401.4176 [hep-ph].

[68] T. Flacke, K. Kong and S. C. Park, "A Review on Non-Minimal Universal Extra Dimensions," arXiv:1408.4024 [hep-ph].

[69] G. Belanger, A. Belyaev, M. Brown, M. Kakizaki and A. Pukhov, "Testing Minimal Universal Extra Dimensions Using Higgs Boson Searches at the LHC," Phys. Rev. D **87**, 016008 (2013) [arXiv:1207.0798 [hep-ph]].

[70] [ATLAS Collaboration], CERN preprint CERN-PH-EP-2013-103 (2013).

[71] [CMS Collaboration], CMS-PAS-HIG-13-005 (2013).

[72] A. Datta, A. Patra and S. Raychaudhuri, "Higgs Boson Decay Constraints on a Model with a Universal Extra Dimension," Phys. Rev. D **89**, 093008 (2014) [arXiv:1311.0926 [hep-ph]].

[73] L. Edelhäuser, T. Flacke and M. Krämer, "Constraints on models with universal extra dimensions from dilepton searches at the LHC," JHEP **1308**, 091 (2013) [arXiv:1302.6076 [hep-ph]].

[74] J. M. Cornell, S. Profumo and W. Shepherd, "Dark Matter in Minimal Universal Extra Dimensions with a Stable Vacuum and the "Right" Higgs," Phys. Rev. D **89**, 056005 (2014) [arXiv:1401.7050 [hep-ph]].

[75] M. S. Carena, T. M. P. Tait and C. E. M. Wagner, "Branes and orbifolds are opaque," Acta Phys. Polon. B **33** (2002) 2355 [hep-ph/0207056].

[76] F. del Aguila, M. Perez-Victoria and J. Santiago, "Bulk fields with general brane kinetic terms," JHEP **0302** (2003) 051 [hep-th/0302023].

[77] F. del Aguila, M. Perez-Victoria and J. Santiago, "Some consequences of brane kinetic terms for bulk fermions," [hep-ph/0305119].

[78] F. del Aguila, M. Perez-Victoria and J. Santiago, "Bulk fields with brane terms," Eur. Phys. J. C **33** (2004) S773 [hep-ph/0310352].

[79] F. del Aguila, M. Perez-Victoria and J. Santiago, "Physics of brane kinetic terms," Acta Phys. Polon. B **34** (2003) 5511 [hep-ph/0310353].

[80] A. Muck, L. Nilse, A. Pilaftsis and R. Ruckl, "Quantization and high energy unitarity of 5-D orbifold theories with brane kinetic terms," Phys. Rev. D **71** (2005) 066004 [hep-ph/0411258].

[81] F. del Aguila, M. Perez-Victoria and J. Santiago, "Effective description of brane terms in extra dimensions," JHEP **0610** (2006) 056 [hep-ph/0601222].

[82] A. Datta, K. Nishiwaki and S. Niyogi, "Non-minimal Universal Extra Dimensions: The Strongly Interacting Sector at the Large Hadron Collider," JHEP **1211** (2012) 154 [arXiv:1206.3987 [hep-ph]].

[83] T. Flacke, A. Menon and D. J. Phalen, "Non-minimal universal extra dimensions," Phys. Rev. D **79**, 056009 (2009) [arXiv:0811.1598 [hep-ph]].

[84] M. Schmaltz and D. Tucker-Smith, "Little Higgs review," Ann. Rev. Nucl. Part. Sci. **55** (2005) 229 [hep-ph/0502182].

[85] M. Perelstein, "Little Higgs models and their phenomenology," Prog. Part. Nucl. Phys. **58** (2007) 247 [hep-ph/0512128].

[86] O. Brandt [CDF and D0 Collaborations], arXiv:1204.0919 [hep-ex].

[87] P. Silva [ATLAS and CMS Collaborations], arXiv:1206.2967 [hep-ex].

[88] J. Alwall, M. Herquet, F. Maltoni, O. Mattelaer and T. Stelzer, "MadGraph 5 : Going Beyond," JHEP **1106** (2011) 128 [arXiv:1106.0522 [hep-ph]].

[89] N. D. Christensen and C. Duhr, "FeynRules - Feynman rules made easy," Comput. Phys. Commun. **180** (2009) 1614 [arXiv:0806.4194 [hep-ph]].

[90] C. Degrande, C. Duhr, B. Fuks, D. Grellscheid, O. Mattelaer and T. Reiter, "UFO - The Universal FeynRules Output," Comput. Phys. Commun. **183** (2012) 1201 [arXiv:1108.2040 [hep-ph]].

[91] P. de Aquino, W. Link, F. Maltoni, O. Mattelaer and T. Stelzer, "ALOHA: Automatic Libraries Of Helicity Amplitudes for Feynman Diagram Computations," Comput. Phys. Commun. **183** (2012) 2254 [arXiv:1108.2041 [hep-ph]].

[92] A. Pukhov, "CalcHEP 2.3: MSSM, structure functions, event generation, batchs, and generation of matrix elements for other packages," hep-ph/0412191.

[93] J. Pumplin, D. R. Stump, J. Huston, H. L. Lai, P. M. Nadolsky and W. K. Tung, "New generation of parton distributions with uncertainties from global QCD analysis," JHEP **0207** (2002) 012 [hep-ph/0201195].

[94] H. C. Cheng, K. T. Matchev and M. Schmaltz, "Bosonic supersymmetry? Getting fooled at the CERN LHC," Phys. Rev. D **66** (2002) 056006 [hep-ph/0205314].

[95] J. M. Smillie and B. R. Webber, "Distinguishing spins in supersymmetric and universal extra dimension models at the large hadron collider," JHEP **0510** (2005) 069 [hep-ph/0507170].

[96] G. Aad *et al.* [ATLAS Collaboration], "Search for squarks and gluinos with the ATLAS detector in final states with jets and missing transverse momentum using 4.7 fb^{-1} of $\sqrt{s} = 7$ TeV proton-proton collision data," arXiv:1208.0949 [hep-ex]. [97]

[97] M. Battaglia, A. Datta, A. De Roeck, K. Kong and K. T. Matchev, "Contrasting supersymmetry and universal extra dimensions at the clic multi-TeV e+ e- collider," JHEP **0507**, 033 (2005) [hep-ph/0502041].

[98] F. J. Petriello, "Kaluza-Klein effects on Higgs physics in universal extra dimensions," JHEP **0205** (2002) 003 [hep-ph/0204067].

[99] S. K. Rai, "UED effects on Higgs signals at LHC," Int. J. Mod. Phys. A **23** (2008) 823 [hep-ph/0510339].

[100] N. Maru, T. Nomura, J. Sato and M. Yamanaka, "Higgs Production via Gluon Fusion in a Six Dimensional Universal Extra Dimension Model on S^2/Z_2," Eur. Phys. J. C **66** (2010) 283 [arXiv:0905.4554 [hep-ph]].

[101] K. Nishiwaki, K. -y. Oda, N. Okuda and R. Watanabe, "A Bound on Universal Extra Dimension Models from up to 2fb^{-1} of LHC Data at 7 TeV," Phys. Lett. B **707** (2012) 506 [arXiv:1108.1764 [hep-ph]].

[102] K. Nishiwaki, K. -y. Oda, N. Okuda and R. Watanabe, "Heavy Higgs at Tevatron and LHC in Universal Extra Dimension Models," Phys. Rev. D **85** (2012) 035026 [arXiv:1108.1765 [hep-ph]].

[103] U. K. Dey and T. S. Ray, "Constraining minimal and non-minimal UED models with Higgs couplings," Phys. Rev. D **88** (2013) 056016 [arXiv:1305.1016 [hep-ph]].

[104] T. Flacke, K. Kong and S. C. Park, "126 GeV Higgs in Next-to-Minimal Universal Extra Dimensions," arXiv:1309.7077 [hep-ph].

[105] A. Datta, K. Nishiwaki and S. Niyogi, "Non-minimal Universal Extra Dimensions with Brane Local Terms: The Top Quark Sector," JHEP **1401**, 104 (2014) [arXiv:1310.6994 [hep-ph]].

[106] A. Datta, U. K. Dey, A. Shaw and A. Raychaudhuri, "Universal Extra-Dimensional Models with Boundary Localized Kinetic Terms: Probing at the LHC," Phys. Rev. D **87** (2013) 076002 [arXiv:1205.4334 [hep-ph]].

[107] A. Datta, A. Raychaudhuri and A. Shaw, "LHC limits on KK-parity non-conservation in the strong sector of universal extra-dimension models," arXiv:1310.2021 [hep-ph].

[108] D. Choudhury, A. Datta and K. Ghosh, "Deciphering Universal Extra Dimension from the top quark signals at the CERN LHC," JHEP **1008** (2010) 051 [arXiv:0911.4064 [hep-ph]].

[109] J. A. Aguilar-Saavedra, "Identifying top partners at LHC," JHEP **0911**, 030 (2009) [arXiv:0907.3155 [hep-ph]].

[110] G. Cacciapaglia, A. Deandrea, D. Harada and Y. Okada, "Bounds and Decays of New Heavy Vector-like Top Partners," JHEP **1011**, 159 (2010) [arXiv:1007.2933 [hep-ph]].

[111] G. Cacciapaglia, A. Deandrea, L. Panizzi, N. Gaur, D. Harada and Y. Okada, "Heavy Vector-like Top Partners at the LHC and flavour constraints," JHEP **1203**, 070 (2012) [arXiv:1108.6329 [hep-ph]].

[112] J. Berger, J. Hubisz and M. Perelstein, "A Fermionic Top Partner: Naturalness and the LHC," JHEP **1207** (2012) 016 [arXiv:1205.0013 [hep-ph]].

[113] A. De Simone, O. Matsedonskyi, R. Rattazzi and A. Wulzer, "A First Top Partner Hunter's Guide," JHEP **1304** (2013) 004 [arXiv:1211.5663 [hep-ph]].

[114] J. Kearney, A. Pierce and J. Thaler, "Top Partner Probes of Extended Higgs Sectors," JHEP **1308** (2013) 130 [arXiv:1304.4233 [hep-ph]].

[115] M. Buchkremer, G. Cacciapaglia, A. Deandrea and L. Panizzi, "Model Independent Framework for Searches of Top Partners," Nucl. Phys. B **876** (2013) 376 [arXiv:1305.4172 [hep-ph]].

[116] J. A. Aguilar-Saavedra, R. Benbrik, S. Heinemeyer and M. Perez-Victoria, "A handbook of vector-like quarks: mixing and single production," Phys. Rev. D **88**, 094010 (2013) [arXiv:1306.0572 [hep-ph]].

[117] P. Bandyopadhyay, B. Bhattacherjee and A. Datta, "Search for Higgs bosons of the Universal Extra Dimensions at the Large Hadron Collider," JHEP **1003** (2010) 048 [arXiv:0909.3108 [hep-ph]].

[118] S. Chatrchyan *et al.* [CMS Collaboration], "Search for the standard model Higgs boson produced in association with a top-quark pair in pp collisions at the LHC," JHEP **1305** (2013) 145 [arXiv:1303.0763 [hep-ex]].

[119] CMS Collaboration, "Search for ttH production in events where H decays to photons at 8 TeV collisions", CMS-PAS-HIG-13-015.

[120] ATLAS collaboration, "Search for ttH production in the $H \to \gamma\gamma$ channel at $\sqrt{s} = 8$ TeV with the ATLAS detector", ATLAS-CONF-2013-080.

[121] K. Nishiwaki, S. Niyogi and A. Shivaji, "ttH Anomalous Coupling in Double Higgs Production," arXiv:1309.6907 [hep-ph].

[122] S. Alekhin, A. Djouadi and S. Moch, "The top quark and Higgs boson masses and the stability of the electroweak vacuum," Phys. Lett. B **716** (2012) 214 [arXiv:1207.0980 [hep-ph]].

[123] CDF [Tevatron Electroweak Working Group and D0 Collaborations], "Combination of CDF and DO results on the mass of the top quark using up to 8.7 fb^{-1} at the Tevatron," arXiv:1305.3929 [hep-ex].

[124] Diploma thesis by D. Gerstenlauer, "Flavor Physics in Universal Extra Dimension Models with Brane Kinetic Localized Terms," Universität Würzburg, May 2011.

[125] R Aaij *et al.* [LHCb Collaboration], "Observation of $D^0 - \overline{D}^0$ oscillations," Phys. Rev. Lett. **110** (2013) 101802 [arXiv:1211.1230 [hep-ex]].

[126] M. Bona *et al.* [UTfit Collaboration], "Model-independent constraints on Δ F=2 operators and the scale of new physics," JHEP **0803**, 049 (2008) [arXiv:0707.0636 [hep-ph]].

[127] M. E. Peskin and T. Takeuchi, "A New constraint on a strongly interacting Higgs sector," Phys. Rev. Lett. **65** (1990) 964.

[128] M. E. Peskin and T. Takeuchi, "Estimation of oblique electroweak corrections," Phys. Rev. D **46** (1992) 381.

[129] T. Appelquist and H. -U. Yee, "Universal extra dimensions and the Higgs boson mass," Phys. Rev. D **67** (2003) 055002 [hep-ph/0211023].

[130] T. Flacke, D. Hooper and J. March-Russell, "Improved bounds on universal extra dimensions and consequences for LKP dark matter," Phys. Rev. D **73** (2006) 095002 [Erratum-ibid. D **74** (2006) 019902] [hep-ph/0509352].

[131] I. Gogoladze and C. Macesanu, "Precision electroweak constraints on Universal Extra Dimensions revisited," Phys. Rev. D **74** (2006) 093012 [hep-ph/0605207].

[132] M. Baak, M. Goebel, J. Haller, A. Hoecker, D. Ludwig, K. Moenig, M. Schott and J. Stelzer, "Updated Status of the Global Electroweak Fit and Constraints on New Physics," Eur. Phys. J. C **72** (2012) 2003 [arXiv:1107.0975 [hep-ph]].

[133] T. Flacke, K. Kong and S. C. Park, "Phenomenology of Universal Extra Dimensions with Bulk-Masses and Brane-Localized Terms," JHEP **1305** (2013) 111 [arXiv:1303.0872 [hep-ph]].

[134] C. Csaki, J. Erlich and J. Terning, "The Effective Lagrangian in the Randall-Sundrum model and electroweak physics," Phys. Rev. D **66** (2002) 064021 [hep-ph/0203034].

[135] M. S. Carena, E. Ponton, T. M. P. Tait and C. E. M Wagner, "Opaque branes in warped backgrounds," Phys. Rev. D **67** (2003) 096006 [hep-ph/0212307].

[136] T. Flacke and C. Pasold, "Constraints on split-UED from Electroweak Precision Tests," Phys. Rev. D **85**, 126007 (2012) [arXiv:1111.7250 [hep-ph]].

[137] M. Baak, M. Goebel, J. Haller, A. Hoecker, D. Kennedy, R. Kogler, K. Moenig and M. Schott *et al.*, "The Electroweak Fit of the Standard Model after the Discovery of a New Boson at the LHC," Eur. Phys. J. C **72**, 2205 (2012) [arXiv:1209.2716 [hep-ph]].

[138] T. Flacke, A. Menon and Z. Sullivan, "Constraints on UED from W' searches," Phys. Rev. D **86** (2012) 093006 [arXiv:1207.4472 [hep-ph]].

[139] S. Chatrchyan *et al.* [CMS Collaboration], "Search for charge-asymmetric production of W ' bosons in top pair + jet events from pp collisions at $\sqrt{s} = 7$ TeV," Phys. Lett. B **717** (2012) 351 [arXiv:1206.3921 [hep-ex]].

[140] R. Kelley, L. Randall and B. Shuve, "Early (and Later) LHC Search Strategies for Broad Dimuon Resonances," JHEP **1102** (2011) 014 [arXiv:1011.0728 [hep-ph]].

[141] G. Aad *et al.* [ATLAS Collaboration], "Search for direct third-generation squark pair production in final states with missing transverse momentum and two b-jets in $\sqrt{s}$=8 TeV pp collisions with the ATLAS detector," arXiv:1308.2631 [hep-ex].

[142] S. Chatrchyan *et al.* [CMS Collaboration], "Search for top-squark pair production in the single-lepton final state in pp collisions at $\sqrt{s} = 8$ TeV," arXiv:1308.1586 [hep-ex].

[143] A. Altheimer, S. Arora, L. Asquith, G. Brooijmans, J. Butterworth, M. Campanelli, B. Chapleau and A. E. Cholakian *et al.*, "Jet Substructure at the Tevatron and LHC: New results, new tools, new benchmarks," J. Phys. G **39** (2012) 063001 [arXiv:1201.0008 [hep-ph]].

[144] M. Dasgupta, A. Fregoso, S. Marzani and G. P. Salam, "Towards an understanding of jet substructure," JHEP **1309** (2013) 029 [arXiv:1307.0007 [hep-ph]].

[145] D. E. Kaplan, K. Rehermann, M. D. Schwartz and B. Tweedie, "Top Tagging: A Method for Identifying Boosted Hadronically Decaying Top Quarks," Phys. Rev. Lett. **101** (2008) 142001 [arXiv:0806.0848 [hep-ph]].

[146] [CMS Collaboration], "A Cambridge-Aachen (C-A) based Jet Algorithm for boosted top-jet tagging," CMS-PAS-JME-09-001.

[147] T. Plehn and M. Spannowsky, "Top Tagging," J. Phys. G **39** (2012) 083001 [arXiv:1112.4441 [hep-ph]].

[148] S. Schaetzel and M. Spannowsky, "Tagging highly boosted top quarks," arXiv:1308.0540 [hep-ph].

[149] J. M. Butterworth, A. R. Davison, M. Rubin and G. P. Salam, "Jet substructure as a new Higgs search channel at the LHC," Phys. Rev. Lett. **100** (2008) 242001 [arXiv:0802.2470 [hep-ph]].

[150] P. M. Nadolsky, H. -L. Lai, Q. -H. Cao, J. Huston, J. Pumplin, D. Stump, W. -K. Tung and C. -P. Yuan, "Implications of CTEQ global analysis for collider observables," Phys. Rev. D **78** (2008) 013004 [arXiv:0802.0007 [hep-ph]].

[151] A. Djouadi, J. L. Kneur and G. Moultaka, "Higgs boson production in association with scalar top quarks at proton colliders," Phys. Rev. Lett. **80** (1998) 1830 [hep-ph/9711244].

[152] A. Djouadi, "The Anatomy of electro-weak symmetry breaking. II. The Higgs bosons in the minimal supersymmetric model," Phys. Rept. **459** (2008) 1 [hep-ph/0503173] and references therein.

[153] W. Beenakker, S. Dittmaier, M. Kramer, B. Plumper, M. Spira and P. M. Zerwas, "Higgs radiation off top quarks at the Tevatron and the LHC," Phys. Rev. Lett. **87** (2001) 201805 [hep-ph/0107081].

[154] A. Djouadi, "The Anatomy of electro-weak symmetry breaking. I: The Higgs boson in the standard model," Phys. Rept. **457** (2008) 1 [hep-ph/0503172] and references therein.

[155] S. Chatrchyan *et al.* [CMS Collaboration], "Search for heavy, top-like quark pair production in the dilepton final state in pp collisions at $\sqrt{s} = 7$ TeV," Phys. Lett. B **716** (2012) 103 [arXiv:1203.5410 [hep-ex]].

[156] G. Aad *et al.* [ATLAS Collaboration], "Search for pair production of heavy top-like quarks decaying to a high-pT W boson and a b quark in the lepton plus jets final state at $\sqrt{s}$=7 TeV with the ATLAS detector," Phys. Lett. B **718** (2013) 1284 [arXiv:1210.5468 [hep-ex]].

[157] [ATLAS Collaboration], "Search for pair production of heavy top-like quarks decaying to a high-p_T W boson and a b quark in the lepton plus jets final state in pp collisions at $\sqrt{s} = 8$ TeV with the ATLAS detector", ATLAS-CONF-2013-060.

[158] A. Leike, "The Phenomenology of extra neutral gauge bosons," Phys. Rept. **317** (1999) 143 [hep-ph/9805494].

[159] P. Langacker, "The Physics of Heavy Z' Gauge Bosons," Rev. Mod. Phys. **81** (2009) 1199 [arXiv:0801.1345 [hep-ph]].

[160] T. Han, P. Langacker, Z. Liu and L. T. Wang, "Diagnosis of a New Neutral Gauge Boson at the LHC and ILC for Snowmass 2013," arXiv:1308.2738 [hep-ph].

[161] T. Sjostrand, S. Mrenna and P. Z. Skands, "PYTHIA 6.4 Physics and Manual," JHEP **0605** (2006) 026 [hep-ph/0603175].

[162] E. Accomando, D. Becciolini, A. Belyaev, S. Moretti and C. Shepherd-Themistocleous, "Z' at the LHC: Interference and Finite Width Effects in Drell-Yan," JHEP **1310** (2013) 153 [arXiv:1304.6700 [hep-ph]].

[163] S. Chatrchyan *et al.* [CMS Collaboration], "Search for heavy narrow dilepton resonances in pp collisions at $\sqrt{s} = 7$ TeV and $\sqrt{s} = 8$ TeV," Phys. Lett. B **720** (2013) 63 [arXiv:1212.6175 [hep-ex]].

[164] K. Kong, S. C. Park and T. G. Rizzo, "A vector-like fourth generation with a discrete symmetry from Split-UED," JHEP **1007**, 059 (2010) [arXiv:1004.4635 [hep-ph]].

[165] A. Datta, U. K. Dey, A. Raychaudhuri and A. Shaw, Phys. Rev. D **88**, 016011 (2013) [arXiv:1305.4507 [hep-ph]].